

COMPUTATIONAL METHOD FOR EARLY-STAGE DESIGN OPTIMIZATION OF NATURALLY VENTILATED TERMINALS

MSc. Thesis | Delft University of Technology
Okan Türkcan

With the utmost gratitude to my true Father...

Delft University of Technology

AR4B025 Sustainable Design Graduation Studio
MSc. Architecture, Urbanism and Building Sciences
Track Building Technology

Okan Fehmi Şaban Fred Türkcan (4309364)

Examiners:

dr. ir. P. Nourian

1st mentor - Design Informatics

dr. ir. P. J. W. van den Engel

2nd mentor - Building Physics & Services

dr. ir. M. J. Tenpierik

3rd mentor - Building Physics & Services

dr. Sang Lee, RA

External examiner – Public Building

Anything that reduces fuel consumption and cuts down on
greenhouse gasses is good news.

...as far back as I can remember, I was sketching designs. My
first subject was an aircraft...

I love flying; I love aircraft, and you could say I've had a love
affair with flight since I was a child.

Every time I've flown an aircraft, or visited a steelworks, or
watched a panel-beater at work, I've learned something new
that can be applied to buildings.

Sir Norman Foster

O

ABSTRACT

ABSTRACT

This thesis focuses on the development of a computational model for early-stage design decision support of naturally ventilated terminal structures. The model is developed in a parametric Rhino Grasshopper environment paired with Python coding and CFD analyses through OpenFOAM. Optimization of air distribution parameters is performed with Galapagos evolutionary solver, while optimization of the subsequent geometry is done manually by means of the CFD results of the best-performing variant.

Within the thesis a background study is made by means of an interview and literature review, after which analytic calculations and CFD studies are used to test various options and narrow down the domain of solutions for the case of the design of a naturally ventilated terminal structure. Finally, the method itself is developed and validated with a case study that is also used during the development of the model.

The result of the thesis is a rapid computational model that allows for the integration of CFD studies into the early-stage design of naturally ventilated terminals with an optimization for the stated objective function. Secondly, the CFD results can be used to give an indication of a more optimal geometry of the hall. The final selection of geometry and the validation are left up to the user to perform afterwards.

O

CONTENTS

0 CONTENTS

ABSTRACT	5
1 INTRODUCTION	11
2 RESEARCH FRAMEWORK	13
2.1 Background	13
2.2 Research Objective	14
2.3 Research Questions	15
2.4 Methodology	16
2.4.1 Research Design	16
2.4.2 Design Method	18
2.5 Research Planning	23
3 LITERATURE REVIEW	25
3.1 Introduction	25
3.2 Energy Performance and Climate Change	25
3.2.1 Influence of the Built Environment	25
3.2.2 Development of Sustainable Architecture	27
3.2.3 Energy Consumption of Buildings	29
3.3 Airport Design	30
3.3.1 Economic Impact of Aviation	30
3.3.2 Airport Development Costs	31
3.3.3 Airport Design Concepts	32
3.3.4 Airport Energy Consumption	36
3.4 Indoor Environmental Quality	39
3.4.1 Aspects of Indoor Environmental Quality	39
3.4.2 Indoor Air Quality	41
3.4.3 Thermal Comfort	42
3.4.4 Adaptive Thermal Comfort	48
3.4.5 Thermal Comfort at Airports	51
3.5 Ventilation	53
3.5.1 Importance of Ventilation	53
3.5.2 Fluid Mechanics and Ventilation	53
3.5.3 Ventilation Mechanics	54
3.5.4 Thermal Buoyancy	55
3.5.5 Wind	57
3.5.6 Venturi Effect	58
3.5.7 Internal Obstacles and Duct Resistance	59
3.5.8 Ventilation Integration	63
3.5.9 Case Study Designs	64
3.6 Optimization in CFD	71
3.7 Literature Review Discussion	74
4 DESIGN & ENGINEERING	77
4.1 Introduction	77
4.2 Design: General Topology (Driving Forces)	77
4.3 Design: Algebraic Topology (Geometry)	79
4.3.1 Airport Design Guidelines	80
4.3.2 Terminal Design	82
4.3.3 Design Scripts	83
4.4 Engineering	87
4.4.1 Thermal Loads and Buoyancy Scripts	87
4.4.2 Air Distribution	93
4.4.3 CFD Simulation	117

5 OPTIMIZATION	126
5.1 Introduction	127
5.2 Optimization I: Air Distribution	127
5.2.1 Description	127
5.2.2 Result Aggregation I	128
5.3 Optimization II: Geometric	129
6 APPLICATION	135
6.1 Introduction	135
6.2 Description of Lelystad Airport	135
6.3 Input Parameters	138
6.4 Genetic Algorithm Results	139
6.5 Geometric Optimization Results	141
7 CONCLUSION	145
7.1 General Conclusion	145
7.2 Research Questions	146
7.3 Limitations	147
7.4 Recommendations	148

1

INTRODUCTION

1 INTRODUCTION

The aviation industry has always been a source of inspiration for me; the development of magnificent machines that allow millions of people each day to travel to other corners of the globe has been a topic that has interested me since I was a child. Not surprisingly, my dream was to become an airplane designer.

It was not until in my high school years that I realized that such a job does not exist, nor has any chance of existing; the sheer complexity of the various fields involved makes it impossible for a single person be able to work in the total field of airplane design.

However, as my interest in the built environment developed over the following years, my interest in *total design* remained. To this day, I believe that any successful architect must have the qualities of all the disciplines that it works with, including the technical ones. Therefore, I chose building technology as a specialization direction, with a particular interest in building physics.

The thesis topic reflects my personal goal to develop the skills I felt lacking most: in computational design, natural ventilation and thermal comfort. So much more than a thesis, the treatise is a silent manifest for learning. Learning from my professors, from literature, and from trial and error. It is my sincere hope that regardless of the outcome as a product itself, the whole process of learning in these fields will broaden my horizon and that the thesis shows this desire for learning.

2

RESEARCH FRAMEWORK

2 RESEARCH FRAMEWORK

2.1 Background

The rising challenge of climate change and the realization that even with immediate action, irreversible damage is done to our ecosystem, forces designers of the built environment to think even harder on the topic of a sustainable and less energy and resource-intensive built environment. This is especially the case as the built environment causes over a third of all energy consumption and generation of CO₂, not even including the fact that it is the number one consumer of global resources. In this context, the development of low-energy and passively ventilated buildings becomes of particular interest: especially because HVAC systems are one of the largest consumers of energy in buildings and contain around 12% of total embodied energy.

On the other hand, the predicted growth of the aviation industry (a doubling of passengers by 2040) is causing serious shortages in infrastructure: the over 1 trillion USD investments to existing and future airport construction are already warned to be insufficient. Especially the increase of low-cost flights and low-cost terminals (LCT's) will be influential to this development.

As a sector under great scrutiny from a sustainability point of view, the energy performance and thermal comfort of airports is often under-researched, even if the terminals form over three quarters of the total energy consumption and around 10-15% of operational expenditures. HVAC systems form -depending on the airport- between 20-60% of this consumption, consistently being the prime consumer of energy at airports.

Within this context, developing a radical solution -a *fully* naturally ventilated terminal- to the energy consumption of this very energy-intensive architectural function is an interesting design challenge. Problems such as the surrounding air quality, high levels of noise, thermal comfort and high internal loads arise quickly to push designs to complicated HVAC systems: after all, such a *natural* solution requires a clear integration into the architectural expression of the building, knowledge of building physics and most importantly: early-stage design decisions.

Therefore, in this high-tech sector dominated by *airflow* and *performance*, it would seemingly be fitting to develop high-performance buildings that also fit into a similar design language that airplanes follow; yet also contrast by focusing on *low-end* rather than *high-end* technologies. Developing a method for designing airport terminals that allows for good indoor environmental quality yet is passively operated therefore poses an interesting challenge, both from an architectural as well as technical point of view.

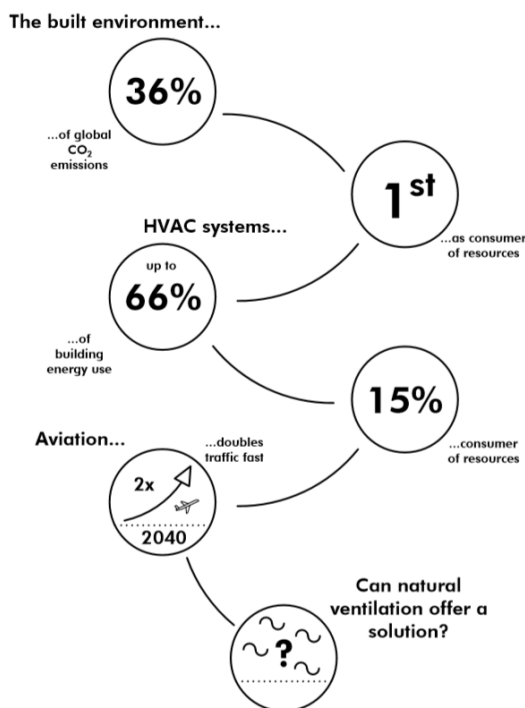


Figure 1 The challenge that the thesis tackles in short.

In order to make such a thesis happen, various scientific disciplines need to be integrated. Besides being an architectural problem and therefore concerning the field of architecture, the topic also integrates the basic disciplines of computer science and physics. Within those disciplines, the branches of building sciences, optimization, numerical analysis, fluid mechanics and thermodynamics are tackled. Specifically, this thesis focuses on the integration of architectural design, building physics and optimization applied to the case of natural ventilation in large terminal structures. A Venn diagram of the integration of these fields is given in figure 2.

2.2 Research Objective

The underlying objective of this thesis is to gain a deeper understanding of the three topics that I desire to learn more about: natural ventilation, computational design and the design of airports. In that sense, the thesis is not just a scientific enquiry, but also a quest of personal interest and development.

The posed design problem is to develop a computational design method for early-stage design of a naturally ventilated terminal in a temperate climate for a given thermal comfort requirement in a parametric and optimized workflow. The developed model allows for a fast integration of natural ventilation into the design from a conceptual phase and can help architects and engineers in analyzing and guiding more detailed designs. By analyzing a multitude of results designers quickly can gain insight into the effect of design decisions. This is also the reason why an integration with Rhino Grasshopper was sought: by implementing a CFD optimization in a parametric workflow for early-stage design, designers can more efficiently analyze alternatives in comparison to more traditional software packages.

Within the goal of developing such a computational model, the objective of the thesis is to gain insight to what effect various parameters influence thermal comfort of a naturally ventilated airport terminal in a temperate climate. Within that scope, there are multiple sub-objectives of the thesis:

- Determine the current state of the climate design of airports and naturally ventilated buildings
- Define appropriate strategies, from a thermal comfort as well as geometry point of view, for the design of naturally ventilated airport terminals
- Determine the appropriate computational design and optimization process(es) for the design
- Optimize air distribution parameters and terminal geometry to achieve the required level of thermal comfort for least amount of inlets/outlets
- Apply the model to an existing low-cost terminal design as a case study

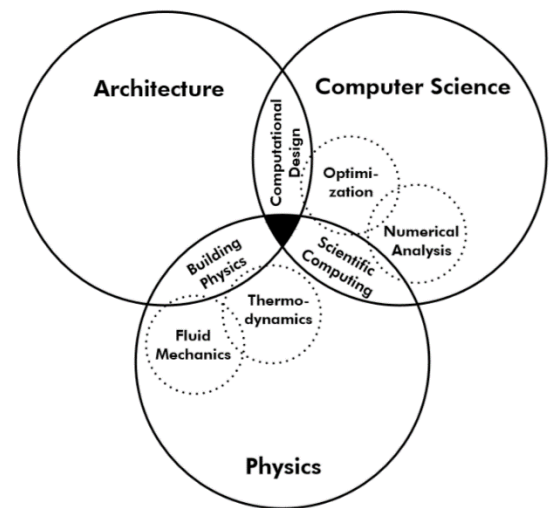


Figure 2 Venn diagram of the disciplines the thesis addresses.

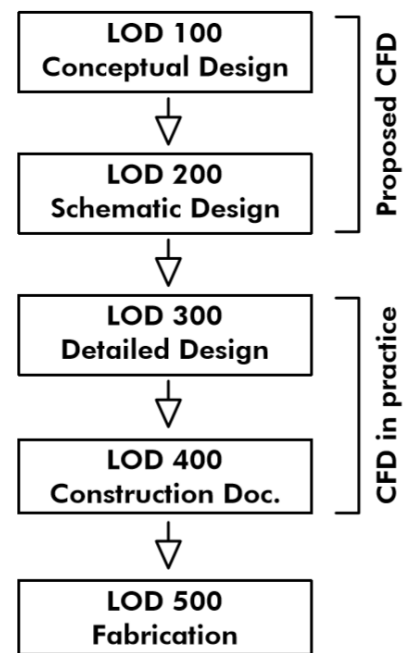


Figure 3 Normally CFD is only integrated in more detailed design stages due to complexity and slowness. The developed method attempts to implement CFD quickly at an early design stage.

- Estimate the energy savings for a peak heating and cooling day of the optimized design against an existing design

The final envisaged product is a computational model for early conceptual design of naturally ventilated terminals in a parametric design environment. The design knowledge gained from a CFD-validated design for a naturally ventilated terminal optimized for thermal comfort subsequently allows for gaining design knowledge. To this extent, knowledge gained from the steps in between will also be included in the final body of conclusions. Additionally, the insights gained from manual design and smaller CFD analyses are also added.

Initial hypotheses would be that that achieving a fully passive ventilation concept paired with a high level of thermal comfort will not be possible without high exceedance hours, unless some sort of additional heating/cooling is provided. Active heating will be universally required, yet active cooling could be avoided easily by using smart design. If lower thermal quality levels are used, for instance category II/III or adaptive thermal comfort or even outdoor comfort levels, the resulting geometry could be much more compact as well.

Some conditions will apply the design to limit it further. Firstly, the plan geometry should not change, nor should the underlying topological layout of the plan. This is because the design of airports is based heavily on other factor such as passenger throughput, security screening and safety. Secondly, we will assume all sides of the building are glass and that the geometry can be simplified to a level of design that is still reasonable. Also, a full annual continuous simulation will not be conducted for the design process; instead, the focus will be on a heating and cooling day and an average annual day.

2.3 Research Questions

By such, this thesis will focus on the following research question: “What are the effects of various air distribution and geometry input parameters on the thermal comfort of a naturally ventilated airport terminal?” Additionally, the following sub-questions will need to be answered:

- What is the underlying design methodology of naturally ventilated large structures, which are designed and built in practice?
- How can the requirements of the design task be translated into a computational workflow and what methods are appropriate in its application?
- What are the optimal air distribution parameters for a naturally ventilated terminal?

- What is the optimal (roof) geometry of an airport terminal to maximize ventilation efficiency?
- What is the energy and comfort performance of the optimized design against a traditionally designed (case study) airport terminal?

For these questions to be answered, some background questions need to be answered as well:

- What are the underlying fundamental theories and applications in airport design, natural ventilation, thermal comfort and optimization in architectural (engineering) design?
- What is the contribution of HVAC systems to energy consumption in buildings?
- What is the topological layout and occupancy for various types of airport terminals?
- What are the current standards and relevant norms in the layout, climate design and thermal comfort of airport terminals?
- How can natural ventilation be integrated into architecture and its expression?

2.4 Methodology

2.4.1 Research Design

The research design is based on four main steps that need to be taken for the research objectives to be achieved. All these steps are conducted by using a case study example to develop the model with. A visual description of the whole research design can be observed in figure 4.

The study is an exploratory research-by-design with firstly a literature review and interviews with experts from practice. The interview was conducted with Arjan Pleysier, Senior Advisor at Deerns BV. An excerpt of this interview can be found in Appendix A. Additionally, two naturally ventilated buildings that are well-documented will be analyzed as case studies. The literature review and case study buildings will yield both qualitative as well as quantitative data, which is then used as input for the design and computational model. Data preparation, methods used within the model and qualitative analysis of the content can be found in the upcoming chapters and conclusion.

The development of the computational model starts with a set of manual drafts that propose alternatives for the design of a naturally ventilated terminal. The designs are then checked using hand calculations and CFD studies performed in Phoenics CFD. These initial manual and CFD designs have the goal to determine the accuracy of the manual estimates and gain insight into the effect of air distribution parameters and terminal geometry on the final thermal comfort of the design.

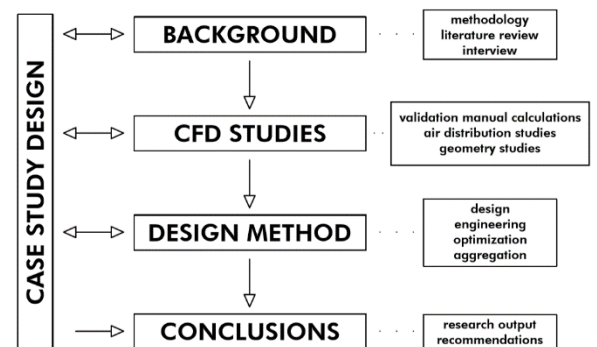


Figure 4 Diagrammatic overview of the thesis' process.

Software	Version	Function
Rhino & Grasshopper	Rhino v5.0 Grasshopper v0.9.0076	Parametric 3D modeling
Python	v2.7.10	Geometric and general programming
Ladybug & Honeybee	v.0.067	Thermal comfort calculations, daylight simulations
Butterfly	v.0.0.05	CFD simulation interface for Grasshopper
Galapagos	-	Genetic Algorithm for Grasshopper
OpenFOAM	v5.x (v.1706+)	CFD solver
BlueCFD-Core	v2017-2	Linux virtual environment
Paraview	v5.6.0	Scientific data visualization
Phoenics	2017 v1.3	CFD studies, final verification

Figure 5 Software used during the thesis.

Insights gained from this process are used as the base for the development of the computational method afterwards. The method is executed in a Rhino and Grasshopper environment supplemented with Python coding for mathematical and geometric operations. The Ladybug/Honeybee plugin is used to generate thermal comfort results from the CFD simulations run using the Butterfly plugin. This plugin acts as an interface for running OpenFOAM simulations in a virtual Linux environment by using BlueCFD-Core. Intermediate result visualization and mesh inspection is executed in Paraview. Finally, Galapagos is used as the optimization plugin to determine which solution complies best with the objective statement. A detailed description of each software package is given in figure 5, while software elaboration and settings are given in the following chapters.

The computational process is finally tested on the case study design that was also used in the development of the method. The case study is elaborated further to also address issues and design requirements that are necessary to implement the design. The result of the whole process is documented to gauge the performance of the proposed method both in general as well as on the case study, after which the study is concluded.

2.4.2 Design Method

The proposed method itself is split into four main parts, consisting of design, engineering, optimization and analysis. This structure for the method is nearly fully visible in the Rhino Grasshopper script and allows users to clearly see and interact with the process itself. It is also summed up in the following figure.

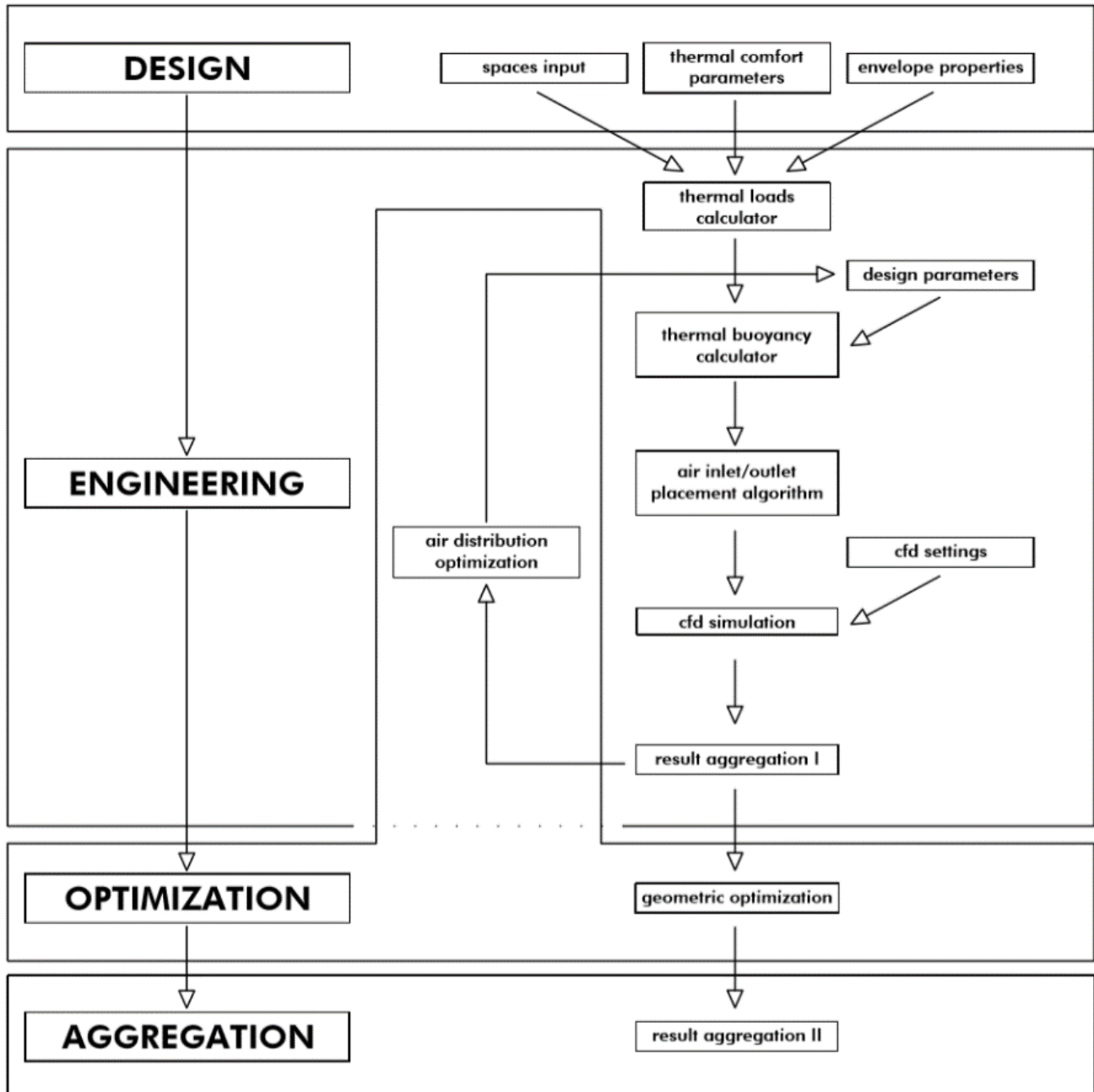


Figure 6 Proposed design method in simplified form.

In the initial design phase, the design is considered both from a general (point-set) topology as well as algebraic topology point of view. Firstly, the correct topology for the case at hand is considered: the type of ventilation, what the driving forces behind air movement are and how air should be distributed in principle. Afterwards the 'algebraic' topology is elaborated, focusing on the geometry of the building and what parameters are influential for natural ventilation.

In more concrete terms, the user inputs the outlines of all spaces in the terminal, the desired thermal comfort levels and parameters and the properties of the envelope. All of these features are always calculated per space, allowing for different levels of thermal comfort in each space.

In the subsequent engineering phase, the influence of influential parameters on thermal comfort and natural ventilation is quantitatively analyzed to explore the domain of feasible solutions in a building design. This is done using manual calculations and CFD studies and includes smaller studies into the practical application of natural ventilation in buildings. The final result of the engineering design is to deliver a naturally ventilated building that will function, but is not yet optimized in terms of its final parameters.

In this phase the script automatically processes data through a mix of GH_Python and C_Python scripts to calculate all thermal loads in the design per space and per grid point of 1m. This data is also used to generate the heat volumes that are then imported into the CFD simulation. According to a predefined set of design parameters, in this case inlet airspeed, inlet and outlet areas and stack heights, a feasible set of air distribution inputs is generated based on thermal buoyancy. Additional requirements can also be put in here, such as extra pressure gains.

After air distribution parameters are defined, the script runs a clustering algorithm coded in C_Python to distribute inlets and outlets geometrically in the spaces. The used algorithm is the K-means clustering algorithm, which is explained in more detail in the subsequent chapters. Inlets are positioned with a weighted K-means script, in which the heat load per grid point 'attracts' the inlets towards spaces with more heat load. This way, uneven heat loads, e.g. due to solar loads, façade transmission and higher localized occupancy can be taken into account. Outlets are then placed in a weightless K-means script, but by using the inlets as initial reference points it is ensured that all outlets service the same number of inlets, ensuring a more even distribution of air.

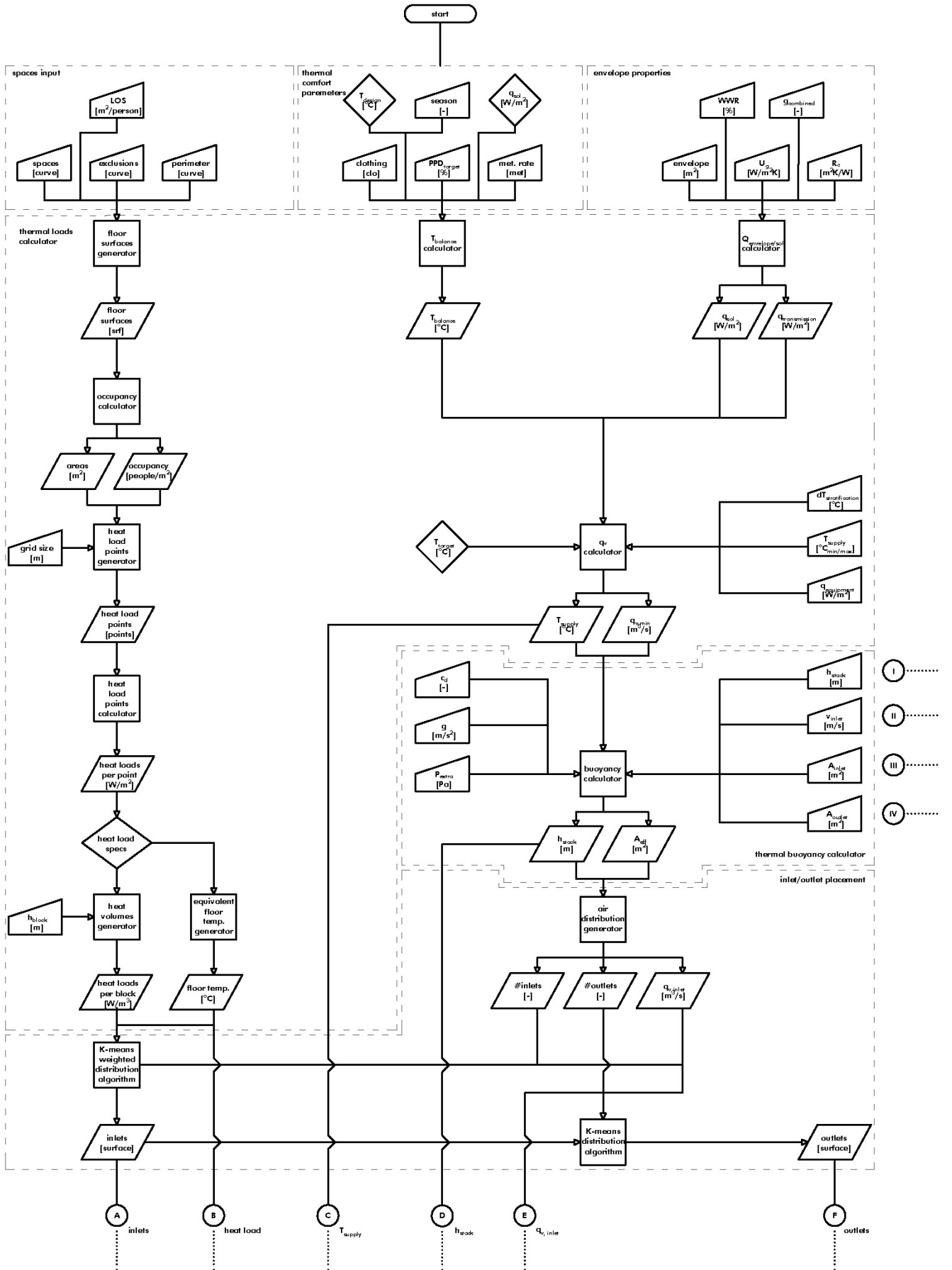
In the final part of the engineering side of the script, the final geometry is prepared for the CFD simulation. Boundary conditions are input and the CFD simulation case is prepared using standard Butterfly components. An additional python script writes two additional files to input the heat loads into the CFD simulation, as Butterfly does not support the input of heat loads out of the box.

Afterwards, a twofold optimization is executed on the design. Firstly, a metaheuristic search algorithm using genetic algorithms scans the possible design space to try and find the right combination of air distribution parameters that still ensures high thermal comfort. The results obtained from the whole process, including data of lesser iterations, are stored and aggregated to gain insight into which parameters are more influential to thermal comfort. Once a satisfactory result is reached from the first optimization process, the 'best' result is put through the second optimization of changing geometry to increase ventilation effectiveness. The resulting geometry gives an indication of what a terminal geometry could be when optimized for maximum air-flow rates while having the same air distribution parameters.

In the script this process is reflected in a Galapagos Evolutionary solver component changing the design parameters that were defined earlier. A CFD analysis is run for each parameter change and the thermal comfort data of these runs are logged and aggregated to define fitness (the objective) of the first optimization solver. In here, the goal minimize the amount of inlets and outlets needed while providing for sufficient thermal comfort. A limit is set on the amount of generations the algorithm will analyze in order to speed up the design process.

The 'best-performing' geometry is selected and voxelated, while inlets and outlets are connected through a set of Bezier curves with parametric start and end tangents. The start and end tangents are controllable by the user, allowing for a certain level of 'design freedom'. However, a supplemental method of checking velocity magnitudes in the hall is also proposed and included in the code, but it does not yield a consistently valid result, which is why it is not proposed as the final solution. Nevertheless it can be used as a guide for optimization of the design.

In the final stage of the method, all results collected are analyzed in order to gain a better understanding of the final performance of the design. The best performing result is visualized and presented in conjunction with additional data for usage in the natural ventilation design, such as the combination with solar chimneys, wind catchers and earth ducts.



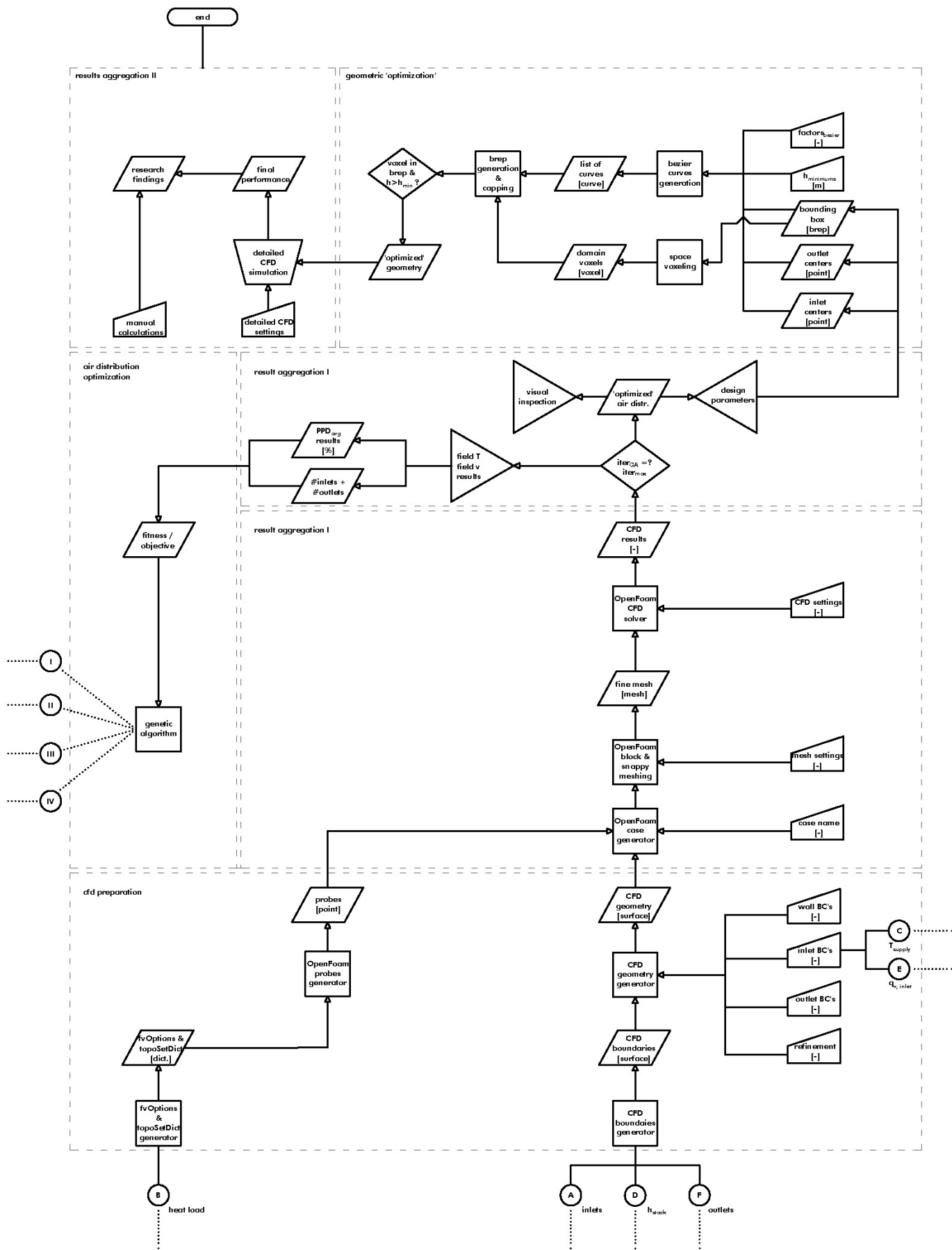


Figure 7 Main flowchart of the design method.

2.5 Research Planning

The planning of the research will follow the outline that was documented at P1 and is split into four main phases:

- P1-P2: Research and Formulation (literature review, interview with relevant companies, design principles and methods, initial model calibration)
- P2-P3: Simulation (initial simulation results, computational model development, report and design set-up)
- P3-P4: Design and Validation (final design analysis and results, report draft)
- P4-P5: Finalization and Presentation (preparing all documents and a model for final presentation)

The research team will consist of the author, supervised by the three mentors. The computational aspect will be mainly with dr. ir. P. Nourian, while the ventilation aspect will be supervised by dr. ir. P. van den Engel. Dr. ir. M. J. Tenpierik will help on the total climate design as well as the indoor environmental quality aspects and the methodology of the whole thesis. No financial burdens are identified for conducting the research.

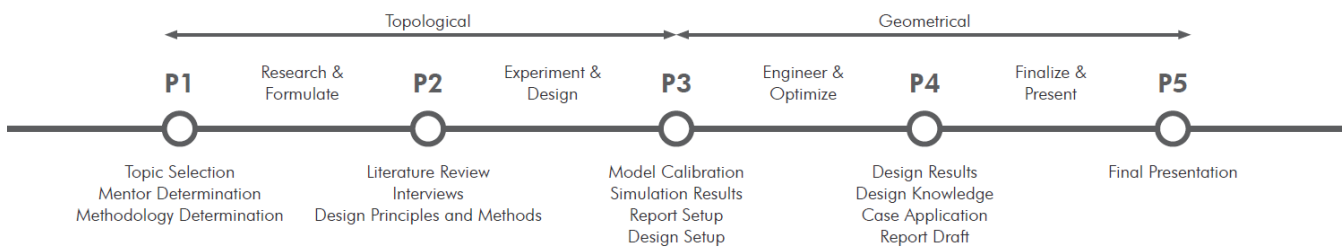


Figure 8 Proposed planning.

3

LITERATURE REVIEW

3 LITERATURE REVIEW

3.1 Introduction

As mentioned in the Methodology section, the literature review is split into multiple categories. Firstly, a general overview will be provided on the energy performance of the built environment, its societal importance and the design of airports in relation to this. An overview will be given of the basics of airport terminal design and its requirements from spatial, indoor environment and energy performance point of view.

Afterwards, a deeper investigation into thermal comfort for indoor and outdoor environments will be provided that will form the base of the design. Then, the focus will be specifically on natural ventilation in the built environment and its physical background, including two case study examples of natural ventilation.

Finally, an overview will be given on optimization techniques for computational fluid dynamics related to the design challenge posed in the thesis.

3.2 Energy Performance and Climate Change

3.2.1 Influence of the Built Environment

Mankind has had and will continue to have a great influence on the climate of the earth. As a species with the power to influence earth so drastically -ranging from large urban developments to alterations of the natural environment and population of the atmosphere and beyond- the effects of human intervention on natural processes and cycles have been thoroughly investigated since the last century, with early measurements of climatic conditions starting as early as the second half of the 19th century (Schlanger, 2018).

The Holocene period in our climate, which started around 10,000BC with the demise of the Last Glacial Period (known as the Pleistocene Epoch/"last ice age") (Zimmermann, 2018), has seen a steep rise in CO₂ levels in the atmosphere exceeding any value seen in the previous 400,000 years. The effect of human activity as the main contributor to this rise has been broadly accepted by scientists with over 95% probability (NASA, 2018).

Currently in Europe, buildings are responsible for over 40% of all energy consumption and 36% of CO₂ emissions annually (European Commission, 2018). Also globally, over 31% of CO₂ emissions is caused by electricity and heat production and another 12% by manufacturing and construction (C2ES, 2018). Annually, nearly 60% of all electricity is consumed in residential and public buildings (GEA, 2012). Evidently, tackling the energy performance of the built environment will continue to be an important aspect in the fight on climate change, not least due to

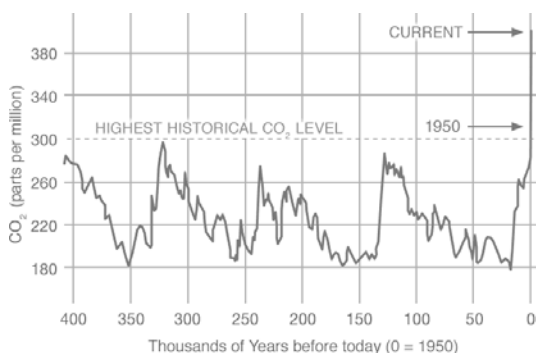


Figure 9: Rising CO₂ levels in our atmosphere (NASA)

the fact that the built environment will continue to grow (Rithcie & Roser, 2018). Additionally, the built environment is a basic need of humanity by providing shelter.

Besides the broad aforementioned consensus however, it would be scientifically valid to also acknowledge the 5% chance that CO₂ reduction is not the right strategy. Even then, the contribution of the building industry to the alteration of the environment is undeniable. Besides the creation of large settlements and infrastructure, the building industry is a large “exploiter of natural resources” (Spence & Mulligan, 1995), causes large losses in soil, agricultural lands, forests and wildlands, pollutes drinking water and generates landfills (Initiafly, 2018). In the United States for instance, the construction sector causes 40% of all drinking water pollution and 50% of landfill wastes, while according to the UK GBC the construction sector annually uses more than 400 million tons of material.

Therefore, the reduction in materials usage and embodied CO₂ is just as important in *sustainable architecture* as is the reduction in energy usage and related CO₂ emissions. In fact, in zero-energy buildings, over 52% of the total CO₂ emissions in a fifty-year lifespan (Autodesk, 2018) are from the building materials. Knowing that around 10-12% of a regular building’s embodied energy is in building services (Hitchin, 2013), it is easily visible that a reduction in building services would lead to less CO₂ emissions.

On the other hand, the building industry’s dependency on financial feasibility means that it is critical for buildings to reduce both operational as well as initial costs. The rising popularity of the concepts of TCO (Total Cost of Ownership) and LCCA (Life Cycle Cost Analysis) are a clear indication of this. In the current Dutch market, for instance, nearly 35% of the initial building costs are spent on building services (Arcadis, 2018) while in general operating costs are in the range of 3-4 times as large in a thirty-year span compared to the construction costs (Fuller, 2016), even though this is dwarfed by personnel costs (92%). Similarly, the operating cost of a HVAC system over 30 years will be slightly larger than the initial costs to build it. Clearly, any reduction in HVAC systems would possibly bear not only energetic, but also economic benefits if designed cost-effectively.

Legal bodies have jumped into the challenges created and to be solved by the built environment in the shape of building regulations. Initially to withhold minimum levels of comfort and health, and afterwards also for the energy performance of buildings.

3.2.2 Development of Sustainable Architecture

In the late 19th century and early half of the 20th century, terms associated with *bioclimatic* or *environmental* architecture were focused mainly on a morphological approach by contrasting the hard nature of industrialized cities against “the beauty of nature” (Attia, 2018). Additionally, basic issues regarding sanitation were tackled at urban scale to provide the working class with better living environments, such as fresh running water and sewage.

Paradigms occurred with the architecture lab set up by the Olgay brothers in the 50s and the notion of *Environmental Architecture* in the 60’s and early 70’s, yet the focus was still not on energy efficiency per se. The shift to focus on that aspect started with the First Oil Crisis of 1973, which forced mainly North American and later European institutions to focus on energy consciousness and passive solar architecture. This was taken up by the development of ideas on *Sustainable Architecture* in the 80s. The Brundtland Report of 1987 (United Nations, 2014) was a clear confirmation of this upcoming trend in energy efficient architecture. This evolved in the 90s to include *Green Architecture* with the development of the Passivhaus by Feist et al and the development of the PlusEnergy concept by Disch, amongst others such as the USGBC, Van der Ryn and ARUP (Attia, 2018).

It was with the signing of the 1997 Kyoto Protocol however that developments occurred that would see radical changes occur in Europe. The EU2020 goals, in which all new buildings have to be zero-energy in 2020, and the later development of regulations for a *decarbonized building stock* by 2050 have all come into display in the recent two decades with the 2010 European Building Performance Directive and the 2012 Energy Efficiency Directive (European Commission, 2018). For instance in The Netherlands, the EPC norm has been steadily tightened and is now going to be replaced by the BENG (Nearly Energy Neutral Buildings) norm from 2020 onward (RVO, 2018). Similarly, accreditations such as BREEAM (1988) and LEED (1998) have focused on both energy performance as well as comfort in buildings. Similarly today, the signing of the Paris Agreement will force states to come up with even more stringent measures to ensure the building stock and construction industry becomes better-performing.

Such energy-saving codes have been able to aid significantly to increase the energy performance of buildings and increase the comfort of its inhabitants. However, it has inevitably also led to an increase in the amount of HVAC systems in buildings, with over 50% of new-built buildings in The Netherlands for instance having a fully balanced mechanical ventilation system

Paradigm	Years	Influencer	Paradigm
Bioclimatic architecture	1908–1968	Olgay, Wright, Neutra	Discovery
Environmental architecture	1969–1972	Ian McHarg	Harmony
Energy conscious architecture	1973–1983	ALA, Balcomb, ASES, PLEA	Energy efficiency
Sustainable architecture	1984–1993	Brundtland, IEA, Feist	Resource efficiency
Green architecture	1993–2006	USGBC, Van der Ryn	Neutrality
Carbon neutral architecture	2006–2015	UN IPCC, Mazria	Resilience
Regenerative architecture	2016–Future	Lyle, Braungart, Benyus	Recovery

Figure 10 Development of sustainable architecture concepts (Attia)

(Prendergast, 2016). By such, the divide on using *more technology* against *less technology* has only deepened.

In this respect, there have been many responses from the architectural community to the aforementioned challenges. On the one hand, more technologically advanced systems have been implemented, while others have proposed a reduction in complexity in favor of more *natural* methods.

An example of such technical solutions is in Germany, where the Passivhaus standard by Wolfgang Feist (Passivhaus Institute, 2018) or the PlusEnergy concept (Disch, 2018) were developed. Both are based on initial passive principles -maximizing insolation, minimizing heat losses- but the primary way of achieving this is with technologically advanced solutions. This includes a very airtight and high-performance thermal envelope, balanced heat recovery systems, highly efficient appliances and HVAC systems and PV power. Arguably, such *technical solutions* increase the dependency on HVAC systems and are often accredited to be partly supported by HVAC manufacturers and engineers. As Short (2018) puts it in his treatise *The recovery of natural environments in architecture*: "...the air-conditioning industry whose simple aim, not unreasonably, is to capture market share and generate profit, or a gestural architecture with no environmental presence or meaning..."

In contrast to the technological approach lies one that focuses on the usage of natural elements and, as Short puts it again, "a poetic imagination combined with an understanding of the operation of the natural physics of the world." Short continues to argue that a view that "the marked reluctance historically in the design community to acquire such expertise for fear of destroying free artistic expression" is "anti-scientific" and "may be the principle barrier to a sustainable future for the built world". He concludes by explaining how the development and marketing of air conditioning in the mid-twentieth century has led to the demise of a stream of architectural design from the late nineteenth century that was both appreciative of and cautious to natural principles.

In the sub-chapter of "case studies" a more detailed and elaborate review will be given of building that perform energetically well yet are based on the natural principles as Short puts it. However, to be able to benchmark this against a common reference, the energy performance of the existing building stock and a breakdown of its components needs to be given. The following paragraphs will give a short recap of various values as reference for later chapters.

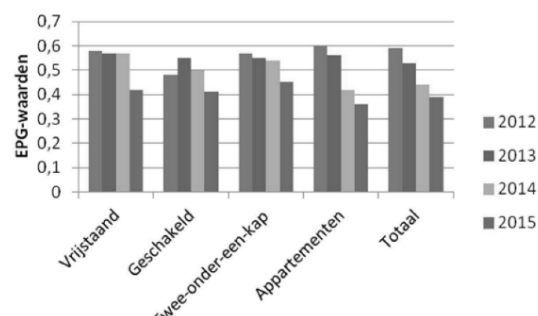


Figure 11 Improvement of energy performance in The Netherlands (Prendergast)



Figure 12 The first Passivhaus (top) (Wikimedia) and the first energy positive building (below), examples of technological approaches (Inhabitat)

Building type	kWh/m ² year	Ratio
Dwellings	147	1
Retail	233	1.6
Schools	262	1.8
Offices	293	2
Hotels	316	2.1
Supermarkets	631	4.3
Hospitals	786	5.3
Restaurants	814	5.5

Year 2003. Source: EIA.

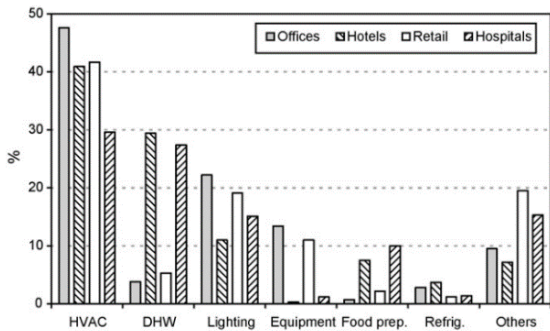


Figure 13 Energy consumption breakdown for different countries combined

Final energy consumption (%)	Commercial	Residential	Total
USA	18	22	40
UK	11	28	39
EU	11	26	37
Spain	8	15	23
World	7	16	24

Figure 15 Weight of building energy consumption (Pérez-Lombard)

End uses in the residential sector (%)	Spain	UE	USA	UK
Space conditioning	42	68	53	62
Domestic hot water (DHW)	26	14	17	22
Lighting and appliances	32	18	30	16

Figure 14 Energy use distribution per country per building type

Energy end uses	USA (%)	UK (%)	Spain (%)
HVAC	48	55	52
Lighting	22	17	33
Equipment (appliances)	13	5	10
DHW	4	10	–
Food preparation	1	5	–
Refrigeration	3	5	–
Others	10	4	5

Sources: EIA, BRE [12] and IDAE.

Figure 17 Energy end use distribution per country

3.2.3 Energy Consumption of Buildings

The energy consumption of buildings depends on many factors that either positively or negatively influence it. The performance of the thermal envelope and glazing, passive features, HVAC system efficiency, climate conditions, occupancy and function all will cause differences in energy performance (European Commission, 2016). Additionally, a change in function will also mean a different breakdown of contributing factors, such as hot water playing a large role in residences and lighting in offices (Pérez-Lombard, Ortiz, & Pout, 2008).

In general, however, it is possible to see that the energy use intensity is lower in housing and higher in commercial buildings, but due to the larger amount of housing it still consumes more in total when compared to commercial buildings (EnergyStar, 2013). Within commercial buildings, hospitals, restaurants and supermarkets stick out with their comparatively high consumption. The general trend however is still the same: HVAC systems are the largest consumer of energy regardless of building type within the existing building stock.

The distribution of consumption per building function can be seen in figures 5 through 9. Similarly, new codes also acknowledge the differences in energy performance per building function. The upcoming BENG norm in The Netherlands (RVO, 2018), for instance, requires that energy demand in residential buildings is half that of commercial buildings, with healthcare buildings even having a higher allowable energy demand. As mentioned previously, decreasing energy consumption of buildings still begins with reducing the largest contributor: HVAC systems.

Building type	USA (%)	Spain (%)	UK (%)
Retail	32	22	22
Offices	18	33	17
Hotels and restaurants	14	30	16
Schools	13	4	10
Hospitals	9	11	6
Leisure	6	–	6
Others	9	–	23

Year 2003. Sources: EIA, IDAE and BRE.

Figure 16 Energy end-uses in the residential sector

3.3 Airport Design

3.3.1 Economic Impact of Aviation

Ever since the advent of flight, flying has been regarded as a fast and safe method of reaching many points of the globe and as an important contributor to the global economy. Besides the direct economic benefits due to employment, airports also contribute by means of indirect and induced jobs, added tourism and the transport of businessmen and freight alike. The aviation sector, with its 900 airlines and 22.000 aircraft serving 1.670 airports, contributes to the global economy with a value of nearly 3 trillion USD, equivalent to 8% of the global GDP (ATAG, 2004). Over 2 billion passengers fly annually and 40% of all international tourists are transported by air. 29 million people are employed by means of direct, indirect, induced and catalytic impacts of air travel.

Currently, airports in Europe give employment to over 12.5 million people and contribute to 4.1% of the GDP with a net value of 675 billion Euros. The economic impact of increased mobility and secondary effects mean that a rise in 10% air travel has been statistically linked to a 0.5% increase in GDP (Cagney, 2018). Especially in Europe and North America, where air travel is most established, the relative and absolute contribution of air travel to the total GDP is considerable.

After the popularization of commercial flight after the Second World War and the 1944 Chicago Convention, which set up the International Civil Aviation Organization (ICAO), commercial aviation saw a large growth thanks to deregulation in the 1970's in the United States. Initially only meant for the wealthy, flying become more accessible thanks to national carriers at first and cheaper, Low Cost Carriers (LCC) after the 1990's.

With the formation of long haul LCC's, increasing globalization, emerging markets outside the classic *Western World* and increased demand for air cargo, air travel is only deemed to grow even more in the upcoming decades. Cargo flights are predicted to increase in all regions of the world by 4.9% over the coming years, while passenger traffic is expected to increase by 4.6% until 2034 (CAPA, 2018a). Passenger traffic is expected to increase mainly in emerging markets, with the Asia-Pacific region continuing to lead the world market of passenger travel. However, many aviation experts and branches warn for a lack of investment into the aviation market -especially in the infrastructure (CAPA, 2018b).

Although predictions of more than 10 years in the aviation market are uncommon (CAPA, 2018a) due to large amounts of uncertainties, the many factors that influence the growth of the aviation market seem positive: fuel prices will remain low, the

global economy will grow, the middle class population will grow threefold and more efficient airplanes will become available.

This growth of the aviation market will not only mean more passenger traffic in existing airports: thanks to an increase in point-to-point flying as opposed to large hubs, there will be more flights globally to smaller destinations (CAPA, 2018a). This means, for instance, that previously unviable direct flights between two low-income cities will become increasingly possible. This, and environmental or planning restrictions around most large hub airports, will mean that smaller airports will be built around the globe. Examples of this include secondary airports of large hubs such as Lelystad Airport in The Netherlands, London City, Gatwick, Luton, Stansted and Southend Airports in the United Kingdom and Istanbul Sabiha Gökçen Airport in Turkey.

3.3.2 Airport Development Costs

In total, over 1.1 trillion USD of investments are currently being made to increase airport capacity around the world but yet seem to fall short in accommodating the large increase in passenger traffic (CAPA, 2018b; IATA, 2018a). Current investments consist of 255 billion USD into new airports and 845 billion USD to upgrading existing ones. The Asia Pacific region leads the charts in both fields, having the highest amount of investment into new airports (130 billion USD) and upgrading existing ones (395 billion USD). Europe comes in second, with investments into new airports (70 billion USD) and existing ones (120 billion USD) being of an order of magnitude two smaller. North America and the Middle East are notable for their low investment into new airports (under 10 billion USD) yet high investment into the existing ones (115 and 145 billion USD respectively). Africa and South America notable due to the lack of investment into the air sector in general.

The monetary investment also shows in the number of airports currently being built or in the pipeline for the coming forty years: over 415 in total. Of these, nearly 220 are in the Asia Pacific region and 58 in Europe, clearly showing that those two regions are leading with respect to the construction of new airports (CAPA, 2018a). Although exact data is not yet available, most of these airports will be relatively small and simple in design, rather than full-fledged large and complex airports.

When considering the total investment it takes to construct a new airport, the cost of the terminal facilities is only a small portion of total costs. These are very much dependent on airport size and capacity, runway length, labor and land reclamation costs and the level quality that is targeted. For instance, in the case of



Figure 18 Construction of new airports globally (CAPA)

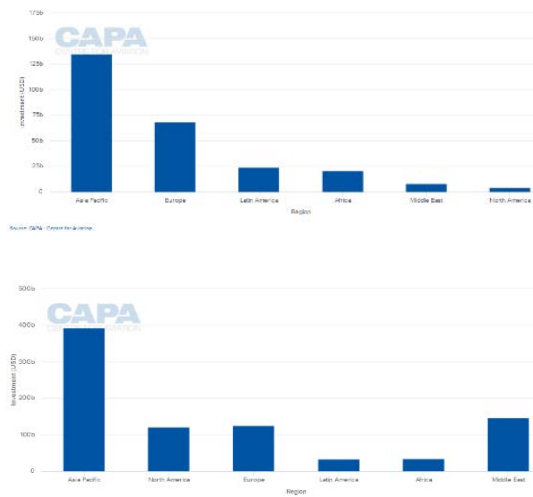


Figure 19 Investments into new airports (top) and existing ones (below) per continent (CAPA)

a financial analysis into the construction of a new regional airport in Ohio (Ohio Airports, 2014), United States, the 700m² terminal building is expected to cost as little as 2% of the total investment costs, at a cost of 1.2 million USD in the most extensive option. Similarly, the expansion of Heathrow Airport Terminal 5 cost 4.2 billion GBP to build, while the addition of a new third runway will cost an estimated 14 billion GBP (Heathrow Airport Limited, 2018).

Cost savings for terminals have become especially important with the rise of terminals for LCC's, referred to as Low Cost Terminals (LCT's) (CAPA, 2018a; International Airport Review, 2017). Although there are many airports fully geared towards low-cost flights in general, such as London Gatwick/Luton/Stansted or Brussels Charleroi, there have also been terminals as part of hub airports designed specifically for LCC's (Hanaoka & Saraswati, 2011). Examples include Piers H and M at Schiphol Airport, Terminal 5 at John F. Kennedy Airport in New York, the 'Budget Terminal' of Changi Airport in Singapore and its current Terminal 4 (The Strait Times, 2017).

In such LCT's, the main point of interest is minimizing taxiing distance (distance between terminal and runway) and passenger walking distance (Hanaoka & Saraswati, 2011). This results in the shortest time spent on the ground and longest time spent in the air: after all, LCC's make profit by increasing the time their fleet is in the air and selecting cheaper airports (Voorde, n.d.). Similarly, LCT's cut costs by offering less passenger facilities, less material quality and often a lowered thermal comfort level (Pleysier, 2018). Higher quality terminals are exactly the opposite: they rely on passengers spending ample amounts of time in the terminal in order to consume (Wendover Productions, 2018). The best example of this is London Heathrow Airport, where passengers spend an average of 2:51 hours in the terminal and net retail revenue per passenger is 13.32 USD. This is thanks to a design that forces passengers to wait in commercial areas, let boarding commence only shortly prior to departure and get as many connecting flights as possible. Unsurprisingly, the thermal comfort levels of Heathrow Airport are of a far higher level, while also following a different plan scheme than low cost terminals.

3.3.3 Airport Design Concepts

An airport complex consist of multiple spaces that cater towards the need of air traffic. Runways and taxiways provide space for planes to land and maneuver, while aprons are used to park, refuel and store aircraft. Passenger or cargo terminals handle the exchange of passengers and goods between planes and the ground. Such main structures are then supported by mainte-

nance hangars, fuel storages, the air traffic control tower, parking lots and any possible offices, hotels or other buildings. The side of an airport before customs checkpoints are referred to as “landside”, while anything after that is referred to as “airside”.

The planning of such all these areas starts at (inter)national scale with a 20-year expected traffic forecasts (people and freight), types of aircraft (large/small, premium or low-cost carriers), destinations (domestic/international), links to (public) transport networks, urban planning and environmental guidelines and expansion opportunities (Neufert & Neufert, 2003). This influences the Runway Design Code (RDC), which determines the level of service for any runway, with small and low-traffic airports having less requirements than bigger ones (FAA Airport Engineering Division, 2014; IATA, n.d.). Topographical and geological conditions are to be investigated, as runways can reach up to 4500m length and all other facilities require considerable space. Such runways need to be aligned with the dominant wind direction to ensure planes can take off or land into the wind. Depending on the RDC, the final Airport Design Criteria (ADC) will be determined, influencing elements ranging from lighting to separation distances.

Areas around airports need to be free of obstructions in a range up to 15km depending on landing systems (Neufert & Neufert, 2003), while buildings need to be at least 150m away from the centerline of any runway. The subsequent 465m will also require buildings to remain below an imaginary 1:7 line starting from 0m at 150m from the runway centerline going up. The air traffic control (ATC) tower is especially important in this respect, as it needs to be high enough to keep a continuous visual connection with all parts of the airport and planes (FAA Airport Engineering Division, 2014).

The layout of airport terminals can afterwards be summed up in two different aspects: the basic terminal configuration and the terminal concept (Poh, 2007). The terminal configuration relates to the relationship between individual terminals, while the terminal concept concerns the basic layout of the terminal.

Currently, there are two main terminal concepts in use: centralized terminals connected to satellites using people mover systems and centralized passenger terminals with attached piers. While in airports with people mover systems the terminals can be fully separated buildings, a centralized terminal will consist of one large whole. The centralized terminals will not require expensive underground or above-ground connections between terminals and allow for more spatial unity, while terminals connected using people movers will be of smaller scale, easier to operate and easier for aircraft to maneuver.

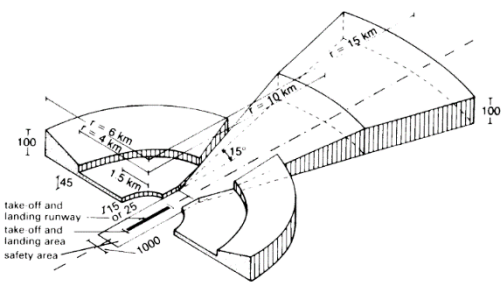


Figure 20 Required clear airspace around airports (Neufert)

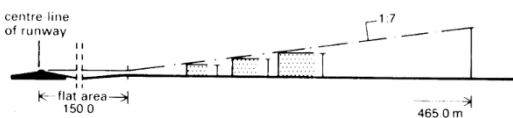


Figure 21 Allowable construction heights besides airports (Neufert)

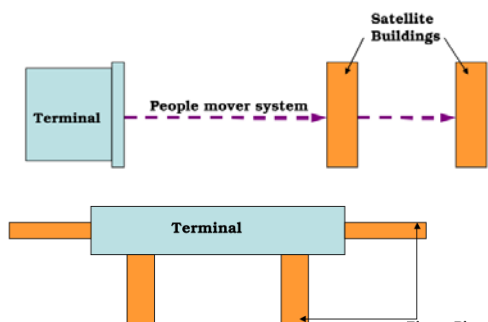


Figure 22 The two basic airport terminal configurations (Poh)

After the basic terminal configuration is chosen, the terminal concept needs to be selected. According to the ICAO there are currently five common topological layouts of a terminal:

- Pier/Finger
- Linear
- Transporter
- Satellite
- Compact Module Unit

Each of the aforementioned terminal concepts cater towards different types of airports and have each a distinct set of advantages and disadvantages. In general, however, operational congestion, passenger and airplane turnaround speeds, expansion possibilities and walking distances are the main reasons for choosing between different terminal concepts.

When looking at hub/premium airports versus low-cost airports, the aforementioned insights allow us to understand why the spatial layout of these two types of airports are different. From a terminal concept point of view, LCT's often avoid expensive transporter systems and keep the amount of terminals limited to only one centralized terminal. Similarly, the terminals themselves are often of a linear or transporter model to keep costs down. A common trait is that a linear or transporter model is used, but transport to the planes is not with jet bridges or buses, but by people walking to the planes themselves.

Within airports, there is a complex flow of passengers through a set of spaces that are carefully designed. This way, both the security as well as fast handling of passengers and luggage is reassured. Firstly, separating the landside zone from the airside zone is of critical importance, as it allows for segregation of screened passengers. Afterwards, there also needs to be a distinction between arriving and departing passengers, although in some airports these still may happen through the same spaces. Both at the landside end as well as the airside end, all flows come together again: departing passengers enter the airplane where arriving passengers came from, while arriving passengers exit to a hall where also departing passengers went through. Depending on the complexity of the airport, such halls can be completely separated, but sometimes also a single one (Neufert & Neufert, 2003).

Departing passengers will often go through a routine of arriving at the airport, checking in, passing customs and security, waiting at waiting lounges with commercial zones finally boarding the airplane. Arriving passengers on the other hand will deplane, go through customs, pick up their bags and exit the airport directly. As arriving passengers spend far less time at the airport and want to get out as soon as possible (Wendover Productions,

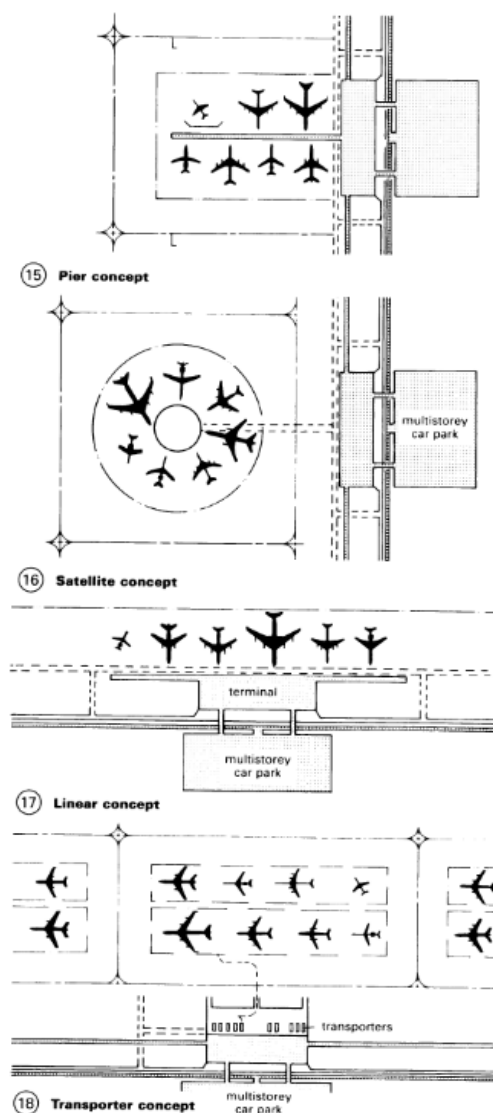


Figure 23 Airport terminal concepts as illustrated by Neufert. Note that the Compact Module Unit is omitted.

	20 mppa	22 mppa	25 mppa
Kerbside to furthest check-in island	195 m	205 m	235 m
Furthest check-in island to nearest gate	265 m	275 m	300 m

Table 2 : Aided Walking Distances

	20 mppa	22 mppa	25 mppa
Furthest check-in island to furthest gate	495 m	515 m	550 m
Furthest gate to gate distance	790 m	840 m	1,000 m

Figure 24 Walking distances for various airport sizes (Poh)

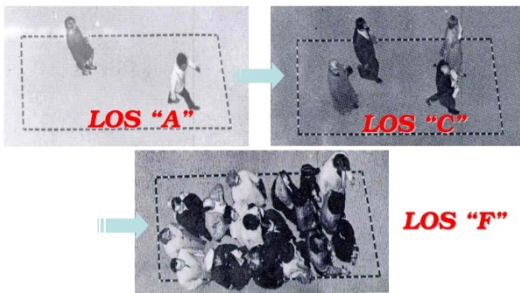


Figure 25 Level of Service explained by Poh

	Level of Service Standards (sq. m per occupant)					
	A	B	C	D	E	F
Check-in queue area	1.8	1.6	1.4	1.2	1.0	-
Wait/circulate	2.7	2.3	1.9	1.5	1.0	-
Hold room	1.4	1.2	1.0	0.8	0.6	-
Bag claim area (excluding claim device)	2.0	1.8	1.6	1.4	1.2	-
Government inspection		1.4	1.2	1.0	0.8	0.6

Figure 26 Level of Service standards for various airport areas (Poh)

2018), the amount of facilities at the arrivals side will be less than at the departures side.

To increase passenger well-being, airport experience and capacity, walking distances and the Level of Service (LOS) are critical. Industry norms as shown in figure 16 show that walking distances should be limited depending on airport size. This concerns both the distance between check-in and boarding, as well as between two gates for transferring passengers. This is why - mathematically speaking- the ideal terminal has a centralized layout with finger piers, with the amount of piers depending being the square root of the amount of gates. Similarly, a practical cap for any terminal is often taken to be around 20-30 mppa (million passengers per annum): nearly all famous airports in the world adhere to the capacity stated by this calculation.

Related to the passenger throughput is the Level of Service at an airport, which determines the density of airport users as well as the amount of throughput and delays for a desired level of quality. For instance, IATA LOS level A will mean there is full free flow without any delays and restriction in user comfort, while LOS F is the worst and has high cross-flows and delays. The LOS applies both for arriving as well as departing passengers and is expressed in available area per user [m²/person]. According to IATA Optimum Waiting Times, these values are in the range of 0.6-2 m²/person depending on the function of the space. Waiting times and IATA LOS standards are given in figures 17 (Poh, IATA). From this it is possible to see that airports have the highest density in security and customs areas, followed by check-in, holding rooms, waiting lounges, and baggage reclamation areas. As mentioned before, Low Cost Terminals adhere to lower level of service than is the case for more premium airports.

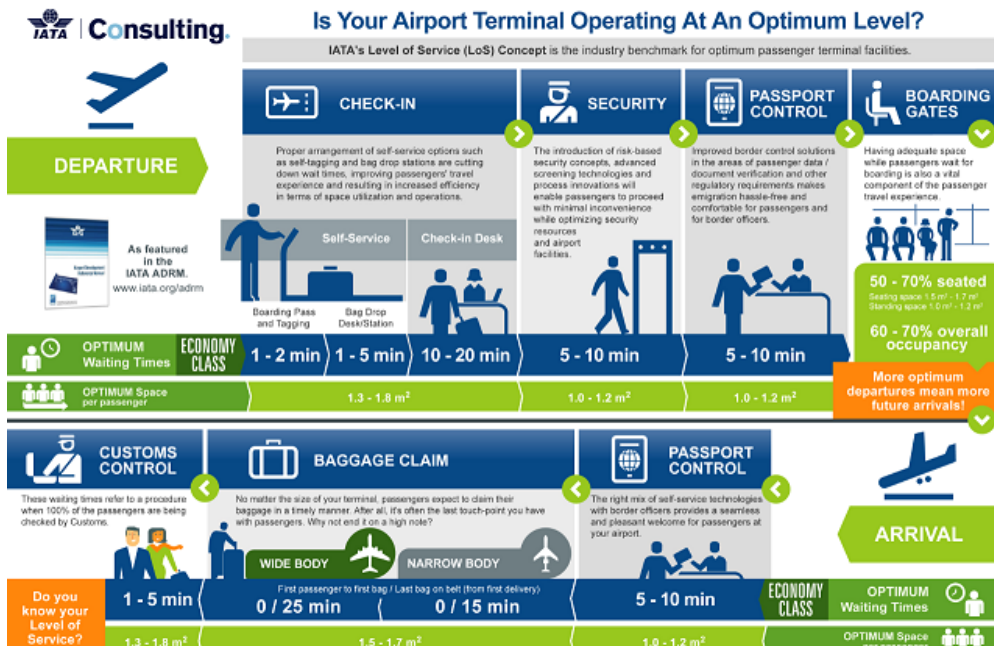


Figure 27 Level of Service with waiting times as explained by IATA Consulting

3.3.4 Airport Energy Consumption

Energy consumption at airports is an important consideration in the OPEX (operational expenditures) of airports and vary greatly depending on the size, climate, airport terminal concept, occupancy, envelope, HVAC systems, maintenance and expected level of thermal quality (Büyükbay, Özdemir, & Üstündağ, 2016). The EPI (Energy Performance Indicator) that is used is either kWh/pax (passenger), kWh/m²a or kWh/m²_{HVACa}; this is different than regular buildings, where kWh/m²a is nearly always the only indicator. As airports handle large amounts of passengers, indicating energy performance per passenger becomes a useful way of gaining insight into the effectiveness of energy spent at an airport. The terminal buildings themselves are the main consumer of energy at airports (Choufani, 2016): 76.6% of all energy goes into the terminal buildings, followed by airfield lighting (6.8%) and radio systems (4.8%).

Correlating the size or amount of passengers directly to the energy consumption of airports is difficult. Not merely because of differences in size, climate, occupancy, terminal concepts, envelope and operating conditions, but also because of differences in terminal quality and levels of expectation. For instance, the largest consumers of energy in a research by CASCADE group (CASCADE, 2012) are London Heathrow, Paris Charles de Gaulle and Frankfurt Airports, each consuming 50% more than average European airports per passenger (~15 kWh/pax) as well as being the largest consumers of energy in absolute terms (Vranes et al., 2012).

When taking into account that these airports offer high levels of quality and attract more premium travel, this could be taken as an explanation. In that case however, Schiphol Airport, which is very similar in terms of size, passenger throughput and climate, stands out as being nearly twice as energy efficient at around 7.6 kWh/pax. Similarly, research by Choufani (2016) also looks into the energy consumption of both less efficient as well as highly efficient airports. However, the total energy consumption seems to be measured differently, becoming incomparable with values from the CASCADE group. Hong Kong Airport and Stavanger Airport are orders of magnitude lower performing than Bergen Airport Terminal 3 and the very energy-consciously designed Galapagos Ecological Airport for instance. A comprehensive list of the energy consumption of airports per passenger and per m² is given in figure 22.

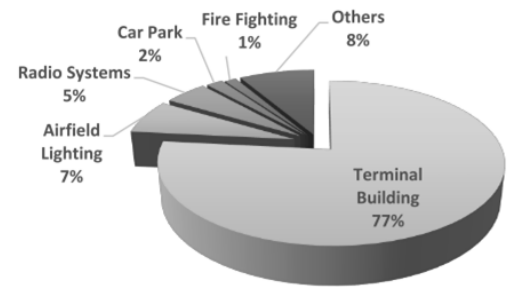


Figure 28 Energy consumption breakdown at Santander Airport (Choufani)

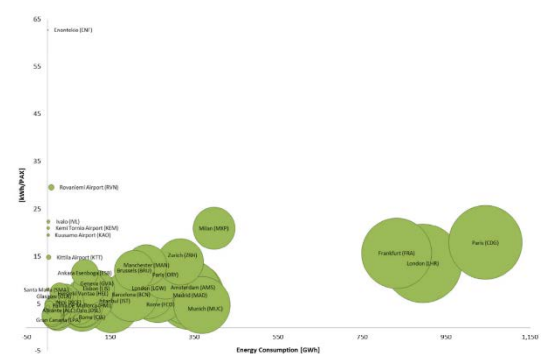


Figure 29 Total energy use (x-axis) plotted against energy use per passenger (y-axis) (CASCADE Research)

Airport	Climate	Terminal Concept	LCT	Passengers '09 [mln]	Total Energy [GWh]	Terminal Area [m2]	Total CO2 [ton]	kWh/pax	kWh/m2	kgCO2/pax	kgCO2/m2
London Heathrow	Cfb		No	66.0	976.0	597,000.0	332,000.0	14.8	1,634.8	5.0	556.1
London Gatwick	Cfb		Yes	32.4	213.8	258,000.0	99,700.0	6.6	828.7	3.1	386.4
London Stansted	Cfb		Yes	20.0	106.1	91,000.0	52,474.0	5.3	1,165.9	2.6	576.6
Paris Charles de Gaulle	Cfb		No	57.9	1,015.0	?	?	17.5	?	?	?
Frankfurt Airport	Cfb		No	50.9	766.1	?	226,100.0	15.0	?	4.4	?
Amsterdam Schiphol	Cfb		No	43.6	331.8	650,000.0	132,000.0	7.6	510.5	3.0	203.1
Eindhoven Airport	Cfb		Yes	1.7	5.8	14,800.0	?	3.4	391.9	?	?
Istanbul Atatürk Airport	Csa		No	29.8	238.1	377,000.0	107,150.0	8.0	631.6	3.6	284.2
Izmir Adnan Menderes	Csa		No	6.2	18.9	295,000.0	6,830.0	3.0	64.1	1.1	23.2
Ankara Esenboga	Csa		No	6.1	95.7	182,000.0	15,460.0	15.7	525.8	2.5	84.9
Zurich Airport	Cfb		No	21.9	305.5	370,000.0	34,326.0	14.0	825.7	1.6	92.8
Hong Kong Airport	Cwa		No	69.7	?	746,000.0	?	4.0	374.0	?	?
Stavanger Airport	Cfb		No	4.5	?	46,000.0	?	3.6	349.0	?	?
Bergen Airport T3	Cfb		No	7.0	?	52,500.0	?	1.1	144.0	?	?
Galapagos Eco Airport	BSh		No	0.5	?	6,027.0	?	1.0	47.0	?	?

Figure 30 Energy consumption and CO₂ generation for various airports based on data from CASCADE Research and Choufani

When looking at the breakdown of the energy consumption of airport terminals, it is also difficult to find a direct correlation in the results available. Again, differences in climate, airport concept, design and level of quality dictate large differences in the contribution of HVAC systems to the total consumption for instance. Research (Alba & Manana, 2016) indicates that HVAC is responsible for 24.5% of Santander airport's consumption, hereby being the largest consumer of energy. They also cite values from other airports, such as Ahmedabad (66%), Izmir Adnan Menderes (80%), Soekarno-Hatta (86%), Tacoma (25%) and Hong Kong (64%). In nearly all cases, lighting comes in at second, together with consumption by ICT systems. Total costs are often not given, and would require further investigation. One indication from Izmir Adnan Menderes Airport (Büyükbay et al., 2016) indicates that 10-15% of all operational expenditure consists of the HVAC system alone.



Figure 31 Energy consumption breakdown between Spanish airports and Hong Kong airport (Choufani)

As HVAC systems and lighting are such a large consumer of energy at terminals, much of the research into reducing consumption has focused on the adjustment of building management systems and using more efficient lighting. According to the Fraunhofer Institute (Klein & Sc, 2015), energy consumption can be reduced in the range of 5-30%, when building management improvements are combined with replacements to the HVAC system. Adaptations to the schedule and operation of the HVAC system on its own will yield an improvement in the range of 1.4-5.93%.

Measures on the HVAC system and improving management include adapting heating and cooling schedules and setback temperatures, overhauling sensors, pumps, fans and generators (Klein & Sc, 2015), adding LED lighting with dimmers and pres-

ence detection (Choufani, 2016; Malik, 2017), doing more detailed thermal camera analyses to detect thermal leaks (Büyükbay et al., 2016), performing energy audits and incorporating energy monitoring and adjustments into management planning and training personnel. However, larger investments with greater payback periods, such as installing PV or solar thermal systems and heat recovery are also mentioned. In any case, improving the energy performance of existing terminals is relatively difficult, while making small yet costly improvements to bad-performing structures, such as implementing a very advanced building management system to a terminal with dated HVAC systems or a bad thermal envelope, will only yield limited energy benefits (C. Alan Short, 2011).

As part of an overarching desire to reduce total CO₂ emissions, the total CO₂ of complete operations and CO₂/pax have also been mapped in recent years by both researchers as well as airports themselves. In 2016, the CORSIA program (Carbon Offsetting and Reduction Scheme) was agreed upon by ICAO members to reduce the emissions by air travel, while many national agreements have forced airports to reduce their emissions. However, a standardized measurement method has not been widely put in scheme yet.

Values from Edinburgh Airport indicate that over 56% of total CO₂ emissions are caused by air traffic movements, with passenger surface access (22%) and utilities (13%) coming in second and third respectively (Vranes et al., 2012). At Schiphol Airport on the other hand, the values of air traffic movements are not incorporated into Schiphol's own CO₂ emissions. In that case, the energy consumed by the airport in gas and fuel amounts to 15% of total emissions, while electricity consumption amounts to 85% of the 103.000t CO₂ in 2017.

Reducing the carbon footprint of airports has been achieved in many airports throughout the world. For instance, in the case of Schiphol airport, the target is to become carbon neutral by using carbon offsetting schemes and reducing emissions to 1.35 kgCO₂/pax by 2020 from today's 1.52 kgCO₂/pax (Schiphol Airport, 2018b). Similarly, Rotterdam The Hague Airport will become carbon neutral in the coming years, while Eindhoven Airport has been carbon neutral since 2012 (Schiphol Airport, 2018a). Important to note, however, is that this neutrality is achieved by financing carbon offsetting schemes elsewhere and reducing emissions caused at the airport. This manifests itself in reducing terminal energy consumption by the aforementioned methods, increasing green mobility of employees and passengers, reducing airplane delays and using more efficient ground equipment.

3.4 Indoor Environmental Quality

3.4.1 Aspects of Indoor Environmental Quality

Indoor Environmental Quality (IEQ) and health of occupants have been important aspects of our built environment ever since mankind has sought shelter. Ample provisions to ventilate a house when a hearth is lit, keeping animals in separate barns/rooms and moving sanitary spaces to outside of the living environment are just some of the simple examples people have done to increase the quality of their interior environment. Already in the first century BC, Vitruvius pointed (Bluyssen, 2009; Vitruvius, 1914) out the importance of arranging cities accordingly:

For when morning breezes blow toward the town at sunrise, if they bring with them mists from marshes and, mingled with the mist, the poisonous breath of the creatures of the marshes to be wafted into the bodies of the inhabitants, they will make the site unhealthy.

Vitruvius, The Ten Books on Architecture



Figure 32 Van Nelle Factory in Rotterdam, with large glazed surfaces for workers to work comfortably (Van Nelle Fabriek)



Figure 33 Amsterdam Open Air School, providing fresh air for the students with open classrooms

It is possible to see that the quality of indoor environments has been judged by both comfort as well as health for a long period of time and has altered the way we have arranged our cities and plan buildings. This *miasmatic approach* (Bluyssen, 2009), based on the idea that unhealthy vapors caused health issues, was the common approach to spread of viruses until the germ theory replaced it. However, exposure to nature and natural environments was and still is today an important aspect of a healthy built environment.

With the advent of the industrial revolution and urbanization in Western Europe, a growing low and middle class formed that had to live in very bad conditions in cities in the 19th century. Concerns on public health dictated new guidelines on sanitation, building ventilation and a desire for natural. Scientific evidence into phenomena such as these were also slowly developing and started their way to enter legislation after the Second World War.

However, a comprehensive view on IEQ, associated factors and scientific research came into existence after the 1960's and was divided into four categories (Bluyssen, 2014):

- Indoor Air Quality (IAQ)
- Thermal comfort
- Acoustic comfort
- Visual comfort

Further research and development in this field, which is a combination of (building) biology, building physics and design, has yielded a comprehensive approach to health in the indoor environment (Bluyssen, 2009). Instead of focusing on individual components and curing mere symptoms, Bluyssen has advocated a wholistic view on healthy indoor environments by looking at all stress factors (stressors) that affect people; health and comfort in buildings are very much linked to each other. The rise of new standards such as WELL, but also BREEAM's HEA criteria and LEED's Indoor Environmental Quality criteria seem to also push for buildings that are not merely energy efficient, but also healthy and comfortable. After all, unhealthy buildings manifest themselves in many ways, including physical complaints (runny noses, coughing, dry eyes, etc.) ("sick building syndrome"), obesity, cardiovascular diseases, lung cancer, chronic respiratory diseases and recently also psychological complaints (depression, lack of concentration, etc.) (Bluyssen, 2018b).

	Thermal comfort	Lighting quality	Acoustical quality	Air quality
Parameters	Temperature (air and radiant) Relative humidity Air velocity Turbulence intensity Activity and clothing	Luminance and illuminance Reflectance(s) Colour temperature and colour index View and daylight Frequencies	Sound level(s) Frequencies Duration Absorption characteristics Sound insulation Reverberation time	Pollution sources and air concentrations Types of pollutants (allergic, irritational, carcinogenic, etc.) Ventilation rate and efficiency
Control	Heating, cooling and air-conditioning systems Design of building (insulation, façade, etc.)	Luminance distribution Integration Artificial and natural lighting Daylight entrance	Acoustical control Passive noise control Active noise control	Source control Ventilation systems Maintenance Air cleaning Activity control
Issues	Dynamic effects Adaptation Integration systems (façade, floor and ceiling) Energy use	Daylight entrance relation to thermal comfort and energy use Health effects and control	Long-term health effects Vibrations and annoyance Degree of annoyance with type of noise	Interpretation and detection Secondary pollution (indoor chemistry and micro-organisms) (Fine) dust Energy use

Figure 34 The four aspects of Indoor Environmental Quality (Bluyssen)

Level	Skin	Eyes	Ears	Nose	Respiratory tract
Discomfort	Warm, cold, sweat, draught	Too much light, too little light, blinding, glare, reflection	Disturbance, hearing and understanding problems	Smell, irritation	Cough; shortness of breath
Systemic effects		Tiredness	Tiredness		Chest pain; wheezing
Allergic or irritant reaction	Contact dermatitis: dry, itchy, red skin	Redness, itching, dry feeling		Runny nose, sneezing, blocked nose	Asthma and bronchitis; hypersensitivity reactions
Infectious diseases	Infection (bacterial, viral or fungal)	Rare: dry-eyes syndrome	Inflammation of the inner ear	Blocked nose, runny nose and stuffy nose; temporary loss of smell	Infection (bacterial, viral or fungal – e.g. bronchitis)
Toxic chronic effects	Radiation-related disorders (such as sunburn)	Damage to the eye by UV light; cataract forming (as a result of long-term infrared light)	Severe and permanent loss of hearing	Permanent loss of smell	Damage and/or tumours

Figure 35 Effects of stressors on parts of our body (Bluyssen)

As humans spend more than 90% of their time indoors, considering indoor environmental quality is not merely about direct threats and discomfort, but the cumulative effect of longer exposure to external stressors as well. Examples include prolonged exposure to carcinogens, pollutants in the air, high noise levels or allergic reactions. Similarly, the exposure over prolonged periods can also influence the state of mind of building users (Parsons, 2014) and, as over 80% of expenditure in offices for instance goes to salaries of employees, improving the health and well-being of workers and reducing sick leave has not

merely a humane, but also an economic aspect to it. Various examples of diseases and disorders are given in figure 26.

In the case of designing for naturally ventilated buildings, aspects regarding indoor air quality and thermal comfort are very important aspects. Therefore, the following section will focus in greater detail on these elements.

3.4.2 Indoor Air Quality

Air quality is expressed in various standards and building codes and concerns the control of pollution sources and ventilating spaces (Bluyssen, 2009). Important is to realize that pollution sources can come from outside, but also from indoor materials, equipment and people. Such pollution can be harmless and cause discomfort, but also become harmful when exposed to for longer periods. Examples of contributors to indoor pollution include outside air pollution (traffic, pollen, dirt), people, polluting activities (smoking, cleaning, cooking), materials and HVAC systems. Pollutants can be either particle-based or gaseous. Particle pollution includes biological particles (fungal, mites, animals, bacteria, pollen), dust particles in various sizes and fibers. Gaseous pollutants include inorganic ones (ozone, CO, CO₂, NO_x) and Volatile Organic Compounds (VOC's) in different ranges.

The basic mathematical description of indoor air quality starts with identifying the production rate of pollutants, the ventilation rate of the space and the (resulting) concentration of pollutants in the space. The resulting concentration of any pollutant is given as:

$$V \cdot \frac{dC_i}{dt} = P_i - \dot{m}_{vent} - \dot{m}_{exfil} - \dot{m}_{decay}$$

In which V=space volume [m³], dC/dt=pollution concentration in indoor air [kg/m³], P_i= production rate of pollutants [kg/s] and m_{vent/exfil/decay} the volume flow rate of air due to ventilation/exfiltration/decay [kg/s].

The efficiency of pollutant removal ventilation is then given as:

$$E_v = \frac{C_e - C_s}{C_i - C_s}$$

Where E_v is the unitless resulting ventilation efficiency, C_e the pollution concentration of the exhaust air, C_s the pollution concentration of the supply air and C_i the pollution concentration inside.

The efficiency of air exchange, showing how well air is distributed in a room, equals:

$$\eta_a = \frac{\tau_n}{2 < \tau >}$$

With τ_n the nominal time constant (shortest time to replace air within the space) [s] and t the mean age of all air particles [s].

Normally, the efficiency will equal to 1 for an ideal displacement ventilation system (piston-type ventilation) and 0.5 for complete mixing. Finally, the nominal time constant of the air is the ratio of room volume to the supplied air volume and equals to the inverse of the commonly used air exchange rate n and will also equal to the mean age of air at the exhaust:

$$\tau_n = \frac{V}{\dot{V}} = \frac{1}{n} = \bar{\tau}_e$$

Where V =space volume [m^3], \dot{V} = volume flow rate [m^3/h], n = ventilation rate [1/h] and t_e = mean age of exhaust air [h].

Generally speaking, the indoor concentration of certain compounds is limited by regulations. For instance, in the case of EN 15251 on indoor environment, the allowable concentration levels are dictated for CO_2 , TVOC's, formaldehyde, ammonia, IARC's and any other odorous materials. Depending on the situation as stated in Annex B, values are followed per person (if people are the only source), per area (if materials are the only source) or combined (in practice). Sometimes values are added, sometimes an in between or highest value is used, which is left up to the user if there are no national decisions. Buildings themselves can be divided into very low polluting, low polluting and non-low polluting buildings. For each building type, there are three categories corresponding to predicted percentage dissatisfied users. For this 3x3 matrix, EN 15251 gives values for minimum airflow per person or per area as illustrated in figures 26-28.

Similarly, BREEAM and LEED also propose values with respect to achieving high indoor air quality. BREEAM HEA 02 criteria for instance include the placement of intakes and exhausts away from pollution sources by more than 20m, incorporating active filtration levels, CO_2 meters and limiting TVOC and VOC concentrations. Similarly, LEEDv4 'Minimum indoor air quality performance' mandates the usage of CO_2 detection, a minimum ventilation are per person and minimum ventilation rates in accordance with ASHRAE standards.

3.4.3 Thermal Comfort

The second important indication in IEQ is thermal comfort and concerns air temperature (T_a), radiation temperature (T_r), relative humidity (RH_a) and air speed (v_a) (Bluyssen, 2009; Parsons, 2014). Additionally, people themselves can adapt by changing their metabolic rate (met) or clothing level (clo). The 'holy grail' with respect to thermal comfort is often accredited to be Fanger's *Thermal Comfort* (1970) (Parsons, 2014). Both before and after Fanger, other thermal models for the human body as

Category	Thermal state of the body as a whole	
	PPD %	Predicted Mean Vote
I	< 6	-0,2 < PMV < + 0,2
II	< 10	-0,5 < PMV < + 0,5
III	< 15	-0,7 < PMV < + 0,7
IV	> 15	PMV<-0,7; or +0,7<PMV

Figure 37 Thermal comfort categories of EN 15251

Category	Expected Percentage Dissatisfied	Airflow per person l/s/pers
I	15	10
II	20	7
III	30	
IV	> 30	< 4

Figure 36 Ventilation rate per person depending on the quality category (EN 15251)

Category	Corresponding CO_2 above outdoors in PPM for energy calculations
I	350
II	500
III	800
IV	< 800

Figure 38 Allowable CO_2 concentration for various levels of PMV (EN 15251)

well as thermal comfort were developed based on either empirical or theoretical research.

However, it was Fanger's research and modelling that was key to a holistic view on thermal comfort by combining the six aforementioned aspects, resulting in a mathematical description of comfort by means of percentages (dis)satisfied for a given set of conditions (Parsons, 2014). As Fanger's comfort model is today still used by EN 15251, ASHRAE Standard 55 and sustainable building codes such as BREEAM or LEED, this model is taken as a base for further elaboration.

According to Fanger, when the aforementioned six values are put in, three conditions on thermal comfort can be determined (Parsons, 2014):

- The body is in heat balance
- Sweat rate is within comfort limits
- Mean skin temperature is within comfort limits

Additionally, an extra criteria is the absence of local thermal discomfort, which will be explained later.

The basic heat balance equation of Fanger describes the heat loss through the skin and respiration with an insulating effect of clothes people wear:

$$H - E_{diff} - E_{sw} - E_{res} - L = K = R + C$$

Where H= metabolic heat production, E_{diff} = heat loss by skin vapor diffusion, E_{sw} = heat loss through sweating, E_{res} = latent respiration heat loss, C_{res} = dry respiration heat loss, K= clothing conduction heat transfer, R=heat transfer through radiation and C= heat transfer through convection.

However, in order to remain comfortable, the sweat rate or vasoconstriction cannot become too high. Therefore, there is a relation between skin temperature and sweat rate depending on the activity level of a person (Rohles and Nevins, 1971). When entered into Fanger's equation, this yields the final comfort equation:

$$\begin{aligned}
 H &= M - W \\
 E_d &= -3.05(5.73 - 0.007(M - W) - P_a) \\
 &\quad (\text{for } t_{sk} = t_{sk,req}) \\
 E_{sw} &= -0.42((M - W) - 58.15) \\
 &\quad (\text{for } E_{sw} = E_{rsw,req}) \\
 E_{re} &= -0.0173M(5.87 - P_a) \\
 L &= -0.0014M(34 - t_a) \\
 R &= 3.96 \cdot 10^{-8} f_{cl}((t_{cl} + 273)^4 - (t_r + 273)^4) \\
 C &= +f_{cl}h_c(t_{cl} - t_a)
 \end{aligned}$$

Where:

$$\begin{aligned}
t_{cl} &= 35.7 + 0.0275(M - W) - 0.155I_{cl}((M - W) \\
&\quad - 3.05(5.73 - 0.007(M - W) - P_a) \\
&\quad - 0.42((M - W) - 58.15) \\
&\quad - 0.0173M(5.87 - P_a) - 0.0014M(34 - t_a) \\
h_c &= \max(2.38(t_{cl} - t_a)^{0.25}, 12.1\sqrt{v}) \\
f_{cl} &= 1.0 + 0.2I_{cl} \text{ for } I_{cl} \leq 0.5 \\
f_{cl} &= 1.05 + 0.1I_{cl} \text{ for } I_{cl} \geq 0.5
\end{aligned}$$

It is important to note that the comfort equation assumes that, when there are a particular set of environmental conditions, people will also wear accordingly. Therefore, all calculations are done with reasonable clothing levels (clo) and activities (met).

However, the thermal comfort equation itself does not provide us with a value that can be used to determine whether (enough) people are comfortable. For instance, ASHRAE Standard 55 dictates that thermal comfort is "that condition of mind which expresses satisfaction with the thermal environment and is assessed by subjective evaluation". To go from the mathematical models of heat balance to thermal comfort, the notions of Predicted Mean Vote (PMV) and Predicted Percentage Dissatisfied (PPD) were introduced. This was based on the thermal load L and was defined by Fanger as "the difference between the internal heat production and the heat loss to the actual environment for a man hypothetically kept at the comfort values of the mean skin temperature and the sweat secretion at the actual activity level."

Generally, thermal comfort is within acceptable limits when people feel either neutral or slightly warm/cold. The PMV is a natural distribution of people's votes on how they feel, with neutral being 0 and hot/cold ranging from -3/+3. The formula is:

$$\begin{aligned}
PMV &= (0.303e^{-0.036M} + 0.028) \cdot ((M - W) - 3.05 \\
&\quad \cdot 10^{-3}(5733 - 6.99(M - W) - P_a) \\
&\quad - 0.42((M - W) - 58.15) - 1.7 \\
&\quad \cdot 10^{-5}M(5867 - P_a) - 0.0014M(34 - t_a) \\
&\quad - 3.96 \cdot 10^{-8}f_{cl}((t_{cl} + 273)^4 - (t_r + 273)^4) \\
&\quad - f_{cl}h_{cl}(t_{cl} - t_a)
\end{aligned}$$

Where:

$$\begin{aligned}
t_{cl} &= 35.7 - 0.028(M - W) - 0.155I_{cl}(3.96 \\
&\quad \cdot 10^{-8}f_{cl}((t_{cl} + 273)^4 - (t_r + 273)^4) \\
&\quad + f_{cl}h_{cl}(t_{cl} - t_a)
\end{aligned}$$

Linked to this formula is the Predicted Percentage Dissatisfied, which gives an indication of how many people will be dissatisfied

with their thermal environment. The PPD is a function of the PMV and is expressed as:

$$PPD = 100 - 95e^{(-0.03353PMV^4 - 0.2179PMV^2)} \text{ [%]}$$

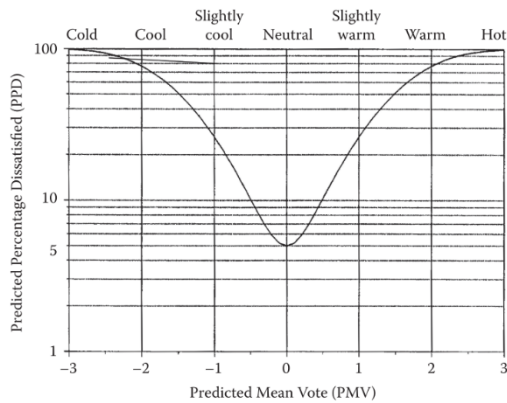


Figure 39 The PMV and PPD relation to how people feel (Parsons)

The resulting table of PPD and PMV in relation to how people feel is given in figure 30. Generally speaking, the level of PPD is dependent on the quality expected from the building. An aim of approximately 80% satisfied is often a mentioned target (ASHRAE), of which 10% is actual PMV (+0.5/-0.5) and 10% for local discomfort, but the final level of quality is left up to the designer. In The Netherlands for instance, the number of hours the PMV is < -0.5 or $> +0.5$ is important and multiplied with a weighting factor. The maximum weighted hours during which PMV is above $+0.5$ or below -0.5 is then limited to 150 annually. The PMV is measured for heights between 0 and 1.8m. It is also important to note that calculations using PMV are generally only valid under the following conditions (Bluyssen, 2009):

- M = metabolic rate between 46-232W/m²
- I_d = thermal resistance of clothing between 0-0.31m²K/W
- T_a = air temperature between 10-30 °C
- T_r = radiant mean temperature between 10-40 °C
- V_a = air velocity between 0-1 m/s
- P_a = partial water vapor pressure between 0-2700Pa
- Resulting PMV is between -2 and +2

As mentioned earlier, there are also other criteria for thermal comfort called 'local thermal comfort' (Bluyssen, 2009; Parsons, 2014). Local thermal comfort is important because, although the whole body may be in comfort, parts of the body may locally be not. Local discomfort consists of draught, vertical air temperature differences, warm/cold floors and radiant asymmetry (NEN, 2005).

Draught is caused by high airspeeds cooling down parts of the body (Bluyssen, 2009). Melikov predicted the dissatisfied percentage when air speed and turbulence intensity is given. The turbulence intensity is determined by:

$$T_u = \frac{\sigma_{v_a}}{v_a} \text{ [%]}$$

Where s_{v_a} is the ratio of standard deviation of air velocity [m/s] and v_a the mean air velocity [m/s].

Afterwards, the percentage of people dissatisfied with draught at neck-level, known as Draught Rating (DR), is expressed as:

$$DR = (34 - t_a)(v_a - 0.05)^{0.62}(3.14 + 0.37T_u v_a) [\%]$$

Where t_a is local air temperature [°C], v_a = local mean air velocity [m/s], T_u =turbulence intensity [%].

Similar to PMV, the DR is only valid under the assumption that people have a thermal sensation close to neutral (PMV~0). Draught is felt less when people have "higher than sedentary activity rates and or people feel warmer than neutral" (Bluyssen, 2009). Also, the draught will be considerably less at arms and feet. Commonly, the turbulence intensity has to be between 30 and 60% for mixed airflow and may be less for displacement ventilation or natural ventilation.

The second aspect of local comfort is vertical air temperature difference between head and ankles. This is commonly taken to be at 0.1m and 1.1m (for sedentary position). The equation that determines the PD (percentage dissatisfied) due to this difference is:

$$PD_{vad} = \frac{100}{1 + e^{(5.76 - 0.856 \cdot \Delta t_{a,v})}} [\%]$$

Where $\Delta t_{a,v}$ = vertical air temperature difference.

However, again, this function is only valid for differences smaller than 8 degrees and for upwards increasing temperatures. Also the air velocity is of great importance in this. Therefore, ISO 7730 contains an additional correction for increase air velocity as shown in figure 31. For sedentary activities in cold conditions, airspeeds above 0.83m/s are often not recommended.

The third local discomfort aspect considers warm or cold floors. For both standing or sedentary activity, the floor temperature determines the PD value according to the formula:

$$PD_{wcv} = 100 - 94e^{(-1.387 + 0.118t_f - 0.0025t_f^2)}$$

Where t_f is the temperature of the floor [°C].

The final local discomfort is labeled as radiant asymmetry. This is generally caused by warm ceilings or cool walls and each type of radiant asymmetry needs to be checked using a separate function. These functions are given as follows:

$$PD_{warm\ ceiling} = \frac{100}{1 + e^{2.84 - 0.174\Delta t_{pr}}} - 5.5 \text{ if } \Delta t_{pr} < 23^\circ\text{C}$$

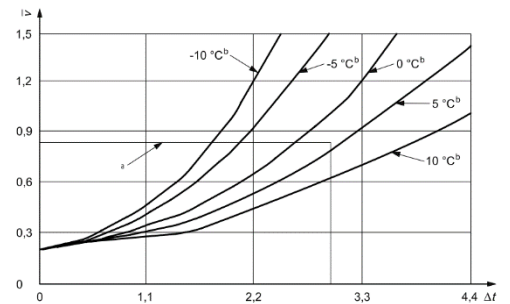


Figure 40 Increase in airspeed required to offset temperature increase (ISO 7730)

$$PD_{cool\ wall} = \frac{100}{1 + e^{6.61 - 0.345\Delta t_{pr}}} \text{ if } \Delta t_{pr} < 15^{\circ}\text{C}$$

$$PD_{cool\ ceiling} = \frac{100}{1 + e^{9.93 - 0.50\Delta t_{pr}}} \text{ if } \Delta t_{pr} < 15^{\circ}\text{C}$$

$$PD_{warm\ wall} = \frac{100}{1 + e^{3.72 - 0.052\Delta t_{pr}}} - 3.5 \text{ if } \Delta t_{pr} < 35^{\circ}\text{C}$$

Where t_{pr} is the plane radiant temperature, the “uniform temperature of an enclosure where the radiance on one side of a small plane element is the same as the radiance in the nonuniform actual environment” (ISO 7726). In this case, it means the radiant difference between to opposing surfaces of an imaginary cube (Parsons, 2014).

The final influential factor in thermal comfort is humidity. Although humidity influences thermal comfort relatively little, it is still an important aspect. The humidity is determined by the amount of water vapor in the air, with absolute humidity being the absolute amount and relative humidity the amount in relation to the amount that can be maximally contained in the air for that temperature:

$$AH = \frac{m_w}{V_a} \left[\frac{g}{m^3} \right]$$

$$RH = 100 \cdot \frac{p(H_2O)}{p^*(H_2O)} [\%]$$

Where AH is the absolute humidity, m_w = mass of water vapor in the air [g], V_a = air volume [m^3], RH= relative humidity, $p(H_2O)$ = partial water vapor pressure in the air [Pa], $p^*(H_2O)$ = saturation water vapor pressure in the air [Pa].

Generally speaking, humidity is ideally between 40 and 60% for indoor environments. Higher humidities are especially an issue at high temperatures and cause microbial growth as well. On the other hand, low humidities (< 15-20%) will cause dryness for eyes air airways (NEN, 2005).

3.4.4 Adaptive Thermal Comfort

As might have been noticed from the aforementioned criteria and formulae, thermal comfort is often considered for closed spaces with sedentary activity for cultures that are mainly accustomed to temperate climates. However, people’s expectations and accustomed conditions vary greatly, especially for those that have become accustomed to outdoor conditions (Brager & de Dear, 2001). People can adapt to their thermal environment by means of behavioral, physiological and psychological changes. Therefore, an important addition to the thermal comfort models of Fanger is de Dear and Brager’s (2002) “Adaptive Thermal Comfort” after initial studies by Auliciems (1981) and Humphreys and Nicol (1970) (Parsons).

The adaptive thermal comfort model focuses on an additional and broader range than is normally predicted by PMV and PPD studies. This also allows for the development of buildings without air conditioning and a greater focus on naturally ventilated buildings. De Dear and Brager identified that in buildings with operable windows and heating settings, people also preferred “a wider range of conditions that more closely reflect outdoor climate patterns” (2002). While in buildings with HVAC control the PMV model was accurate, in naturally ventilated ones the PMV model had only taken into account “half the climatic dependence of comfort temperatures.”

According to the added Adaptive Thermal Model, resulting 90% and 80% acceptability is still predictable by using the following formula (Brager & de Dear, 2001):

$$T_{comf} = 0.31 \cdot T_{a,out} + 17.8 \text{ [}^\circ\text{C]}$$

Where $T_{a,out}$ = mean outdoor temperature [$^\circ\text{C}$].

In order to reach 90% acceptability, the T_{comf} line can be stretched 2.5 degrees up or down from the calculated value, while for 80% acceptability the band can be stretched 3.5 degrees as illustrated in figure 33. Similarly, the thermal comfort ranges can be plotted on the psychrometric chart both for PMV and Adaptive Thermal Comfort models for various parameters using the CBE Thermal Comfort Tool (CBE, 2018).

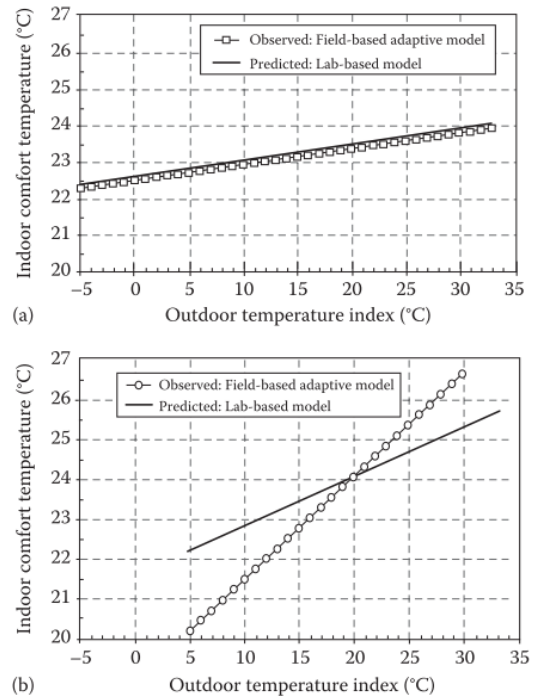


Figure 41 Temperature range for regular air conditioned buildings (PMV) (top) and naturally ventilated ones (adaptive) (bottom) (Parsons)

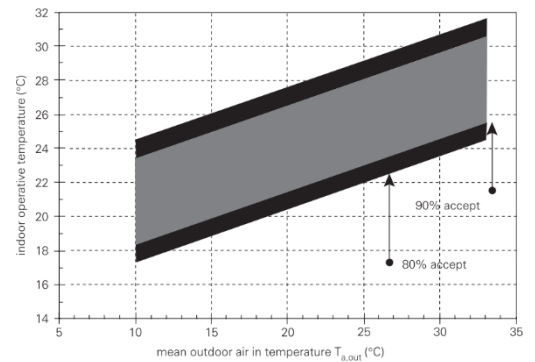


Figure 42 80% and 90% satisfied with the adaptive thermal comfort model (Bluyssen)

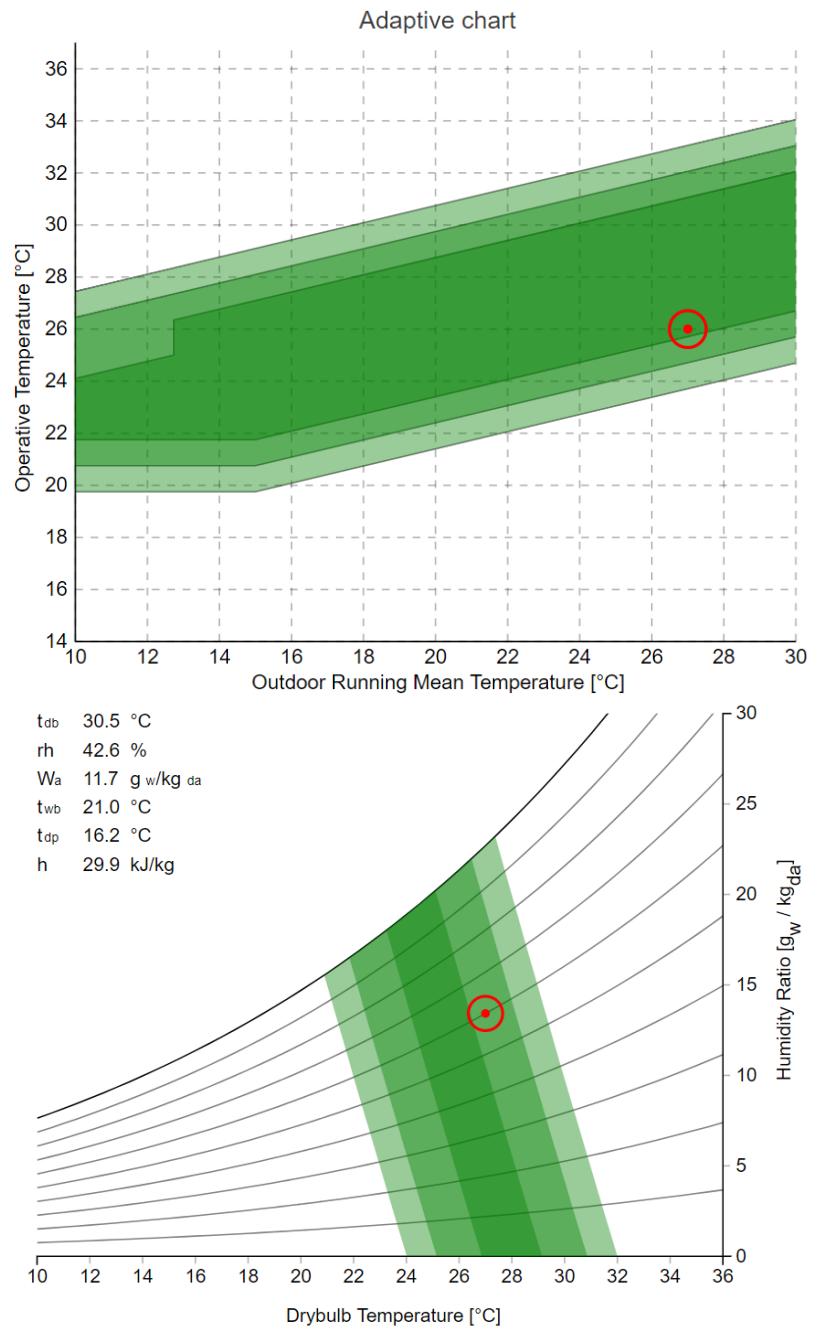


Figure 43 Images from the CBE Thermal Comfort Tool with 27°C T_{air} and 25°C $T_{radiant}$ and $v=0.2m/s$. Note that in the adaptive case (above) we are in category I (better), while in the PMV model (below) we only end up in category II

Part of this adaptation is caused by a change in clothing levels. As clothing is one of the six basic parameters of the thermal comfort equation, it is possible to “relate the total effect of all adaptive behavior to the equivalent effect of adjusting clothing” (Parsons, 2014). This new I_{equiv} will take into account multiple adaptations to be entered into the original PMV equation and is determined by the starting clothing levels and adjusted clothing level as follows:

$$I_{EQUIV} = I_{start} - (I_{ADJ} \cdot I_{start}) \text{ in the heat}$$

$$I_{EQUIV} = I_{start} + (I_{ADJ} \cdot I_{start}) \text{ in the cold}$$

Where I_{ADJ} is given in the table of figure 35.

However, it is important to note that the scope of this definition was for buildings that allowed for occupant control of windows with easy access. Additionally, spaces cannot have a mechanical cooling system (but heating is allowed), but are allowed to have mechanical ventilation with unconditioned air (but windows should still be the primary source of air). Similarly, people should engage in “near sedentary activity (1-1.3 met)”. Similarly, as the data was only validated between 10-33 degrees C (yet measured between 5-33C) outdoor temperature, extrapolation beyond these limits is not suggested.

Studies into comfort conditions in extremely cold or extremely hot temperatures and buildings have been conducted however. For instance Gou, Gamage, Lau, & Lau (2018) have focused on thermal comfort naturally ventilated dormitories in Singapore’s tropical climate. There, they found that the occupants were “exposed to higher operative temperatures than what ASHRAE comfort standards recommended for naturally conditioned spaces” yet still found them acceptable. This was attributed mainly to increased air velocity due to fans, which increased the adaptive thermal comfort range from the expected 5882h (67.1%). The respondents felt comfortable even in the case of air temperatures around 30 °C with 70% RH and wind speeds between 0.2 and 1.5m/s. However, sample size was small and exact outdoor climate data was missing.

Similarly, but now for outdoor conditions, a study was performed in the cold climate of Harbin, China (Chen, Xue, Liu, Gao, & Liu, 2018). They also gave a large overview of research into thermal comfort in outdoor conditions according to various climate zones. The measurements were for a whole year and focused on the thermal sensation experienced by the inhabitants

Adaptive Opportunity	I_{ADJ}
Minimum	0
Low	0.25
Medium	0.5
High	0.75
Maximum	1.0

Figure 44 Adjustment for clothing index in adaptive thermal comfort I_{ADJ} (Parsons)

of the city under outdoor conditions. In Harbin’s cold land climate, reaching between -2.5 and -12.92 °C in winter, the acceptable range was still between 2.5 and 30.9 °C of the PET (physiologically equivalent temperature). A neutral temperature in winter was found to be 18 °C, but wind conditions were left out of the scope of research.

Wind is an important factor in thermal comfort though. For outdoor conditions, NEN 8100 “Wind comfort and wind danger in the built environment” gives information on external wind speeds that are still deemed acceptable.

External wind speeds are dependent on the wind speeds at reference height (60m), area aerodynamic roughness (NPR 6097), buildings and trees and the building design itself. Wind speeds are calculated at 1.75m (v_{LOK}) height and have to be limited to a number of exceedance hours over the threshold speed ($v_{DR,H}$) annually. There are five quality levels ranging from A to E and three activity classes ranging from I to III. Quality level A will yield the lowest exceedance probability while class I activity is walking, II is strolling and III is sitting for longer periods. The chart that depicts the exceedance probability, quality classes and activity levels is given below.

Overschrijdingskans $p(v_{LOK} > v_{DR,H})$ in procenten van het aantal uren per jaar	Kwaliteitsklasse	Activiteiten		
		I. Doorlopen	II. Slenteren	III. Langdurig zitten
< 2,5	A	Goed	Goed	Goed
2,5 – 5	B	Goed	Goed	Matig
5 – 10	C	Goed	Matig	Slecht
10 – 20	D	Matig	Slecht	Slecht
> 20	E	Slecht	Slecht	Slecht

Figure 45 Exceedance hours, quality class and activity levels for the resulting wind comfort levels according to NEN 8100

In general, outdoor airspeeds that are considered to cause hindrance are speeds above 5m/s ($v_{DR,H}$). This means the blowing of hairs and movement of clothes and umbrellas. However, when sitting outdoors at terraces, for instance, speeds should be limited much further to 3m/s (Pleysier, 2018).

3.4.5 Thermal Comfort at Airports

The reason why external thermal comfort is of importance is because airports are often discussed on whether they should be classified as internal, transitory or outdoor spaces (Pleysier, 2018). For instance, in the case of train stations such as Rotterdam Central Station, the conditions could best be described as “outdoor”. On the other hand, Schiphol airport provides levels of comfort identical to other indoor spaces, while at the new Lelystad Airport the building is split into various climate zones, with the entrance plaza and boarding area having more semi-

outdoor conditions compared to the security and waiting areas, which provide for a higher degree of thermal comfort.

Kotopoulos & Nikolopoulou (2016) identified the difficulty of defining the comfort levels of airport terminals. The difference was especially big between passengers and employees, with passengers showing considerably larger possibilities of adaptation compared to employees. Such challenges include:

- Difference in expectation between passengers (transient) and airport employees (stationary)
- Possibility of adaptation in clothing for passengers
- Possibility of changing activity level (seating/standing)
- Difference in exposure times between passengers and employees

Research into the thermal environment at airports is generally limited however, and especially the case for Low Cost Terminals where a lower level of thermal quality can be deemed acceptable (Pleysier, 2018). Kotopoulos & Nikolopoulou (2016) give a brief overview of available research and cite sources that focus mainly on large (hub) terminals in Greece, China, Brazil and India. However, none of the studies focus on adaptive performance and rather investigate the thermal comfort parameters according to PMV or temperature indices.

A similar problem can be seen in guidelines into the thermal environment of airports by the CIBSE and ASHRAE. According to the ASHRAE HVAC Applications Handbook the ideal temperature in airports is between 23 and 26 degrees with humidities varying between 30 to 55% depending on the season. The CIBSE has more detailed temperature charts, including values per terminal are as well as season for a target PMV value of ± 0.5 . This is given in the figure below:

	Summer ^a	Winter ^a	Activity (met)
Operative temperature (°C)			
Baggage reclaim	21–25 ^b	12–19 ^b	1.8
Check-in areas ^c	21–23	18–20	1.4
Concourse (no seats)	21–25 ^b	19–24 ^b	1.8
Customs area	21–23	18–20	1.4
Departure lounge	22–24	19–21	1.3

^a For clothing insulation of 0.65 clo in summer and 1.15 clo in winter.

^b Based on PMV of ± 0.5 . At other cases based on PMV of ± 0.25 .

^c Based on comfort requirements of check-in staff.

Figure 46 Target temperatures for various airport zones according to the CIBSE (Kotopoulos)

3.5 Ventilation

3.5.1 Importance of Ventilation

Ventilation is an important aspect of architecture as already explained in the section on indoor environmental quality, both from a health as well as comfort point of view. Ventilation has been an integral part of architectural design for years and often has formed distinct elements of traditional architecture, which will be elaborated on later.

The advantages of natural ventilation include a greater comfort and satisfaction experienced by the users (Brager & de Dear, 2001) due to adaptive behavior, a better link to nature (Engel & Roaf, 2017), potentially better IAQ (Bluyssen, 2018a), less chance of the sick building syndrome, lower heating or cooling energy thanks to mixed mode possibilities, no fan power and potentially less noise. It is also proven by many sources that allowing for control over windows and ventilation rates is preferred by building users (Brager & de Dear, 2001).

3.5.2 Fluid Mechanics and Ventilation

Ventilation -air movement- is considered to be part of fluid mechanics, as this field encompasses both liquids as well as gases (Nakayama, 1998). Liquids are characterized by their incompressibility and viscosity, the tendency resist sliding over each other. On the other hand, gases will compress easily under relatively large pressures, but if pressure differences are small, that effect may also be neglected. If a fluid is theoretically incompressible and has zero viscosity, it is called an ideal fluid; if a gas adheres to the Boyle's Law, it is called an ideal gas. This means that the relation between pressure, volume, amount of substance and temperature according to the following formula:

$$PV = nRT$$

Where P=pressure [Pa], V= volume [m³], n= amount of substance [mol], R= gas constant, T= temperature [K].

Fluid flows can be either laminar or turbulent or something in between. Laminar flows are flows in which there is minimal momentum convection, meaning the fluid flows "straight". Turbulent flows on the other hand have high convection momentum, causing the flow to be erratic. In the case of a frictionless laminar flow, the mass flow rate entering any control volume has to equal the mass flow rate exiting it, referred to as the equation of continuity. In the case of laminar and frictionless flow, the volume flow rate (flux) will also remain constant).

$$\begin{aligned}\dot{V}_1 &= \dot{V}_2 \\ A_1 v_1 &= A_2 v_2\end{aligned}$$

Where V' = mass flow rate/flux [m^2/s], A = area [m^2] and v = flow speed [m/s].

Similarly, the conservation of energy states that the entering energy should equal the energy exiting a control volume. This means that the sum of all work, potential energy and kinetic energy remains the same, called the Bernoulli equation (Khan Academy, 2018):

$$W_1 + KE_1 + PE_1 = W_2 + KE_2 + PE_2$$
$$P_1 + \frac{1}{2}\rho_1 v_1^2 + \rho_1 g h_1 = P_2 + \frac{1}{2}\rho_2 v_2^2 + \rho_2 g h_2$$

In which W = work done [J], KE = kinetic energy [J], PE = potential energy [J], P = pressure [Pa], ρ = density of the fluid [kg/m^3], v = flow speed [m/s], g = gravitational constant [m/s^2] and h = height [m].

However, it is important to note that this equation only applies to incompressible flows. Also, the simplified form is only used for laminar cases and for fluids that are not viscous.

Viscosity in fluid flows will mean that the fluid is very difficult to get moving due to high internal sliding resistance. This is why in pipes or ducts, the speed of a fluid will be slower towards the encasing, as it encounters more drag resistance there. Once the speed increases past a critical speed, turbulent flows start to occur. The critical speed is determined by the Reynold's number, the viscosity of a material, the pipe diameter and density of the fluid. However, as turbulent flows are ideally avoided and difficult to calculate, it is left outside further scope of this thesis. Similarly, the topic of surface tension, which is caused by the cohesion of molecules in liquids, is left outside the scope of this research.

However, a very important topic that applies to both fluids and gases is the Venturi effect. The Venturi effect is based on Bernoulli's principle, which dictates that the total energy level in a flowing fluid has to remain the same, meaning the flux has to remain the same. This means that in a constriction, the fluid speed will increase and the pressure will drop, causing less pressure on the sides. This can be useful when negative pressure is desired, for instance for extracting air using a Venturi roof that will be explained later.

3.5.3 Ventilation Mechanics

In the case of ventilation, the basic rules of fluid mechanics are adapted and often simplified. The basic principles however, remain the same, with many of ventilation formulas being applicable for laminar flows that are assumed to be incompressible. The basic formula for the pressure difference between entry and exit in a simplified cylindrical volume equals:

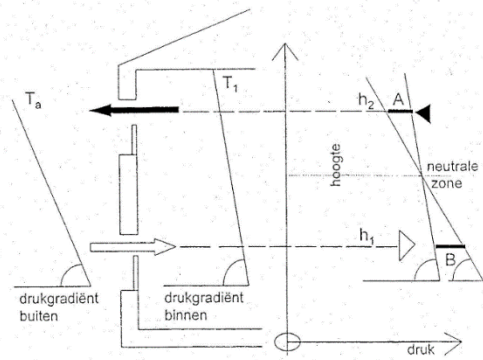


Figure 47 Pressure gradients of imaginary interior and exterior stacks (Cauberg)

$$\Delta P = \frac{1}{2} \zeta_1 \rho v_1^2 + \frac{1}{2} (\zeta_c + \zeta_2) \rho v_2^2 \text{ [Pa]}$$

Where ζ_1 = flow resistance at the inlet, ρ = density [kg/m³], v_1 = flow speed at the inlet [m/s], ζ_c = flow resistance of the construction the flow passes through, ζ_2 = flow resistance at the outlet and v_2 = flow speed at the outlet [m/s].

The resulting volume flow rate (often written as Q) is given by the generic formula:

$$\Delta P = \frac{\dot{V}^2 \rho}{2A^2 C_d^2} \text{ [Pa]} \leftrightarrow \dot{V} = C_d A \sqrt{\frac{2\Delta P}{\rho}} \left[\frac{\text{m}^3}{\text{s}} \right]$$

Where \dot{V} = volume flow rate [m³/s], ρ = density [kg/m³], A = orifice area [m²], C_d = discharge coefficient of the opening and dP = pressure difference [Pa].

An important aspect is the geometric behavior of the openings. Every opening will have its own discharge coefficient, which is dependent on its geometry and Reynolds number. Generally, a discharge coefficient of 0.8 can be assumed for the built environment with purpose-built openings. Additionally, if there are opposing openings, the effective area between them has to be used directly. The effective area of two openings is calculated as follows:

$$\frac{1}{A_e^2} = \left(\frac{1}{A_{in}^2} + \frac{1}{A_{out}^2} \right)$$

$$\frac{1}{A_{in/out}^2} = \frac{1}{\sum_1^x A_{in/out,x}^2}$$

Where $A_{in/out}$ is the calculated sum of inlet/outlet openings [m²].

The pressure difference required to get the air moving can be caused by:

- Buoyancy/Stack effect
- Wind
- Venturi effect

3.5.4 Thermal Buoyancy

Buoyancy of air is also known as the stack effect and is based on the principle that temperature differences cause differences in pressure. Two imaginary air columns of varying temperatures, one inside and one outside, will have different pressures exerted below. The pressure differences within a single column will be

due to a difference in height, while the pressure differences between inside and outside are due to temperature. The pressure at a given height in an isothermal air column is given as:

$$P(h) = P_0 \cdot e^{-\frac{\rho_0}{P_0}gh}$$

Where P_0 = the pressure at the base height [Pa], ρ_0 = air density at base height [kg/m^3], g = gravitational acceleration [m/s^2] and h = height above base height [m].

However, for the relatively low height of buildings, the formula can be linearized to (Caugberg):

$$P_i(h) = P_{i,0} - \frac{P_{0,0}}{RT_i}gh$$

In which case the rate of change can be described as:

$$\frac{dP}{dh} = -\rho g = -\frac{P}{RT}g$$

Where R = gas constant, T_i = interior temperature [K].

As can be seen from the formula, when a stack with temperature T_1 is compared to a stack of temperature T_2 , the density difference as one goes up will also change. The difference between these two stacks for any given height can then be calculated by:

$$(P_1 - P_2)(h) = \Delta P_{1,2}(h) = P_{1,0} - P_{2,0} - \frac{P_{0,0}}{R(T_1 - T_2)}gh$$

$$\Delta P(h) = \frac{P_{0,0}}{R(T_1 - T_2)}gh \text{ (for } P_{1,0} = P_{2,0}\text{)}$$

When looking at the two air columns, it is possible to conclude that the pressure differences below and at the top of the two columns are reversed and that there is a point at which the interior and exterior pressure become equal, called the neutral zone. When inside of a building is warmer than outside, this means air will enter from below and exit from above; when the outside air is warmer, air will enter from above and exit from below. The height of the neutral zone can be calculated using:

$$h_0 = \frac{A_1^2 h_1 + A_2^2 h_2}{A_1^2 + A_2^2}$$

However, the stack formula can be simplified yet again because in most building cases, the pressure difference within the building is small compared to atmospheric pressure. From the Boyle-Gay Lussac law, the pressure and temperature of a gas are then linked to each other by means of:

omgeving	K	a	h _a in m
vrije veld	0,68	0,17	250
landschap met bomen en struiken	0,52	0,20	300
bebouwde omgeving, dorp	0,35	0,25	400
stedelijk centrum	0,21	0,33	500

Figure 48 Values for wind speed calculations of coefficients a and K (Caugberg)

$$\frac{\rho_1}{\rho_2} = \frac{T_2}{T_1}$$

By approximating that T_1 and T_2 and p_1 and p_2 are very close to each other, these values can be entered into the aforementioned formula, resulting in:

$$\Delta P_b = \rho_i g h \frac{\Delta T}{T_a} = (\rho_o - \rho_i) g h$$

Where ρ_i = interior air density [kg/m^3], dT = temperature difference between inside and outside [K], T_o = outside air temperature and ρ_o = outside air pressure [kg/m^3].

The airflow that is caused due to thermal buoyancy is finally given by the following two equations:

$$\Delta P = \frac{\dot{V}^2 \rho}{2A_e^2 C_d^2}$$

$$\dot{V}_b = C_d A_e \sqrt{\frac{2\Delta P}{\rho}} = C_d A_e \sqrt{2gh \frac{P_{0,0}}{\rho R(T_1 - T_2)}} \sim C_d A_e \sqrt{2gh \frac{\Delta T}{T_2}}$$

Where V' = air flow rate [m^3/s], ρ = air density [kg/m^3], A_e = equivalent area [m^2], C_d = opening discharge coefficient, $P_{0,0}$ = air pressure at base height [Pa], T_1 = outlet air temperature [K], T_2 = inlet air temperature [K].

3.5.5 Wind

Besides buoyancy, wind is the second important driving factor for air pressure. Wind speeds will vary depending on height and will be zero at ground level and increase as an exponential function until a boundary height is reached, after which the air will remain at constant speed. The wind speeds under the boundary layer are influenced by terrain roughness, which depends on the amount of buildings, trees etc. at ground level. Windspeeds until the boundary layer can be calculated using:

$$v_h = v_{ref} \left(\frac{h}{h_{ref}} \right)^a$$

$$v_h = v_0 K h^a$$

Where v_h = wind speed at height h [m/s], v_{ref} = reference wind-speed [m/s], h_{ref} = reference height [m], a = exponential factor, v_0 = wind speed at zero height [m/s], K = coefficient.

The reference speed is often defined as the wind speed at 10m height (Caugberg), but is sometimes also given at 60m. Additionally, wind speeds at roof height of the imaginary (to-be-built) building can also be taken. A wind rose for any given location, showing the frequency of wind speeds for any given direction,

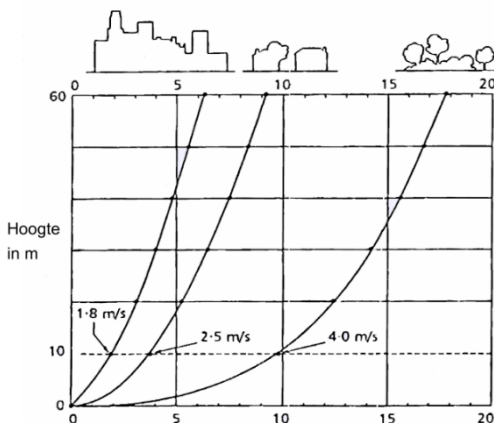


Figure 49 Wind speed profiles depending on surroundings (Caugberg)

are useful in determining the most critical directions and can - for The Netherlands- be generated using NPR 6097. The resulting wind pressure on any geometry can then be given as:

$$P_{wind} = C_p \frac{\rho v^2}{2}$$

Where C_p = pressure coefficient, ρ = air density [kg/m³], v = air-speed [m/s].

The important factor here is that the C_p value will depend on geometry and on the location of the geometry. For basic shapes, C_p values are given in norms and are very difficult to find analytically. In all cases, the side at which wind hits (luff side) will have positive C_p values (hence, positive or overpressure), while the side at which it doesn't will have negative or under pressure. The resulting airflow due to wind will then become:

$$\dot{V}_w = C_d A_e v_r \sqrt{\Delta C_p}$$

With V' = volume flow rate [m³/s], C_d = opening discharge coefficient, A_e = effective opening area, v_r = airspeed, ΔC_p = difference between supply and removal side C_p values.

3.5.6 Venturi Effect

Finally, the Venturi effect can be used to generate pressure differences. As stated earlier, the Venturi effect is caused by Bernoulli's law, which states that pressure decreases as speed increases when a fluid flow is constricted. The resulting pressure difference can be calculated using the following formula:

$$\Delta P = \frac{1}{2} \rho v_1^2 \left(\left(\frac{A_1}{A_2} \right)^2 - 1 \right)$$

Where ρ = air density [kg/m³], v_1 = supply airspeed [m/s], $A_{1/2}$ = supply/removal areas.

An interesting case is when wind and thermal buoyancy are present together, as is most likely to occur in real life. The total pressure difference and resulting flow rate depends on the situation that is considered. For a single room with a ventilation opening on two sides, the total pressure difference will be due to wind and buoyancy combined. The formula then becomes:

$$\dot{V}_{b+w} = C_d A_e \sqrt{\frac{2\Delta P_{b+w}}{\rho}} = C_d A_e \sqrt{\left| 2gh \frac{\Delta T}{T_o} - \Delta C_p v^2 \right|}$$

Meaning it follows the basic principle outlined by Cauberg:

$$\dot{V}_{b+w} = \sqrt{\dot{V}_b^2 + \dot{V}_w^2}$$

Where V'_b = air flux thanks to buoyancy [m^3/s] and V'_w = air flux thanks to the wind [m^3/s].

3.5.7 Internal Obstacles and Duct Resistance

The above equations are meant for single-room models without internal obstacles. However, partitions, large objects and furniture could all pose potential blockages in the expected airflow pattern (Chu & Chiang, 2013). Recalling the original airflow formula, this internal resistance was expressed in the factor ζ_c :

$$\Delta P = \frac{1}{2} \zeta_i \rho v_i^2 + \frac{1}{2} (\zeta_c + \zeta_o) \rho v_a^2$$

Chu and Chiang found out that external pressures that drive the ventilation will remain the same regardless of resistance inside, meaning that external wind speeds, building sizes and opening configurations do not influence the internal resistance factor. If supply openings are smaller than 3% of the façade area, referred to as porosity, the internal resistance can even be neglected as ζ_o will be far greater than ζ_c . Similarly, if the internal resistance, called blockage ratio, is smaller than 30% (meaning the obstacle is not bigger than 30% of the cross-section through which the air is flowing), the reduction on total airflow will be below 5% and can also be neglected.

The resistance factor for large objects is determined as a function of internal blockage ratio and location and was empirically deducted from CFD simulations. The values are given in figure

The internal resistance that air encounters will be especially important in multi-zone airflows, in ducts and for various-shaped openings. When air flows through multiple zones, the air will encounter a resistance at each boundary between internal spaces as mentioned before. The airflow rate through an opening with known capacity of the resistances is:

$$\dot{V} = C_w (\Delta P)^{\frac{1}{n}}$$

Where C_w = capacity of the openings and n = flow number (1 for laminar and 2 for turbulent).

For many types of ventilation apertures, C_w values will be given by the manufacturer. Similar to how electric resistances are calculated, the resistance between the spaces can therefore be calculated to determine the total airflow.

Resistances are also important in airflow through ducts. The capacity of a duct is given by its cross-section, length, duct resistance and resistance of other internal elements:

$$C = \frac{A \sqrt{\frac{2}{\rho}}}{1 + \sqrt{\frac{\lambda}{D} \cdot l + \sum \zeta_i}}$$

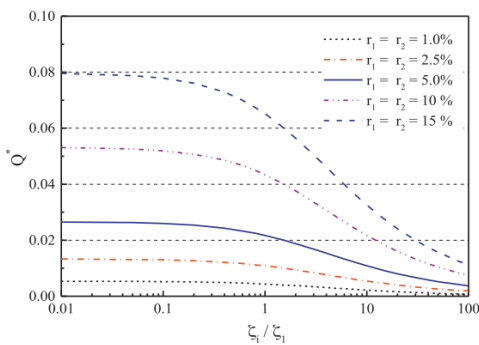


Figure 50 Research by Chu and Chiang showing the effect of internal blockage on total airflow. The different linetypes r_1 etc. represent facade porosity, or the relative size of the supply opening in the facade.

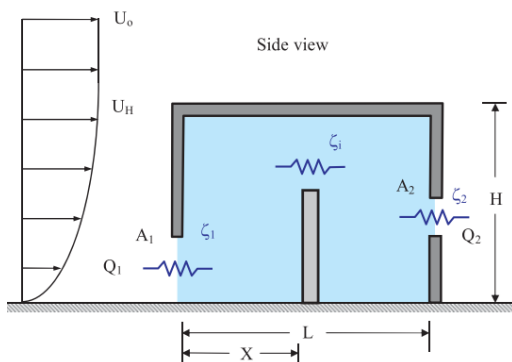


Figure 51 Diagram of Chu and Chiang's experimental model

Where A= duct cross-sectional area [m²], ρ= density [kg/m³], lambda= wall friction coefficient, l= duct length [m], D= hydraulic diameter (4x Area/Circumference), s_i= resistance of any additional element i (turns, grilles etc.).

Similarly, the capacity of an opening is given as:

$$C = A\mu \sqrt{\frac{2}{\rho}}$$

Where A= net opening of a cross-section [m²], m= contraction coefficient, ρ= air density [kg/m³].

Values for these factors are given in common HVAC books and are also included in the following page.

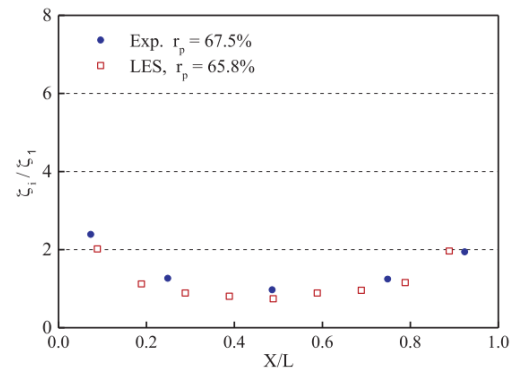
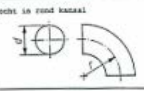
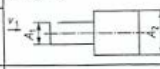
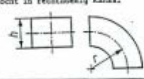
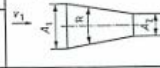
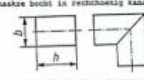
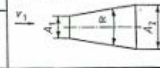
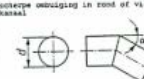
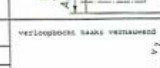
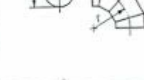
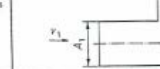


Figure 52 Resistance factor for large plates plotted (y-axis) against their relative location from the supply/removal side (Chu and Chiang)

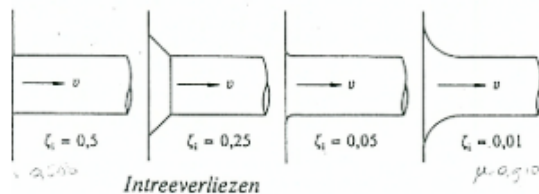
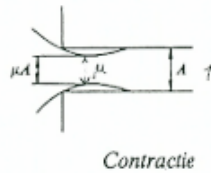
	r/d	f	verlooptoets haaks verwijdend	A_2/A_1	t.o.v. γ
	0,5 0,75 1,0 1,5 2,0	1,0 0,5 0,35 0,25 0,20		0,8 0,6 0,5 0,4 0,3	0,04 0,14 0,24 0,34 0,44
	r/d	f	verlooptoets omhoog verwijdend	μ	t.o.v. γ
	0,5 0,75 1,0 1,5 2,0	1,0 0,5 0,35 0,25 0,20		0,8 0,6 0,5 0,4 0,3	0,02 0,07 0,12 0,17 0,22
	h/b	f	verlooptoets omhoog verwijdend	μ	t.o.v. γ
	0,25 0,5 1,0 2,0	2,1 1,7 1,2 0,4		0,8 0,6 0,5 0,4	0,17 0,28 0,40 0,59
	μ	f rond f vierkant	verlooptoets haaks verwijdend	A_2/A_1	t.o.v. γ
	10° 30° 45° 60° 90°	0,1 0,2 0,3 0,4 0,5		0,2 0,4 0,6 0,8 1,0	0,04 0,14 0,24 0,34 0,44
	r/d	Aantal opgevoeren 1 2 3	verlooptoets haaks vernauwend	A_2/A_1	t.o.v. γ
	1,0 1,5 2,0 3,0 4,0	0,5 0,4 0,35 0,3 0,25		0,2 0,4 0,6 0,8 1,0	0,02 0,07 0,12 0,17 0,22
	A_2/A_1	t.o.v. γ	kap	f	
	0,75 0,5 0,25 0,2	0,5 0,3 0,2 0,1			1,1

waarden voor de weerstandsfactor $\zeta [-]$	
bocht	0,5
scherpe toevoeropening	0,5
rooster voor kanaal	1,0
kap	1,5
waarden voor de wandwrijvingscoëfficiënt $\lambda [-]$	
glad kanaal (metaal, PVC)	0,035
ruw kanaal (gemetseld)	0,045
waarden voor coëfficiënt $n [-]$	
grote openingen	2,0
spleten, kieren en naden	1,5
poreus materiaal met aansluitnaden	1,33
poreus materiaal	1,0
waarden voor weerstandcoëfficiënt $C [m^3/h]$	
grote openingen (per cm^2 opening)	0,30 (n = 2)
goed sluitend raam (per m kierlengte)	0,43 (n = 1,5)
redelijke sluitend raam (per m kierlengte)	1,15 (n = 1,5)
slecht sluitend raam (per m kierlengte)	3,9 (n = 1,5)
deur met tochtstrip (per m kierlengte)	4,3 (n = 1,5)
deur zonder tochtstrip (per m kierlengte)	5,3 (n = 1,5)
naden tussen kozijn / gevel (per m kierlengte)	1,4 (n = 1,5)
buitengevel (per m2 geveleppervlak)	0,14 (n = 1)

Intreeverliezen (ζ_i)

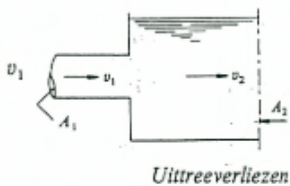
ζ_i wordt bepaald door de afronding. Er treedt bij binnenstromen *contractie* op.

De *contractie-coëfficiënt* is $\mu = \frac{1}{1 + \sqrt{\zeta_i}}$,
dus $\zeta_i = \left(\frac{1}{\mu} - 1\right)^2$



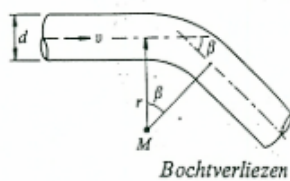
Uitreeverliezen (ζ_u)

$\zeta_u = \left(1 - \frac{A_1}{A_2}\right)^2$ betrokken op v_1
 $h_v = \zeta_u \frac{v_1^2}{2g}$



Bochtverliezen (ζ_b)

ζ_b is een functie van de bocht-hoek β en de waarde r/d , zie tabel A (volgens Hütte).

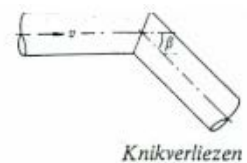


Tabel A. ζ_b -waarden voor bochten bij verschillende β -waarden

β	15°	22,5°	30°	45°	60°	90°
r						
d	0,03	0,045	0,085	0,14	0,19	0,21
$2d$	0,03	0,045	0,060	0,09	0,12	0,14
$4d$	0,03	0,045	0,055	0,08	0,10	0,11
$6d$	0,03	0,045	0,050	0,075	0,09	0,09
$10d$	0,03	0,045	0,045	0,07	0,07	0,11

Knikverliezen (ζ_k)

Tabel B geeft waarden van ζ_k afhankelijk van de waarde van β (volgens Hütte).

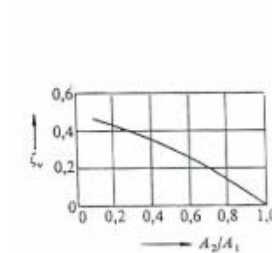
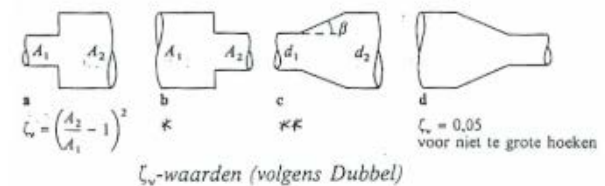


Tabel B. ζ_k -waarden voor knikken bij verschillende β -waarden

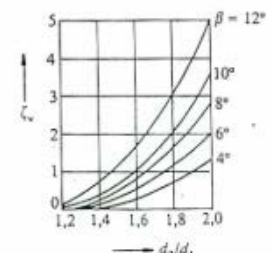
	10°	15°	22,5°	30°	45°	60°	90°
glad	0,034	0,042	0,066	0,130	0,236	0,471	1,129
ruw	0,044	0,062	0,154	0,165	0,320	0,684	1,265

Verliezen t.g.v. vernauwing en verwijding (ζ_v)

De verliezen worden gegeven voor de uitgangssnelheid v_2 .



Figuur * ζ_v -waarden voor geval b



Figuur ** ζ_v -waarden voor geval c

Ducts are often used in conjunction with fans to overcome drag and ensure a steady supply rate. As stated before, the pressure in a horizontal duct equals the kinetic energy (Pren-dergast, van den Engel):

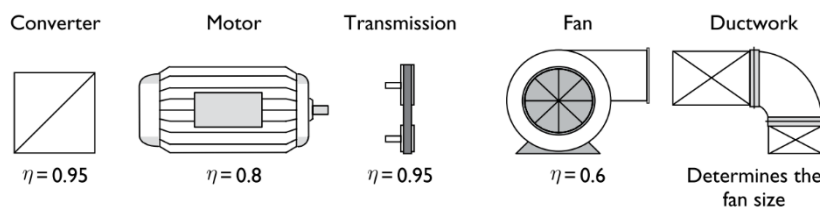
$$P = \frac{1}{2} \rho v^2$$

The energy consumption of a fan is linearly scaled with the pressure it provides (engineeringtoolbox):

$$P_{fan} = \frac{\Delta P \cdot \dot{V}}{\eta} [W]$$

Where ΔP = pressure difference caused by the fan [Pa], \dot{V} = volume flow rate [m^3/s] and η = efficiency [%].

Therefore, using low pressure fans, meaning larger ducts and lower speeds, is very beneficial for the total energy consumption. The chart below gives the typical efficiency of various HVAC components and the energy consumption for moving $1 m^3$ of air for typical as well as energy efficient systems:



Use of ventilated room	Typical systems ($Wh m^{-3}$)	Energy-efficient systems ($Wh m^{-3}$)
Dwelling	0.42	0.17
Office and meeting rooms	0.56	0.35
Shop	0.35	0.22
Shopping center	0.90	0.56
Classroom, auditorium	0.35	0.22
Hospital room	0.35	0.22
Hotel room	0.56	0.35
Restaurant	0.35	0.22
Professional kitchen	0.42	0.28
Workshop	0.35	0.22
Toilets	0.14	0.08
Couloirs, archives	0.28	0.17
Garage (private)	0.14	0.0 ^a
Garage (public)	0.28	0.0 ^a
Computer room (exhaust air only)	0.14	0.08

^a Natural ventilation.

Figure 53 Efficiency of various HVAC components and typical energy consumption values for moving air (Awbi)

3.5.8 Ventilation Integration

The integration of ventilation into the architectural design has arguably been since the first man-made enclosures for living in. Primitive huts of the stone age for instance incorporated openings on top to act as a chimney for hearths, while even today nomadic tribes from all around the globe still have huts that incorporate ventilation provisions. Even today, the idea of a chimney is associated with European housing quintessentially. In the following section, a short overview will be provided of the integration of ventilation into architectural design and the challenges associated with this integration.

Natural ventilation can occur through different architectural elements and can either enter the space directly, or through an intermediate space (Engel & Roaf, 2017). Direct natural ventilation access is provided by openable windows or ventilation grills and are integrated into the façade where direct access to fresh air is possible. Indirect access is also possible, such as through lightwells, atria and glasshouses, where air can be pre-heated or cooled, (de)humidified and slowed down. Similarly, the outside obstructions can be used to slow down wind speeds and increase comfort, such as the case with *hagen* in The Netherlands. Chimneys and ventilation towers, but also ground ducts are elements that can be used to supply or remove air.

Using natural ventilation has, however, particular design challenges (C A Short & Cook, 2015). This includes the need for large openings, adequate sound insulation, blocking out the possible negative effects of wind or backflows, controllability and possible discomfort in very hot or cold conditions. In the following section, where ventilation strategies will be discussed for various climate zones, such challenges will also be mentioned alongside examples from traditional architecture.

In temperate climates, the challenge for natural ventilation is twofold; both for hot as well as cold periods. It is critical to ventilate the building only to minimum levels when it is cold, and maximally when it is too warm (Engel & Roaf, 2017). Night cooling can help in cooling down the building for the next day. Often, heating the building will be more problematic, which is why air should be pre-heated using ground ducts, greenhouses, atria and supplied at sufficient height (1.8m in Dutch standards for instance) to allow for sufficient mixing with indoor air. Air can then be extracted through regular openings, but also chimneys. Especially in European architecture, the chimney has gained an extremely important role for the final architectural expression of the building. The same applies for cold climates, but with less risk of overheating.



Figure 54 Mongolian Ger's/Turkish Yurts with distinct central openings for ventilation (Suntimeyurts)



Figure 55 Distinct chimneys in this 15th century English housing (Homebuildingrenovation)



Figure 57 Wind catchers in Yazd, Iran



Figure 56 Chimneys of the kitchens of Topkapı Palace, Istanbul, by Mimar Sinan (Wikimapia)

In hot climates on the other hand, the strategy is to create large amounts of airflow consistently. If the region is dry, night cooling can be used to cool down the building for the next day. Dry regions also work well with evaporative cooling, which is why many Middle Eastern buildings will feature a combination of wind catchers (*malqaf*) with ponds to precool the air. Similarly, such buildings will often have many porous openings that allow for cross-ventilation, such as through *mashrabiya*'s.

As Short argues, after the late 19th century knowledge on natural ventilation was lost in the Western world. In the 1960's, ventilation grills were made mandatory in The Netherlands to provide sufficient fresh air, while from the 80's onward mechanical extraction systems with natural supply became standard (Prendergast, van den Engel). Fully mechanical ventilation systems started to become more popular as well, especially for commercial buildings. In general, any system that has natural supply falls into the category of naturally ventilated buildings, regardless of the fact if it has mechanical exhaust or not.

3.5.9 Case Study Designs

A common problem in many traditional buildings with natural ventilation is that a systematic way of calculating and documenting the performance is absent. In that respect, naturally ventilated theater designs by Alan Short are one of the best documented designs that are naturally ventilated. Therefore, one example from his theatres will be taken as an example for further investigation. While Short's design is in the temperate climate of Manchester, a second example will be a design in the hot sub-tropic climate of Zimbabwe by Mick Pearce.

Climate data for Manchester, NH													[hide]
Month	Jan	Feb	Mar	Apr	May	Jun	Jul	Aug	Sep	Oct	Nov	Dec	Year
Record high °F (°C)	69 (21)	63 (17)	69 (32)	94 (34)	97 (36)	100 (38)	103 (39)	100 (38)	100 (38)	87 (31)	75 (24)	74 (23)	103 (39)
Average high °F (°C)	33.1 (0.6)	36.9 (2.7)	44.9 (7.2)	57.6 (14.2)	68.7 (20.4)	77.5 (25.3)	82.4 (28)	81.0 (27.2)	72.6 (22.6)	61.0 (16.1)	49.8 (9.9)	38.2 (3.4)	58.6 (14.8)
Daily mean °F (°C)	24.4 (-4.2)	28.0 (-2.2)	36.0 (2.2)	47.3 (8.5)	58.1 (14.5)	67.0 (19.4)	72.5 (22.5)	71.0 (21.7)	62.6 (17)	50.8 (10.4)	41.5 (5.3)	30.4 (-0.9)	49.1 (9.5)
Average low °F (°C)	15.7 (-9.1)	19.0 (-7.2)	27.2 (-2.7)	37.0 (2.8)	47.5 (8.6)	56.6 (13.7)	62.7 (17.1)	60.9 (16.1)	52.5 (11.4)	40.6 (4.8)	33.1 (0.6)	22.5 (-5.3)	39.6 (4.2)
Record low °F (°C)	-17 (-27)	-20 (-29)	-10 (-23)	13 (-11)	25 (-4)	38 (3)	46 (8)	41 (5)	28 (-2)	19 (-7)	11 (-12)	-15 (-26)	-20 (-29)
Precipitation inches (mm)	3.02 (76.7)	2.78 (70.6)	4.33 (110)	3.86 (98)	4.05 (102.9)	3.79 (96.3)	3.80 (96.5)	3.63 (92.2)	3.81 (96.8)	4.16 (105.7)	4.07 (103.4)	3.28 (83.3)	44.58 (1,132.3)
Snowfall inches (cm)	14.4 (36.6)	10.5 (26.7)	6.0 (15.2)	2.5 (6.4)	0 (0)	0 (0)	0 (0)	0 (0)	0 (0)	0 (0)	1.9 (4.8)	11.4 (29)	46.7 (118.6)
Avg. precipitation days (≥ 0.01 in)	9.8	8.0	9.7	11.2	11.0	11.1	10.3	10.0	9.9	9.4	10.6	9.5	120.5
Avg. snowy days (≥ 0.1 in)	5.2	4.1	2.5	0.7	0	0	0	0	0	0	1.1	3.7	17.3

Climate data for Harare (1961–1990, extremes 1897–present)													[hide]
Month	Jan	Feb	Mar	Apr	May	Jun	Jul	Aug	Sep	Oct	Nov	Dec	Year
Record high °C (°F)	33.9 (93.0)	35.0 (95.0)	32.3 (90.1)	32.0 (89.6)	30.0 (86.0)	27.7 (81.9)	28.8 (83.8)	31.0 (87.8)	35.0 (95.0)	36.7 (98.1)	35.3 (95.5)	33.5 (92.3)	36.7 (98.1)
Average high °C (°F)	26.2 (79.2)	26.0 (78.8)	26.2 (79.2)	25.6 (78.1)	23.8 (74.8)	21.8 (71.2)	21.6 (70.9)	24.1 (75.4)	28.4 (83.1)	28.8 (83.8)	27.6 (81.7)	26.3 (79.3)	25.5 (77.9)
Daily mean °C (°F)	21.0 (69.8)	20.7 (69.3)	20.3 (68.5)	18.8 (65.8)	16.1 (61.0)	13.7 (56.7)	13.4 (56.1)	15.5 (59.9)	18.6 (65.5)	20.8 (69.4)	21.2 (70.2)	20.9 (69.6)	18.4 (65.1)
Average low °C (°F)	15.8 (60.4)	15.7 (60.3)	14.5 (58.1)	12.5 (54.5)	9.3 (48.7)	6.8 (44.2)	6.5 (43.7)	8.5 (47.3)	11.7 (53.1)	14.5 (58.1)	15.5 (59.9)	15.8 (60.4)	12.3 (54.1)
Record low °C (°F)	9.6 (49.3)	8.0 (46.4)	7.5 (45.5)	4.7 (40.5)	2.8 (37.0)	0.1 (32.2)	0.1 (32.2)	1.1 (34.0)	4.1 (39.4)	5.1 (41.2)	6.1 (43.0)	10.0 (50.0)	0.1 (32.2)
Average precipitation mm (inches)	190.8 (7.51)	176.3 (6.94)	99.1 (3.90)	37.2 (1.46)	7.4 (0.29)	1.8 (0.07)	2.3 (0.09)	2.9 (0.11)	6.5 (0.26)	40.4 (1.59)	93.2 (3.67)	182.7 (7.19)	840.6 (33.09)
Average precipitation days	17	14	10	5	2	1	0	1	1	5	10	16	82
Average relative humidity (%)	76	77	72	67	62	60	55	50	45	48	63	73	62
Mean monthly sunshine hours	217.0	190.4	232.5	249.0	269.7	264.0	279.0	300.7	294.0	285.2	231.0	198.4	3,010.9
Mean daily sunshine hours	7.0	6.8	7.5	8.3	8.7	8.8	9.0	9.7	9.8	9.2	7.7	6.4	8.2

Figure 58 Climate data of Manchester (top) and Harare (below) (Wikipedia)

The Contact Theater for the University of Manchester was one of the designs that drew from lessons learnt earlier from the auditoria of the Queens Building (C A Short & Cook, 2015). The theater operates mainly by buoyancy ventilation assisted by wind and fans. The 390m² theater allows for 386 occupants for prolonged periods of time (7 hours).

Air enters the theater from below the seating area through four compartments with dampers. The air is pre-cooled by means of a concrete labyrinth as well as concrete blocks and heating elements are placed under each seating platform. Air flows upward into five stacks that each have H-pots to generate a favorable C_p value for any wind direction. The size of each opening equals 4m², while racks are suspended beneath the towers to catch rain from entering inside.

The theatre is able to handle a heat load of 100kW, of which 40kW is from the occupants and 60kW from theater lighting. The inlet area of 12m² is slightly less than the outlet area of 20m², with the total inlet and outlet area per person for both this design as well as others given in figure 62. The stack pressure difference of 2.13Pa would theoretically allow for a maximum airflow of 15.2m³/s. However, in reality, such values are of course not attained due to internal resistance and heating time of the interior. Short indicates that temperatures in the auditorium with fans running minimally was no higher than 22 °C, while the design differential of 3 degrees was attained nearly everywhere without any fans.

From Short's other theater designs, a basic extrapolation is performed to see the required inlet and outlet area for the ventilated theatres and the theoretical maximum resulting airflow for the five stack pressures.



Figure 59 Contact Theater (contactmcr)

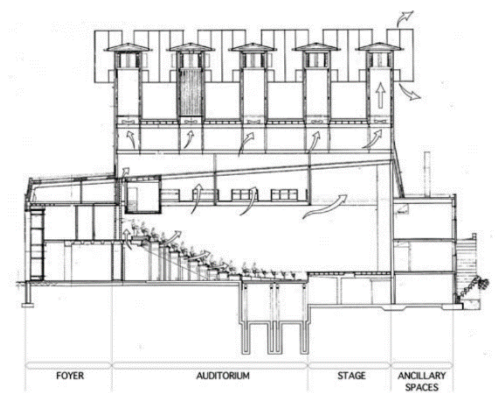


Figure 60 Section of the main hall of the theater (Short)

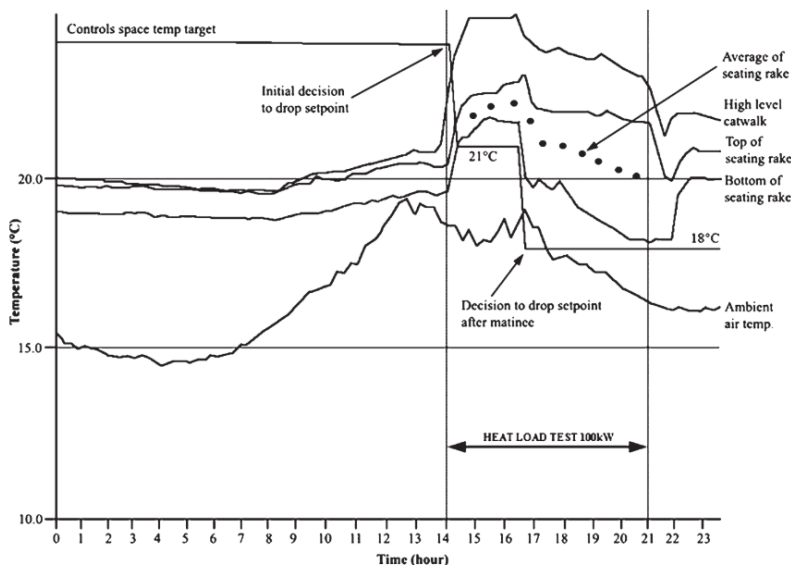


Figure 61 Temperature inside the main hall during a 100kW heat test load (Short)

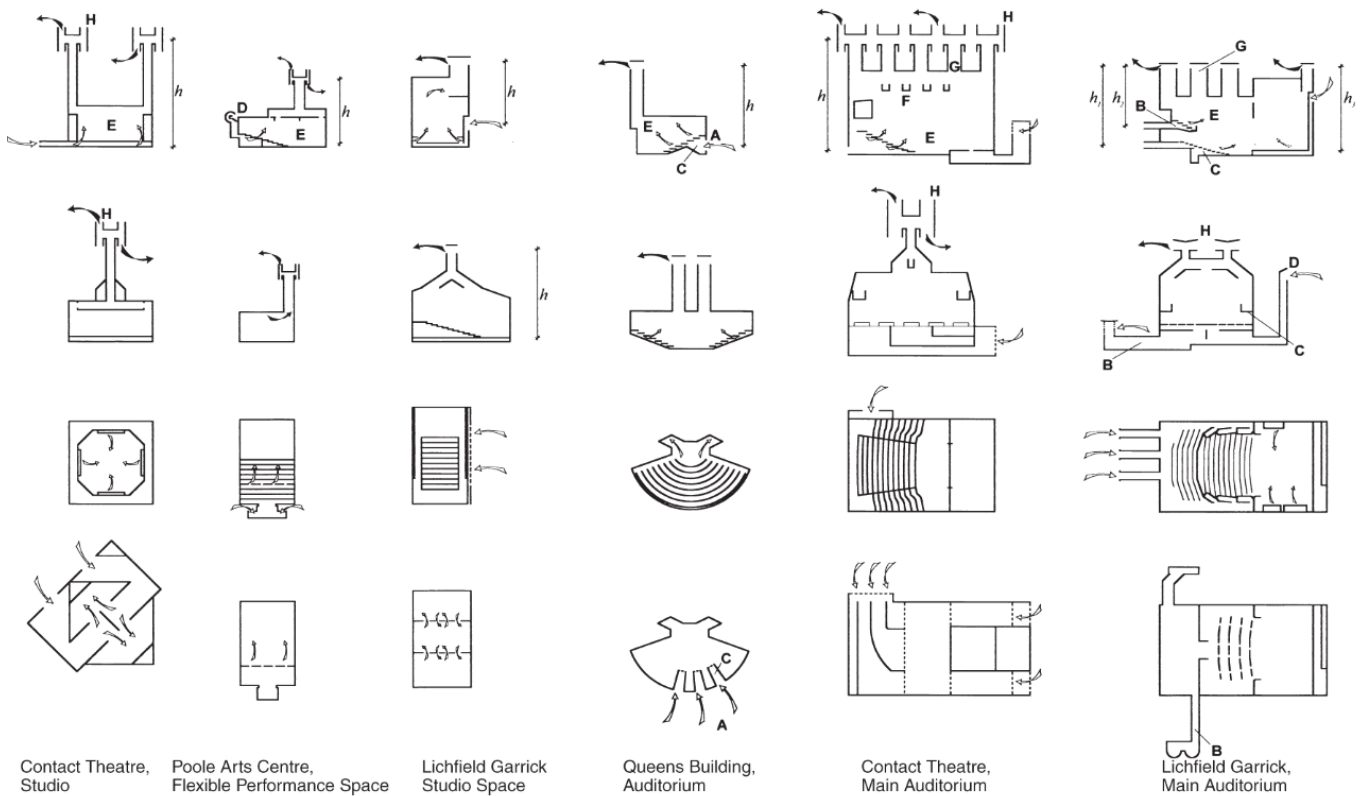


Figure 63 Short's naturally ventilated theater designs (Short)

Building	Queens (Leicester)		Contact Theatre (Manchester)		Poole Arts Centre	Lichfield Garrick Centre	
	Auditorium 1	Auditorium 2	Main auditorium	Studio	Flexible performance	Main auditorium	Studio
Client	De Montfort University		Contact Theatre Company		Poole Borough Council	Lichfield District Council	
Noise rating value	NR30	NR25	NR25	NR20	NR25	NR20	NR20
Max. occupancy	150		386	110	140	500	180
Max. casual heat gains	17.6 kW		100 kW	31 kW	34 kW	110 kW	66 kW
Total cost, cost per m ²	£9.1 M, £910/m ²		£3.4 M, £825/m ²		£5.7 M, £200/m ²	£5.2 M, £910/m ²	
Year construction completed	1993		2000		2002	2003	
Net floor area	350 m ²		390 m ²	90 m ²	144 m ²	395 m ²	154 m ²
Free inlet area	5.86 m ² (0.04 m ² /person)		12 m ² (0.03 m ² /person)	8 m ² (0.07 m ² /person)	1.5 m ² (0.01 m ² /person)	37.6 m ² (0.08 m ² /person)	8.7 m ² (0.05 m ² /person)
Free outlet area	6.11 m ² (0.04 m ² /person)		20 m ² (0.05 m ² /person)	2.25 m ² (0.02 m ² /person)	1.5 m ² (0.01 m ² /person)	30.8 m ² (0.06 m ² /person)	4.2 m ² (0.02 m ² /person)
Stack height (from centre of lowest inlet to centre of highest outlet)	14.5 m		19.7 m	19.7 m	10.93 m	$h_1 = 14.85$ m, $h_2 = 11.15$ m, $h_3 = 15.7$ m	10.25 m
Estimated stack pressure based on external temperature = 24°C; internal temperature = 27°C	1.57 Pa		2.13 Pa	2.13 Pa	1.18 Pa	1.60 Pa, 1.20 Pa	1.11 Pa

Figure 62 Technical description of Short's Theater designs (Short)

The second example is the Eastgate Center in Harare, designed by Zimbabwean architect Mick Pearce (Pearce, 2018b). Inspired by a termite hill, Pearce designed the seven-story high office and shopping center as an antithesis to the “old order of steel and glass”, intended to be an ecosystem and not a “machine for living in” (Pearce, 2018a).

The Eastgate Center in Harare is located in a temperate sub-tropical climate, which is relatively cool thanks to its altitude yet considerably warmer than the climate of Manchester. The architecture is representative of the “traditional stone architecture of Great Zimbabwe” and is based on termite mounds. As in an early stage the costs for an air conditioning system were deemed far too large, the climate design had to be cheaper, hence the resulting biomimetic approach.

Termite mounds work by thermal buoyancy through their relatively porous shell. Large passages going upward in excess of 3m high will allow for air to exit the mound, while the soil keeps the interior cool (National Geographic, 2018). Similarly, the Eastgate Center has a very high thermal mass construction of concrete and brickwork, which is also supposed to symbolically represent “Zimbabwe’s lichen-covered rocks” (Pearce). By jagg-ing the concrete, more surface area is created for the structure to cool off at night, while they also provide overhangs for shading of the already small windows. Two of such facing blocks are connected through a glass-covered atrium (representative of the old colonial order), that also make the atrium cooler than outdoors.

Air that is supplied to the spaces comes from this atrium through 32 low and high volume fans. The air is filtered and sucked up higher through cool air shafts. Per floor, the shafts give air into a hollow-core concrete slab where air passes through, pre-cooling the air further. The air enters the room low at the façade and rises back towards the vaulted ceiling. The air is sucked towards the hot air duct, where it is extracted to one of the 48 chimneys. By using lighting systems that reflect light upward and which are partly hidden within a concrete panel, the heat gains due to lighting are nearly directly absorbed by the construction.

Such an approach was found to be very effective, providing comfortable indoor conditions for 50/52 weeks of the year. Internal temperatures are 3 degrees cooler than outdoor conditions on average, with peak temperatures occurring at 16:00h of 27-28 degrees. Internal heat loads cause the office to heat up by 1.5°C during daytime, but the high room height ensures there is a level of stratification that keeps temperatures more comfortable.



Figure 64 The Eastgate Center from afar (archnet)



Figure 65 Atrium view of the center (National Geographic)

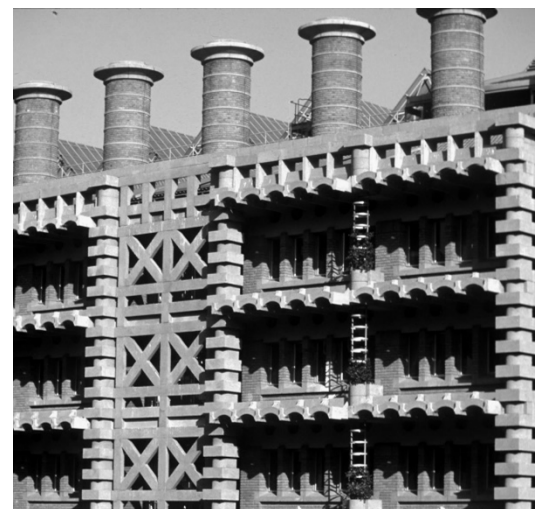


Figure 66 Close-up of the facade (Archnet)

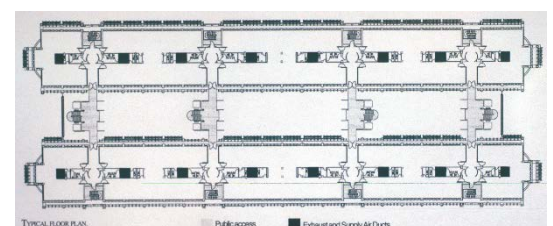


Figure 67 Typical floor plan (Archnet)

The Eastgate Center in total used 35% less energy compared to six other similar buildings in Harare with HVAC systems. The cost savings were in the range of 10% of total costs compared to a structure with a full HVAC system, resulting in a reduction of 3mln USD on the total price of 30mln USD. The 55.000m² building with a ground floor area of 9313m² was constructed in three years and designed in only one by the architect in conjunction with ARUP engineers.

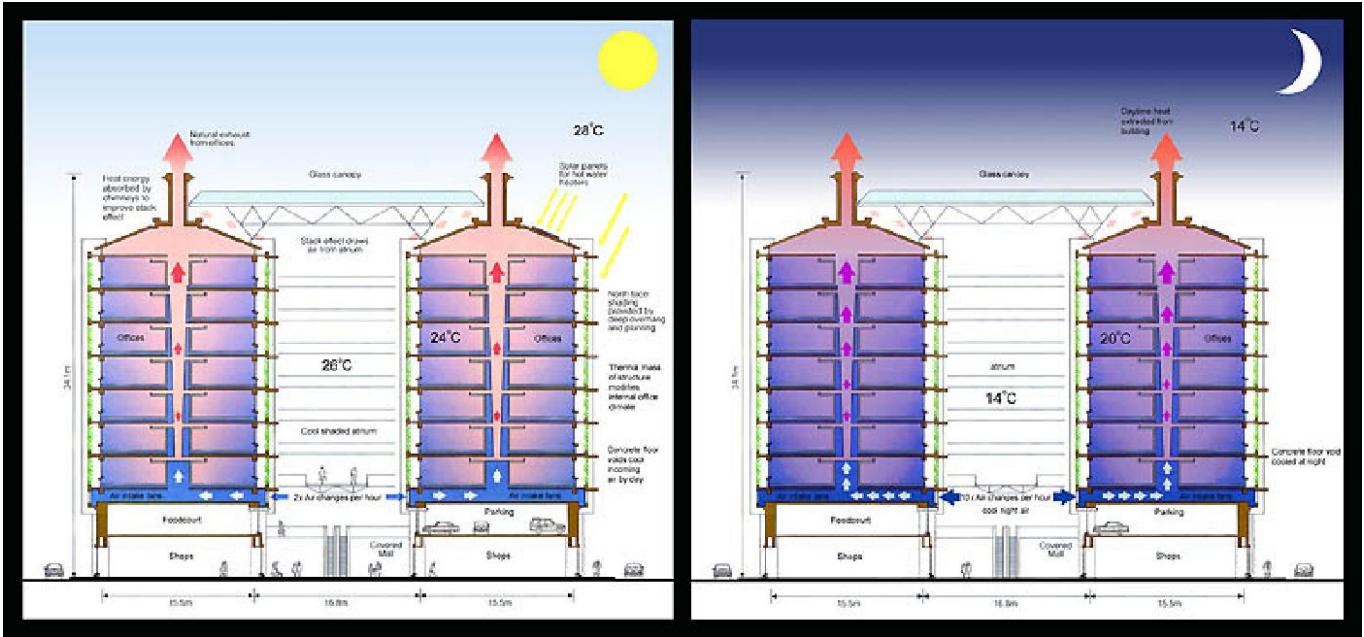


Figure 69 Climate concept of the Eastgate Center (Pearce)

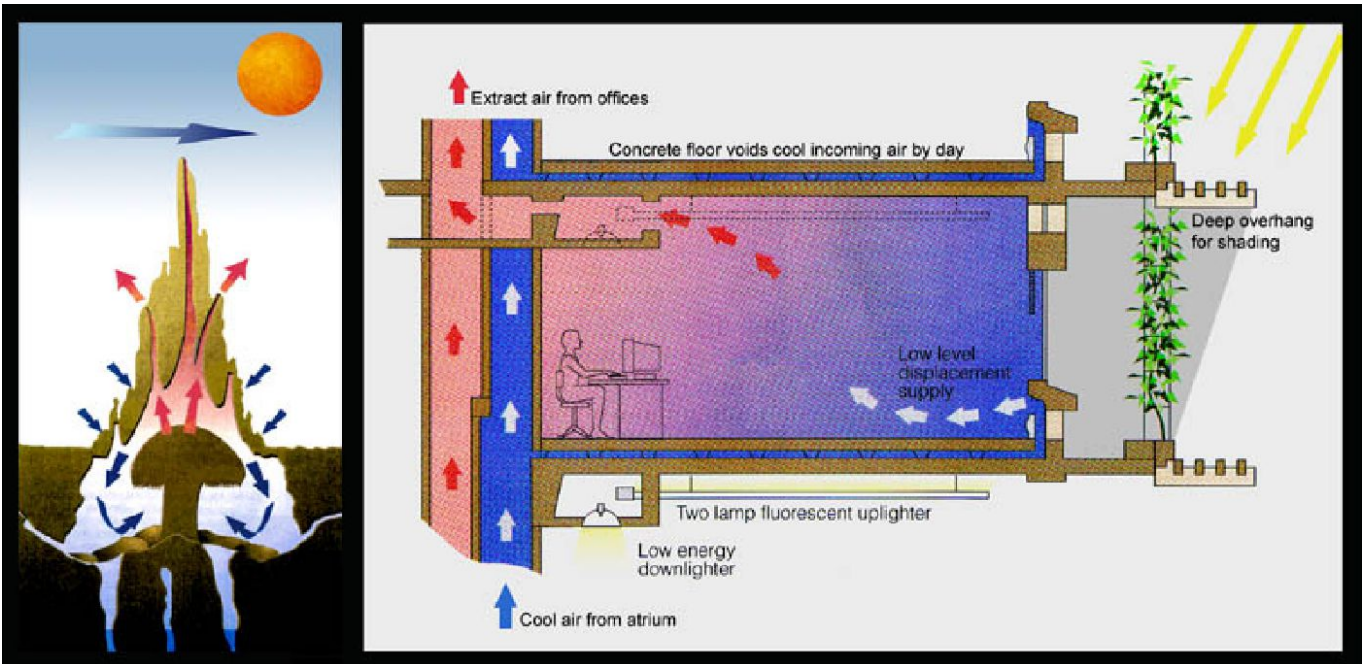


Figure 68 Section of the generic office space (Pearce)

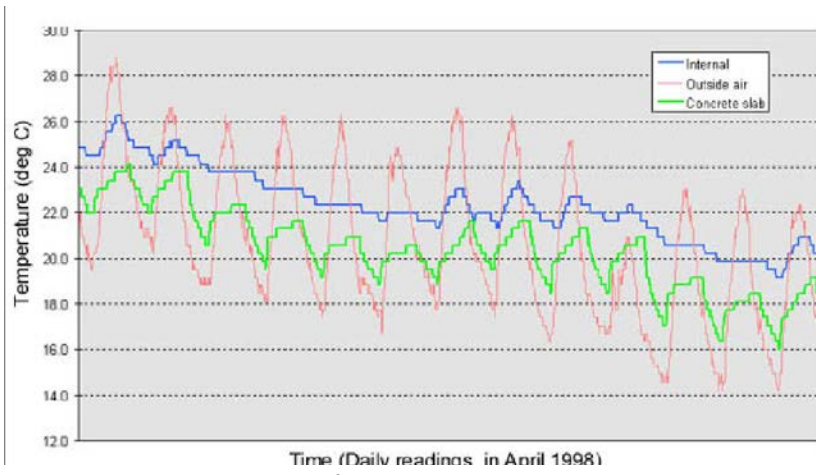


Figure 70 Interior temperatures of April (Pearce)

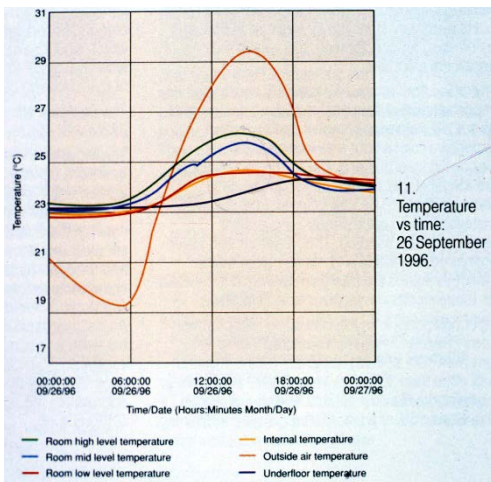


Figure 71 Interior temperatures for 26th of September (Archnet)

3.6 Optimization in CFD

Computational Fluid Dynamics (CFD) is a numerical approach to fluid mechanics and allows for the simulation of fluid flow in many different cases. Many software packages allow for the analysis of fluids, both commercially as well as free of charge. Generally speaking, optimization of CFD problems is very difficult and literature on the topic is very little.

Parry et al. (2004) identify many reasons for such difficulties, including the resource-intensiveness of CFD simulations, possible local minima, meshing and non-linear objectives and constraints. Similarly, Nitsopoulos et al. (2009) doubt the efficiency of classic parametric design methods using conventional Response Surface Models (RSM), because to generate the surface a high count of analyses is required, which is resource-intensive.

Therefore, research into “optimization” using CFD is often performed by combining best practices and applying a set of iterations to a known, given design. Guo, Liu, & Yuan (2015) developed a flowchart for such a CFD workflow for three scales of building design as shown in figure 64. Bhardwaj & Agrawal (2018) used the Taguchi Method with an orthogonal array of 32 solutions to find the best input parameters for a solar chimney, including the air gap, glazing material, season, window-to-wall ratio and orientation. Similarly, Su, Lei, & Xue (2013) designed a tapered solar chimney which prevented turbulent flow and improved flow rate by 25% by basing the design on good practices. Liu et al studied various options for the optimized design of an exhibition space, while Liu, Wang, & Zhang (2013) studied various solutions for an underground mains power station. Sacht et al. (2016) researched the optimal placement of ventilation grilles in a façade, while Méndez et al. (2008) proposed alternative air supply locations to a two-bed hospital room. Ma et al. (2011) analyzed the design of the new traffic center of terminal 3 of Beijing International Airport.

The continuous problem with the aforementioned analyses is that there is no certainty that the found results actually depict the best possible combination of input parameters or not. Similarly, this form of design requires an initial, working design to start with; it is not possible to generate a design based on the principles. Realizing these shortcomings, various other approaches to CFD optimization were developed, including:

- Global optimization with local trust regions
- Genetic Algorithms (GA) supported by Artificial Neural Networks (ANN)
- Topology Optimization

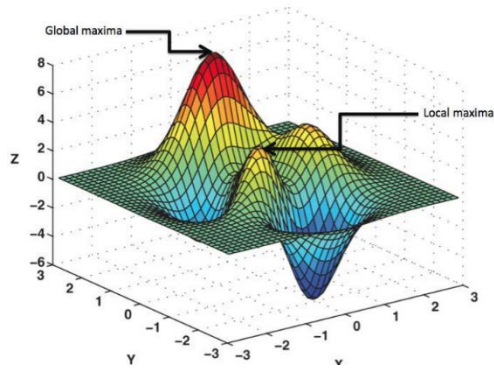


Figure 73 A Response Surface Model plotted in 3D (Nourian)

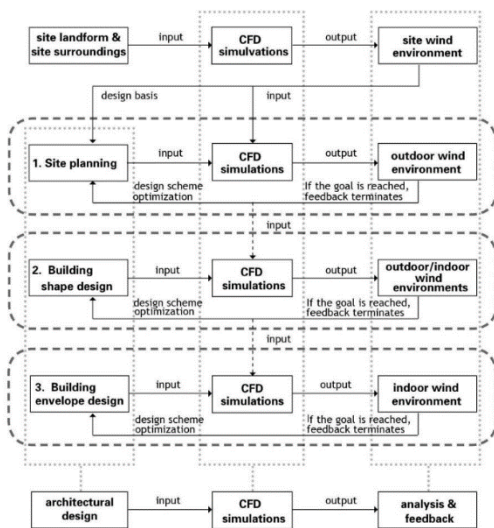


Figure 72 CFD Workflow proposed by Guo et al.

By opting for a global optimization strategy with local trust regions, Parry et al. (2004) were able to optimize the design of a heat sink for computer applications. They formulated global optimization goals after which they created a latin hypercube design (LHD) to generate starting points. Afterwards, for each starting point, a local optimization approach is used to find the nearest optimum. A Trust Region is used to find the direction to which the improvements should go, which is repeated until 30 experiments are conducted. Finally, a global optimization is performed in which the best performing local optimized variants are optimized further. The resulting design is found much faster than with a traditional approach and allows for different options to be analyzed and the best performing one selected.

However, a more advanced method is based on using genetic algorithms (GA) with artificial neural networks (ANN) to quickly reach a good solution and has research applied to the field of natural ventilation and thermal comfort. Li et al. (2013) for instance developed a genetic algorithm that was able to optimize an indoor flow pattern. Instead of simulating a large amount of flow scenarios (inlet and outlet), a GA was used to reduce the amount of simulations that needed to be run. By optimizing for the highest PMV value when supply velocity, temperature and angle are parameters, the study was able to develop an effective CFD-based model to “predict and optimize the inlet flow control in various confined spaces.”

Similarly, Li et al. (2013) used a GA model combined with a proper orthogonal decomposition (POD) based model to optimize for multiple objectives, including PMV, space temperature gradients, indoor air quality and energy usage in a single office room. The final model was able to generate an optimized design faster than comparable methods and yielded the idealized balance between temperature, airflow, CO₂ and PMV.

The most comprehensive usage of GA’s with ANN’s was however performed by Zhou & Haghigat (2009a). An objective function was designed, in which comfort and indoor air quality could be optimized without increase in energy consumption. The ANN was used to speed up fitness evaluations inside the GA loop for response surface approximation (RSA). The network contained 8x30x7 neurons with roughly 150 CFD results entered into it. A single office room was analyzed and optimized to that extent, with considerable speed improvement over the traditional fitness method: 17 hours against 10 minutes. The final ventilation system produced better PMV values, higher CO₂-based ventilation effectiveness and less cooling load (Zhou & Haghigat, 2009b).

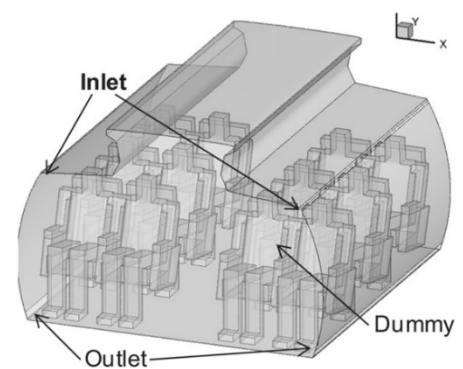


Figure 74 Li et al.'s optimization for an airline cabin

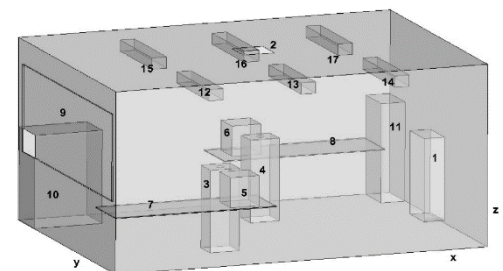


Figure 76 Li et al.'s optimization for an office layout

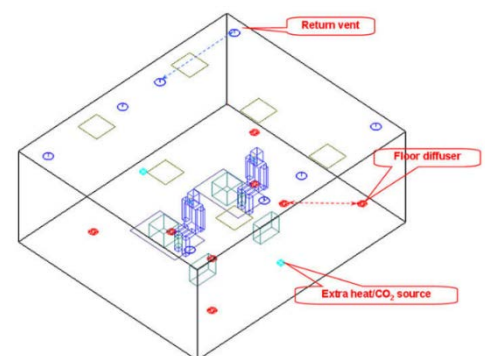


Figure 75 Zhou & Haghigat's research on a single office layout

The final computational optimization method focuses more on form-finding than the other examples so far: topology optimization allows for the ideal shape to be found for a given set of boundary conditions. Currently, commercially available programs such as ANSYS and COMSOL allow for topology optimization embedded within their software, or with third party additions. Different than the parametric optimization that constituted the previous examples, topology optimization starts from an “available design space” rather than a design itself. Within the given design space, individual cells can be populated to form a final geometry based on optimality criteria (OC’s). There is no mathematical convergence: only when adding to the geometry stops adding significantly to the desired criteria is the simulation complete.

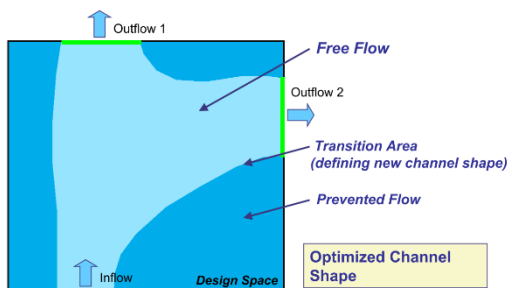


Figure 77 Example of a topology optimization solution for a 2D space (Nitsopoulos)

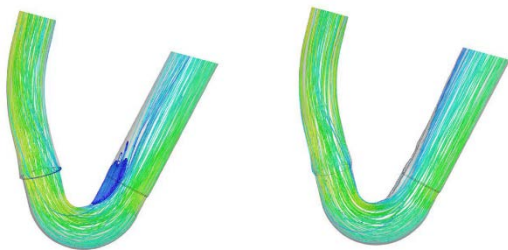


Figure 78 Example of an intercooler intake hose optimization (Nitsopoulos)

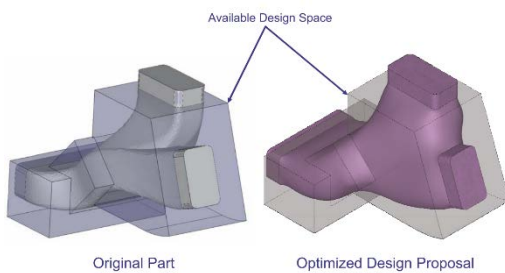


Figure 79 Example of a HVAC flow splitter optimized for lowest pressure drop (Nitsopoulos)

Multiple examples of this are documented by (Nitsopoulos et al., 2009) using ANSYS Fluent with TOSCA Fluid, where in 2D or 3D optimality criteria can be defined and applied to a mesh geometry. For instance, for the case of a channel structure, the topology optimized can guide it in such a way as to prevent backflow and recirculation. This could be called a “re-design rule” as such.

Another example is the design of a connection piece for two known directions of flows. When a design space is given, the optimizer can direct the population of cells as to allow for minimal pressure drops for instance. This is applied to many industrial examples, such as a HVAC splitter manifold, an intercooler intake of an automotive engine and the design of an automotive exhaust gas cooler. In all cases, the topology optimization allows for a better performance with greater uniformity and lower pressure losses in the system in the range of 20%.

3.7 Literature Review Discussion

The literature review focused on multiple aspects related to the final goal of the thesis and included a review of relevant literature on energy efficiency in the built environment, the design of airports, indoor environmental quality, natural ventilation and optimization topics in Computational Fluid Dynamics. General literature on the underlying principles and a review of recent developments in all these fields were investigated in order to provide for information a relevant context for the thesis.

The need to improve the performance of the built environment is clear from the fact that at this stage, it and construction sector are very big consumers and polluters. Over a third of all CO₂ emissions in Europe are caused by the built environment and nearly 40% of all energy in Europe is consumed by it. On the other hand, the consumption of vast amount of resources, waterway pollution and waste generation are added problems that easily make the built environment and construction sector the most polluting and energy and resource-intensive sector in the world. Tackling the issue of embodied carbon of building materials, however, is only a viable strategy once the energy performance of a building is drastically improved. Therefore, both future stock (2020) and existing stock (2050) need to be energy neutral in Europe, as well as continue to improve on its materials sustainability.

Although architecture cannot influence the energy performance of all the other large global polluters, the development of sustainable transport buildings could help to nudge the sector towards decreasing consumption. In that respect, the growing demand for aviation -both from a passenger as well as a freight point of view- is an important development. Passengers and freight are expected to increase by nearly 5% in all regions of the world, and with the expected rise of Low Cost Carriers (25% market share) and Point-to-point travel, the demand on airline infrastructure is big. Over 1 trillion USD is currently being invested into the upgrading of existing airports and the construction of new ones, but aviation experts estimate that more investments are needed to cater for the demand. This is especially the case in the Asia-Pacific region, Europe and North America, where both existing traffic and airports, but also future growth is large.

The development of Low Cost Terminals poses an interesting challenge in this growing aviation context. Terminals consume over three quarters of all energy at airports and HVAC systems are universally the biggest consumer of energy at them. The share of HVAC to the total consumption varies roughly between 20-60% of the terminal consumption and is followed only by lighting and ICT systems. Low Cost Terminals often save on such

expenses by choosing simple layouts with lower standards of comfort. This is not only the case to reduce energy consumption, but also operating costs as well as initial costs.

However, indoor environmental quality is nevertheless important and critical. Therefore, indoor air quality and thermal comfort are investigated in greater detail and aspects are covered together with their mathematical formulation. Similarly, natural ventilation is tackled in greater depth with its underlying physical principles. Two case study buildings, a naturally ventilated theater in Manchester and a naturally ventilated shopping and office center in Harare are investigated in greater detail as well. Three aspects directly gather the attention: assistance by fans is often required (yet systems can perfectly run often without them), thermal buoyancy is the largest driving force of natural ventilation (with wind being either neutral or as an assisting force) and high levels of thermal comfort can be achieved by only passive methods.

However, there is also another underlying principle for designing with natural ventilation in mind: it needs to be incorporated into the design from the start and requires it to form a clear element of the architectural design.

Of the investigated optimization methods for Computational Fluid Dynamics, topology optimization and the usage of genetic algorithms stand out as following that philosophy of embedding natural ventilation into the design from the beginning. While topology optimization allows for the generation of 2D and 3D forms that follow a set of criteria within a given design space, genetic algorithms (especially when supplemented by artificial neural networks) allow for fast evolutionary analysis into which parameters give approach the desired result best. However, only a handful of sources that tackle the optimization issue in that frame of mind are found, pointing out the fact that most optimization techniques are only meant for feedback. The real challenge therefore lies in developing a feedforward way of design on the topic of natural ventilation in architectural design.

4

DESIGN & ENGINEERING

4 DESIGN & ENGINEERING

4.1 Introduction

This chapter elaborates on the development of the design and engineering phases of the computational model. This is done by both explaining the background studies performed for these two phases as well as an in-dept elaboration of the model itself.

As the first step of the model, decisions are input for the general and algebraic topology of the design. This means that the ventilation method is selected and parameters that influence the final geometry are identified. In the final model these are based on user inputs, while in this chapter an elaboration of the various possible options and their advantages and disadvantages are also discussed.

Afterwards, the engineering of the design that has been envisioned takes place with calculations, CFD studies and testing of parameters. The purpose of the engineering phase is to develop a valid and workable design that satisfies technical requirements (design constraints), but is itself not fully optimized yet.

4.2 Design: General Topology (Driving Forces)

As an initial design step, the 'point-set' or 'general topology' of the naturally ventilated terminal needs to be decided. This mathematical term can be translated in the case of our design into a question of 'What will the driving force be behind our air movement?'

This seemingly basic decision, however, is the first and most critical decision in the design, as it influences all other aspects ranging from geometry to performance. Analogically, this could be compared to the question what function our building should have in the first place, or if our vehicle should have wheels, be amphibious or flying.

In the case of ventilation, the driving force is always pressure difference. For incompressible flows, as mentioned earlier, the Bernoulli equation states that the sum of the pressure energy (static pressure), kinetic energy per unit volume (dynamic pressure) and potential energy per unit volume are constant:

$$W_1 + KE_1 + PE_1 = W_2 + KE_2 + PE_2$$
$$P_1 + \frac{1}{2}\rho_1 v_1^2 + \rho_1 g h_1 = P_2 + \frac{1}{2}\rho_2 v_2^2 + \rho_2 g h_2$$

In which W = work done [J], KE = kinetic energy [J], PE = potential energy [J], P = pressure [Pa], ρ = density of the fluid [kg/m^3], v = flow speed [m/s], g = gravitational constant [m/s^2] and h = height [m].

Additionally, we also know that the sum of static and dynamic pressure is constant over a given streamline, better known as the

total pressure. By combining these two descriptions from fluid dynamics, it is possible to understand what factors can cause pressure differences: a change in kinetic energy (due to speed or density) or a change in potential energy (due to density or height).

The formula also hints at what is the most effective way to generate pressure differences in the built environment: wind. This is because even slight changes in windspeeds cause large pressure differences as the velocity term is squared and airspeeds outside are generally far larger than indoor airspeeds. However, as was visible from the various case study designs and literature, wind is not always a suitable design method as it is not always available depending on climate. Thermal buoyancy (density difference) on the other hand can always be available when ventilation is needed: when the building is occupied and heat loads are generated inside. To understand the advantages and disadvantages of thermal buoyancy and wind for indoor ventilation, a matrix was designed to help in the design.

As can be understood from the matrix, both wind and buoyancy come very close in terms of comparative performance. Especially in the case of The Netherlands, where wind is year-round prevalent. However, the caveat is that it is also multi-directional, with a weak dominant western direction. This also means that the design should work with winds from various directions, which adds another (albeit small) challenge to the design. Additionally, wind speeds not only vary from day to day, but they also do so from one instant to another. Sudden wind gusts can upset a delicately balanced opening so that more air flows through, causing discomfort for instance.

Thermal buoyancy, however, works year-round reliably. As long as the terminal is occupied -hence, when ventilation is needed-thermal buoyancy will be available to make air rise. A simple calculation assumption, in which each square meter of surface area generates 20W/m² of heat, shows us that buoyancy alone would be sufficient to supply enough ventilation:

- 15L/s of ventilation
- 1 m² of floor area with 5% opening
- 20W of heat
- 1.09° increase from 20°C temperature

$$\dot{Q} = \dot{m}c_p\Delta T$$

$$\Delta T = \frac{20}{0.015 * 1.21 * 1008} = 1.09^\circ C$$

$$h_{stack} = \frac{\dot{V}^2 T_2}{2C_d A_e g \Delta T}$$

Criteria	Wind	Buoyancy
Predictability/ 'Robustness'	++	+++
	Wind has a level of uncertainty and dynamic behavior	Thermal buoyancy behaves more predictable than wind
Effect on pressure	+++	+
	Wind affects pressure to the second power	The effect of density difference is small
All-year availability	++	+++
	Depending on geographic location and always fluctuating	Permanently available when the structure is occupied and used
Incorporation into design	++	++
	Wind-based elements can be incorporated to the architectural design	Buoyancy-based elements can be incorporated to the architectural design
Thermal comfort	+	++
	Wind-based ventilation has higher risk of draught due to wind gusts	Buoyancy-driven flows are often slower, but overheating and vertical temperature difference are small issues
TOTAL	+10	+11

Figure 80 Matrix comparing wind and buoyancy suitability for indoor ventilation.

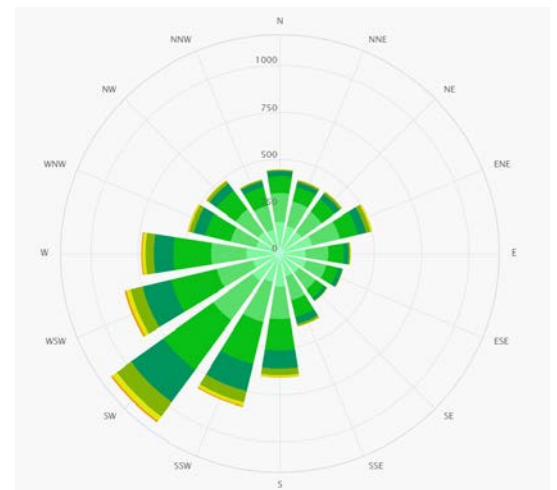


Figure 81 Wind rose of Rotterdam, showing that there is a weak dominant southwest wind direction (Meteoblue, 2019)

$$h_{stack} = \frac{0.015^2 * (273 + 21.09)}{2 * 0.6 * \frac{0.05}{\sqrt{2}} * 9.81 * 1.09} = 0.145 [m]$$

As the required stack height is minimal, it is very plausible that a ventilation design based on such assumptions can easily be made. Even if the load is reduced to 5W/m², the required stack height would merely end up at 1 m.

From this initial calculation and matrix, it is possible to see that a design that is based on buoyancy is more feasible, predictable and robust. This is also the reason why the case study designs rely primarily on thermal buoyancy. However, in the case that buoyancy is taken as the driving force of ventilation, the problem of reverse flows needs to be addressed.

Reverse flows will occur in the design when the interior of the structure is cooler than outside air: in that case, the heavy indoor air will displace the hotter air outside at the lower openings and allow hot air to enter the building from the openings above. This would add considerably to the heating of the structure, making comfort conditions more difficult to attain.

Solutions to circumvent this problem include the usage of fans, wind catchers or solar chimneys to reverse the airflow. Many of such examples to force airflow in a particular direction are also explained in the literature review chapter and can be commonly and easily integrated into a natural ventilation design.

4.3 Design: Algebraic Topology (Geometry)

After having decided on the primary way of ventilating the structure -thermal buoyancy- we must decide on the shape of our building and which parameters influence this. In mathematics, this is called the algebraic topology of a function, often dubbed 'rubber-sheet geometry' (Weisstein, 2019): one can distort the geometry of any shape by many parameters, but by tweaking the right set of parameters the underlying topology will remain identical. An example could be any polygon, which could be distorted by an innumerable amount of translations or rotations and yet remain a polygon. Another example would be a mug, which is topologically the same as a torus, even though both shapes have vastly differing looks.



Figure 82 Although geometrically different, a mug and torus are topologically the same. They can be 'stretched' from one shape to another, the 'rubber-band geometry' (Math Stack Exchange, 2019)

Therefore, the focus of the algebraic topology section is first on discovering what parameters influence the thermal comfort, air distribution and geometry of the structure. To this extent manual designs, hand calculations and CFD studies are implemented to address the influence of various parameters on the design goals.

4.3.1 Airport Design Guidelines

As mentioned earlier, the design requirements for airports are many and range from external guidelines (for non-terminal parts) to internal ones (the terminal itself). For the case of a parametric workflow as described in the thesis, the manual design is not so much considered for a specific case, but rather for a generic layout of an airport terminal. Note that 'manual design' still involves a mix of hand calculations and manual numeric simulations.

The first decision to make regarding airport guidelines is the scope of the airport itself: its size and runway alignments. Often, such runways are placed parallel with the dominant wind directions. If multiple runways are needed, these can be used either in parallel as well (for simultaneous approach or landings), or can be aligned in different directions in order to account for various dominant wind directions. The specific rules and regulations that determine runway alignment are explained in the Literature Review chapter. However, important is to realize that the placement of runways is far more important than the placement of the terminal: the sheer size and directionality of a runway poses a much bigger (initial) design challenge and can cause severe economic losses when airplanes have issues with landing due to crosswinds or geometric limitations.

Examples of airports with single, parallel or crossing runways are many. From the airports examined earlier in the Literature Review for their energy efficiency, a similar list is made explaining their runway alignments. Additionally, a couple of examples of more complicated runway layouts are also given.

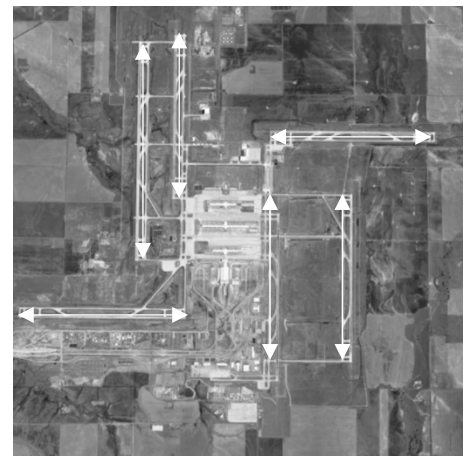


Figure 83 Several airports with complicated crossing runway alignments. Note that for these airports, (semi)parallel approaches are possible for both wind directions. From top to bottom: San Francisco International Airport, Denver International Airport and Dallas Fort Worth Airport (Google Maps, 2019)

<p>London Heathrow 66 mln pax ('09)</p> 	<p>London Gatwick 32.4 mln pax ('09)</p> 	<p>London Stansted 20 mln pax ('09)</p> 
<p>Paris Charles de Gaulle 57.9 mln pax ('09)</p> 	<p>Frankfurt Airport 50.9 mln pax ('09)</p> 	<p>Amsterdam Schiphol Airport 43.6 mln pax ('09)</p> 
<p>Eindhoven Airport 1.7 mln pax ('09)</p> 	<p>Istanbul Atatürk Airport 29.8 mln pax ('09)</p> 	<p>Izmir Adnan Menderes Airport 6.2 mln pax ('09)</p> 
<p>Ankara Esenboğa Airport 6.1 mln pax ('09)</p> 	<p>Zurich Airport 21.9 mln pax ('09)</p> 	<p>Hong Kong Airport 69.7 mln pax ('09)</p> 
<p>Stavanger Airport 4.5 mln pax ('09)</p> 	<p>Bergen Airport T3 7.0 mln pax ('09)</p> 	<p>Galapagos Eco Airport 0.5 mln pax ('09)</p> 

If looked at closely in the case of smaller airports with a single runway, it is notable that runways and the long direction of the terminal are often parallel. This is of course favorable for the linear terminal model, as it allows for the longest surface area being exposed to the apron, meaning more planes can park at the gates. Examples of this can be seen at many airports, including Lelystad Airport, Izmir Adnan Menderes Airport or London Stansted.

From the analysis it is possible to decide that the orientation of the terminal is not a parameter we should influence for the design of a naturally ventilated terminal. Issues of aircraft movements, apron times and relation to highway and other infrastructure plans often already determine such a layout greatly. Therefore, it is taken as a constraint and once more confirms that a design should not be based on wind, but rather on thermal buoyancy.

Afterwards, the maximum height of the terminal and its rough location need to be considered. The first 150m from the runway centerline needs to be free of any structures, while the subsequent distance until 465m from the center of the runway have a height limitation that follows a 1:7 slope running upward. Similarly, taxiing times on the apron need to be limited, yet enough space needs to be left for traffic as well as future expansion capabilities. Various distances to the runway centerline for smaller airports are given in the figure.

After the runway is oriented and the required apron size is determined, the terminal itself needs to be placed. This is sometimes done towards one side of the runway, or in the middle. This all depends on the expected growth of the airport (expansion capabilities), the urban surroundings and infrastructure and mobility integration. However, what is often more certain, is the size required for the terminal and its surrounding facilities.

4.3.2 Terminal Design

The design of the passenger terminal is only a small task within the spectrum of the design of a whole airport; maintenance hangars, parking lots, fuel storages and other offices and security spaces can all be considered one large design challenge. However, within the scope of this thesis, the focus lies on the terminal, which is why only it is considered.

The placement of the terminal is determined by external factors as explained earlier, however the internal layout is similarly very much already fixed. Due to safety and logistics requirements, the sequence in which passengers travel upon arrival or departure is fixed. Sizes are also determined through standards such as the Level of Service concept (IATA, 2018b). Within the scope of this

Airport	Distance Runway Centerline – Terminal [m]	Allowable Height [m]
Lelystad	360m	30m
Eindhoven	420m	38.5m
Izmir Adnan Menderes	600m	-
Ankara Esenboğa	440m	45m
Brussels Charleroi	410m	37m

Figure 84 Various airports with the distance between the runway centerline and the terminal.

thesis, the layout of an airport in plan and associated Level of Service is therefore considered a constraint.

The layout of the terminal is the second step of the design. As mentioned earlier in the literature review, there are various so-called *terminal configurations* and *concepts*. A centralized terminal with a linear concept is the most common one for smaller airports, while variants with piers and satellites are often used for larger airports. Evidently, centralized terminals and spaces where people spend more time (terminal spaces), rather than just walk by (piers), are more interesting to design with thermal comfort as an objective. For all terminal configurations and concepts, the proposed parametric workflow can generate a valid and optimized naturally ventilated design based on thermal buoyancy.

4.3.3 Design Scripts

The design with its general and algebraic topologies is reflected in the computational model as a set of three inputs, consisting of the input of spaces, thermal comfort parameters and envelope properties.

In terms of spatial input, the user is prompted to enter each space's outline, any exclusion zones that should be kept outside the analysis and the outermost perimeter of whole the structure. These can be directly entered in the script by referencing relevant Rhino geometry or generating them within the Grasshopper environment. This data is then merged with the input of the space names as a list and the LOS per space in a Python component. This component returns each space's area and occupancy through element-wise multiplication. Important is to note that when Rhino Geometry needs to be handled by Python, a GH_Python component is used which actually runs on IronPython, while a GH_CPython component is used when there is a need for for importing specialized Python libraries such as numpy or scipy.

The occupancy script contains the following code (see next page):

Occupancy Calculator

```
import rhinoscriptsyntax as rs
import math

for i in range(len(spaces)):
    centroids= rs.SurfaceAreaCentroid(spaces)
    space_centerpoints=centroids[:,2]

area_per_space_list = rs.SurfaceArea(spaces)
area_per_space=area_per_space_list[:,2]
area_per_space_list= []
LOS_per_space_list=list(LOS_per_space)
occupancy_per_space= []

for i in range(len(spaces)):
    a=area_per_space[i]
    b=LOS_per_space[i]
    c=a/b
    occupancy_per_space.append(round(c))
```

After the initial layout of the terminal is entered, the thermal comfort parameters and envelope properties can be entered to calculate the thermal loads in the design.

The thermal comfort parameters can be entered per space, meaning each space can have a different level of thermal comfort if desired. The designer enters the analysis season (summer, winter or intermediate) and expected metabolic rate of the occupants, while pre-programmed databases load the external design temperatures, solar irradiation data and clothing levels per season. These can also be linked directly from an external data source if desired. Per space target PPD values are input as a list.

For the specific case of The Netherlands, external design temperatures of 27°C, 10°C and -10°C are taken respectively for summer, intermediate and winter seasons within the database. Solar radiation on the vertical plane is taken to be 500, 300 and 0W/m² for the respective seasons as an average of east, south, west and north facades. Clothing levels are set at 0.5clo, 0.7clo and 1.0clo respectively for summer, intermediate and winter seasons. These values are all coded into Python using a GH_CPython component with the following code:

Thermal Comfort Parameters I

```
dT_balance_list = []
design_condition_list = []
category_output_list = []

for i in range(len(_PPD)):
    if _season == 1:
        season_output = "Winter"
        clothing_level = _clothing_level[0]
        T_outside_ = -10
        q_sol_ = 50
        if _PPD[i] <= 5:
            dT_balance = 0
        elif 6 <= _PPD[i] <= 10:
```

```

        dT_balance = -0.5
    elif 11 <= _PPD[i] <= 15:
        dT_balance = -2.5
    else:
        dT_balance = 0
    dT_balance_list.append(dT_balance)
elif _season == 2:
    season_output = "Intermediate"
    clothing_level = _clothing_level[1]
    T_outside_ = 10
    q_sol_ = 500
    if _PPD[i] <= 5:
        dT_balance = 0
    elif 6 <= _PPD[i] <= 10:
        dT_balance = -1.5
    elif 11 <= _PPD[i] <= 15:
        dT_balance = -2.5
    else:
        dT_balance = 0
    dT_balance_list.append(dT_balance)
elif _season == 3:
    season_output = "Summer"
    clothing_level = _clothing_level[2]
    T_outside_ = 27
    q_sol_ = 500
    if _PPD[i] <= 5:
        dT_balance = 0
    elif 6 <= _PPD[i] <= 10:
        dT_balance = 1.5
    elif 11 <= _PPD[i] <= 15:
        dT_balance = 2.5
    else:
        dT_balance = 0
    dT_balance_list.append(dT_balance)
else:
    season_output = "ERROR - WRONG SEASON"

category_note = "EN 15251 - Category "
if _PPD[i] <= 5:
    category_output = category_note + "I"
elif 6 <= _PPD[i] <= 10:
    category_output = category_note + "II"
elif 11 <= _PPD[i] <= 15:
    category_output = category_note + "III"
else:
    category_output = "ERROR - TOO HIGH PPD"
category_output_list.append(category_output)

design_condition = 'Season: ' + str(sea-
son_output[i]) + ""
"" + 'Comfort Category: ' + str(cate-
gory_output[i])
design_condition_list.append(design_condi-
tion)

dT_balance_ = dT_balance_list
design_condition_ = design_condition_list

```

The values from this script are used to calculate the thermal gains and losses for the setpoint temperature of each space. To calculate the setpoint temperature of each space, the balance

temperature of each space is calculated based on the target PPD level mentioned earlier. A standard library is set up in which the balance temperature for a PMV=0 environment is added or subtracted by a fix temperature differential that shifts the thermal comfort between classes I (PPD<6%), II (6<PPD<10%) and III (11%<PPD<15%) and according to heating or cooling season. The thermal comfort classes are the ones defined in ISO 7730. This is done using a mix between the PMV calculator tool from Ladybug/Honeybee and a GH_CPython script.

A third Python script that estimates heat gains and losses through the envelope is then used to calculate the total heat balance of the terminal. The user enters the envelope data including envelope area, WWR (Window-Wall Ratio), combined g factor and thermal properties of opaque (R_c) and glazing (U_g) elements. Setpoint and outdoor temperatures are then used to analytically determine the heat balance per room as follows:

Envelope Calculator

```
import math
import numpy as np

q_solar_list = []
q_solar_floor_field_list = []
q_solar_in_zone_list = []
q_transmission_list = []
q_transmission_floor_field_list = []
q_transmission_in_zone_list = []
q_combined_list = []

for i in range(len(_area_per_space)):
    a = _facade_area[i]
    b = _glazing_percentage[i]
    c = _glazing_g_factor[i]
    d = _q_sol
    e = _area_solar_zone[i]
    f = _area_transmission_zone[i]
    g = _area_per_space[i]
    q_solar = float(a*0.01*b*c*d)
    q_solar_list.append(q_solar)
    q_solar_floor_field = q_solar / g
    q_solar_floor_field_list.append(q_solar_floor_field)
    q_solar_in_zone = q_solar / e
    q_solar_in_zone_list.append(q_solar_in_zone)
    h = _facade_Ug[i]
    j = _facade_Rc[i]
    k = _T_outside
    l = _T_inside
    q_transmission = a*0.01*b*h*abs(k-l)
    q_transmission_list.append(q_transmission)
    q_transmission_floor_field = q_transmission/g
    q_transmission_floor_field_list.append(q_transmission_floor_field)
    q_transmission_in_zone = q_transmission/e
    q_transmission_in_zone_list.append(q_transmission_in_zone)
    q_combined = (q_transmission + q_solar)/g
```

```

q_combined_list.append(q_combined)

q_solar_floor_field_ = q_solar_floor_field_list
q_solar_in_zone_ = q_solar_in_zone_list
q_transmission_floor_field_ = q_transmission_floor_field_list
q_transmission_in_zone_ = q_transmission_in_zone_list
q_sol_and_transmission_ = q_combined_list

```

4.4 Engineering

4.4.1 Thermal Loads and Buoyancy Scripts

After the total space loads are known, the required ventilation rate for each space is calculated for a naturally ventilated space. The various thermal comfort parameters and heat loads per space are used as input for another GH_CPython script in which the total energy balance is set to zero to determine the required ventilation rate per space. An extra correction for thermal stratification within the comfort zone can be added, considering the fact that thermal comfort is measured at 1.50m height, while heat generation mainly occurs in the first 2m height of the occupied zone, meaning that the highest temperature calculated in the script is actually not the temperature experienced by the occupants. Additionally, floor heating or cooling can be added, reducing the total airflow required because air is used less for climatization purposes. The input for thermal stratification correction is left up to the user and reflects the placement of inlets and outlets, as well as the usage of floor heating/cooling.

The python script considers minimum recommended ventilation rates as stated in EN15251 too, meaning that the final ventilation rate is either derived from climatization or minimum recommended ventilation rates for indoor air quality. Because the natural ventilation concept relies heavily on free cooling/heating from large volume flow rates, often indoor air quality minimum ventilation rates are always met. The full python script to determine the required ventilation rate is as follows:

Ventilation Rate Calculator

```

import numpy as np

Q_per_space_per_m2_ = []
Q_per_space_total_ = []
Q_people_eq_per_space_ = []
Qperspaceperm2 = int
Qperspacetotal = int
Q_ventilation_per_space_ = []
heatingperm2 = int(_heating_per_m2)
Qventilationperspace = int

for i in range(len(_area_per_space)) :
    a= _occupancy_per_space[i]
    b= _metabolic_rate
    c= _area_per_space[i]
    d= _Q_internal[i]

```

```

    e= _Q_transmission[i]
    f= heatingperm2
    Qperspaceperm2 = (a*b)/c+d+e
    Qperspacetotal = a*b+(d+e)*c
    Q_per_space_per_m2_.append(Qperspaceperm2)
    Q_per_space_total_.append(Qperspacetotal)
    Qventilationperspace = a*b+(d+e)*c-f*c
    Q_ventilation_per_space_.append(Qventila-
tionperspace)
    Q_people_eq_per_space = ((a*b)/c)+d
    Q_people_eq_per_space_.append(Q_peo-
ple_eq_per_space)

qvminclimatization = int

if _season == 1:
    Tsupply = _T_supply_max
    T_supply_ = _T_supply_max
elif _season == 2:
    Tsupply = _T_supply_max
    T_supply_ = _T_supply_max
elif _season == 3:
    Tsupply = _T_supply_min
    T_supply_ = _T_supply_min
print('Supply temperature = ' + ' ' + str(Tsup-
ply))

q_v_min_per_space_list = []
q_v_min_climatization_list = []
q_v_min_en15251_list = []
_T_target_list = []

for i in range(len(Q_ventilation_per_space_)):
    a= Q_ventilation_per_space_[i]
    b= 1.20
    c= 1008
    d= _T_balance + _dT_balance[i] ##+ _dT_ther-
mal_stratification
    e= Tsupply
    qvminclimatization= a/(b*c*(d-e))
    q_v_min_climatization_list.append(qvmincli-
matization)
    _T_target_list.append(d)

T_target_ = _T_target_list

qvminen15251 = int
qvperperson = int
qvperarea = int
qvperperson_list = []
qvperarea_list =[]

for i in range(len(_PPD)):
    if _PPD <= 10:
        qvperperson = 0.01
        qvperarea = 0.001
    else:
        qvperperson = 0.007
        qvperarea = 0.0007
    qvperperson_list.append(qvperperson)
    qvperarea_list.append(qvperarea)

for i in range(len(Q_ventilation_per_space_)):
    a= _occupancy_per_space[i]

```

```

b= qvperperson_list[i]
c= _area_per_space[i]
d= qvperarea_list[i]
qvminen15251= a*b + c*d
q_v_min_en15251_list.append(qvminen15251)

#print('qvminen15251 =' + ' ' +
str(qvminen15251) + ' ' + 'm3/s')
print(q_v_min_en15251_list)

q_v_min_per_space_list = list(map(max,
zip(q_v_min_en15251_list, q_v_min_climatiza-
tion_list)))
print('q_v_min_per_space = ' +
str(q_v_min_per_space_list))
q_v_min_per_space_ = q_v_min_per_space_list
q_v_min_total_ = sum(q_v_min_per_space_)

```

When the required ventilation rates are calculated for the space, the total energy balance per space is solved. However, this is the average value over the whole floor field of each space, meaning that it does not consider the distribution of this heat. Therefore, the heat load needs to be 'distributed' geometrically over the floor field. To this extent the various zones that contain different heat loads need to be put in as a set of closed curves. The model currently contains heat loads due to occupancy and equipment, solar loads and façade transmission. All values are calculated as W/m^2 heat load per analysis gridpoint. These gridpoints are created as the center of 1×1 m grids in the building and are selected using a GH_Python script.

In order to work with extra heat load values per square meter, the script runs an inclusivity test for each curve and gridpoint. The heat load in W/m^2 is translated into a new list based on the index in the total gridpoints list. Points within a curve are assigned a heat load value, appending that initial list value. However, once this operation is finished it is not possible to export these points again: this is because of the fact that the whole operation is run in a nested for loop, which causes a list in list of points, something that GH_Python and Grasshopper cannot read back to geometry easily. However, the thermal values are correctly added using the following script:

Heat Load Points Calculator

```

import Rhino.Geometry as rg
import Grasshopper as gh
import rhinoscriptsyntax as rs
import clr
clr.AddReference("Grasshopper")
import Grasshopper.Kernel.Data.GH_Path as ghpath
import Grasshopper.DataTree as datatree
from Grasshopper.Kernel.Data import GH_Path
import System
import ghpythonlib.components as ghc

is_inside_list=[]

```

```

is_inside_transmission_list=[]
transmission_points_list=[]
transmission_curves=list(transmission_zone_curves)
heat_load_points_list = list(heat_load_points)
datatuples=[]
for i in range(len(heat_load_points)):
    dataTuple=tuple(heat_load_points[i])
    dataTuple=(dataTuple[0],dataTuple[1],dataTuple[2])
    datatuples.append(dataTuple)

out_points_list=[]
heat_points_out_list=[]
ylist=[]
zlist=[]
xlist=list(zip(*datatuples))
z_coordinates_list=[]
is_inside_occupancy_list=[]
occupancy_points_list=[]
is_inside_solar_list=[]
solar_points_list=[]

for i in range(len(heat_load_points)):
    z_coordinate=heat_load_points[i][2]
    z_coordinates_list.append(z_coordinate)

for i in range(len(transmission_zone_curves)):
    for j in range(len(heat_load_points)):
        is_inside_occupancy= (spaces[i].Contains(heat_load_points[j]) == rg.PointContainment.Inside)
        is_inside_occupancy_list.append(is_inside_occupancy)
        if is_inside_occupancy==True:
            occupancy_points_list.append(heat_load_points)
            z_coordinates_list[j]=z_coordinates_list[j]+occupancy_equipment_heat_load[i]

        is_inside_transmission= (transmission_zone_curves[i].Contains(heat_load_points[j]) == rg.PointContainment.Inside)
        is_inside_transmission_list.append(is_inside_transmission)
        if is_inside_transmission==True:
            transmission_points_list.append(heat_load_points)
            z_coordinates_list[j]=z_coordinates_list[j]+transmission_heat_load[i]

        is_inside_solar= (solar_zone_curves[i].Contains(heat_load_points[j]) == rg.PointContainment.Inside)
        is_inside_solar_list.append(is_inside_solar)
        if is_inside_solar==True:
            solar_points_list.append(heat_load_points)
            z_coordinates_list[j]=z_coordinates_list[j]+solar_heat_load[i]
heat_load_values=z_coordinates_list

```

The results per heat load point are additionally colored for visualization purposes and used as a base for creating volumetric heat load boxes. These boxes of 1x1x2m represent the area heat load for each gridpoint as a volumetric heat load in W/m^3 in the first two meters of the floor field. These boxes represent heat generation more accurately in the space, especially for the case of people as a heat source. The boxes are then deconstructed, with their two outermost corner coordinates being extracted for usage in generating input data for the CFD simulation later.

The thermal buoyancy in the space is afterwards calculated through an analytical formula in a GH_CPython script. Additional pressures can be specified per space, increasing the stack height required. The script returns the stack height per space and effective area required for the airflow to occur and is constructed as follows:

Buoyancy Calculator

```
import numpy as np
A_effective_per_space_list=[]
dT_per_space_list=[]
h_max_per_space_list=[]

for i in range(len(_q_v_min_per_space)):
    a=float(_g)
    b=float(_c_d)
    c=_q_v_min_per_space[i]
    d=float(_T_supply)
    e=float(_T_target[i])
    f=_h_stack[i]
    g=abs(e-d)/(e+273)
    h=np.sqrt(2*a*f*g)
    Aeffperspace=float
    Aeffperspace= c/(b*h)
    A_effective_per_space_list.append(Aeffper-
space)
    A_effective_per_space_=A_effec-
tive_per_space_list
    j=abs(e-d)
    dT_per_space_list.append(j)
    dT_per_space_=dT_per_space_list

dP_initial_list = []
h_stack_new_list = []

for i in range(len(_h_stack)):
    d=float(_T_supply)
    e=float(_T_target[i])
    f=float(_dP_extra[i])
    dh = f/(1.21*9.81*(abs(e-d)/(e+273)))
    h_stack_new = round(_h_stack[i] + dh)
    h_stack_new_list.append(h_stack_new)
    dP_initial = 1.21*9.81*_h_stack[i]*(abs(e-
d)/(e+273))
    dP_initial_list.append(dP_initial)

dP_initial_ = dP_initial_list
h_stack_ = h_stack_new_list
```


4.4.2 Air Distribution

4.4.2.1 Background

After the necessary stack height and effective airflow area is calculated, the effective area needs to be translated to a number of inlets and outlets that have the same effective area as the calculated value. For any ventilation design, mechanical or natural, the placement of these air inlets and outlets is of critical importance to the final thermal comfort. Especially the placement and properties of air inlets is important, as air supply is considered the more difficult and delicate part of air distribution. To quote D. van der Beijl, Conceptual Designer at Croonwolter & dros:

“You can easily blow out a candle, but not suck out a candle. It is the air supply that is more important.”

To this extent, various hand sketches and designs are discussed and presented to see how air distribution can best be implemented in a naturally ventilated building and the computational script. In directional terms, air can enter and leave the terminal from below, above or from the sides of the structure. Methods to do this include:

- Simple openings
- Plenum spaces
- Tall stacks

Combining the three directions and the three methods of air distribution yields nine different alternatives for the whole ventilation concept in the design. Supplying and removing air through plenums and tall stacks, both of which are able to provide for high airflow rates without direct openings outward, seems to stand out above other options. Additionally, the usage of stacks on the roof side and the usage of a central plenum-like space under the terminal allows for ventilation to be provided deeply into the terminal, allowing for fresh air to enter there as well.

From an architectural composition point of view, however, there are also less technical arguments. For instance, the usage of large plenums around the building could give the terminal a closed look and would require an alteration to the floor plan (larger footprint). Tower stacks on the other hand have a very particular architectural expression, that needs to be carefully designed. All too easily could it turn into a ‘medieval’ or ‘romantic’ sort of expression, while the main goal of this thesis is to come up with an architectural geometry that is optimized for ventilation performance.

When looking at the various options, supplying in air from below and extracting it from above is the best option as mentioned earlier. Using a supply plenum below and exhaust stacks above will provide for the desired air effect. Additionally, by using a solar chimney at the exhaust stacks in combination with wind-driven exhaust flaps, it should be possible to adequately channel airflow from below to above in summer situations.

Placing inlets at floor levels require additional care in placement and execution. If more open floor diffusers are used, the risk of people or equipment falling in them is large. If diffusers are made fully walkable, however, their effective area decreases, requiring more air inlets. As such, a proper solution needs to be decided on before floor diffusers are placed: each of them has specific pressure drops and ventilation rates. If very closed diffusers are selected, the total resistance they produce might be in the range of 20Pa, which would be far more than the pressure difference provided for by thermal buoyancy.

Another possibility is the usage of vertical air diffusers that are supplied from the floor. Although they are visually more prominent, they allow for more horizontal distribution of air and can create a more usable floor area. Examples of vertical air diffusers are many, also in airports, such as shown in the figure for Istanbul Airport.

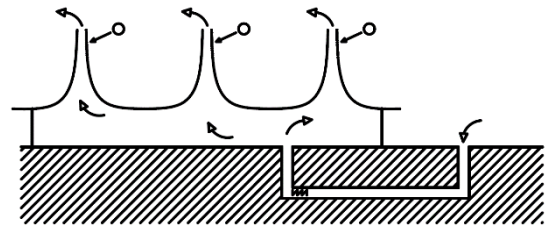


Figure 85 The preferred air distribution solution as a diagram.



Figure 86 Vertical diffusers implemented at Istanbul Airport.

4.4.2.2 Experimentation Setup

The computational (design) process is preceded by initial CFD exploration to explore the available design space and the inter-relation between various input parameters and outcomes. By decreasing the size of the to-be-analyzed domain and the possible number of outcomes, the computational process later is streamlined towards faster generation of an optimized design. This experimental design phase is conducted using the manual design based on initial topological decisions and the Python scripts and is entered into Cham Phoenix 2018 v1.3.

For any architectural engineering design, the initial design steps and assumptions made are both extremely important as well as very determining for the later outcome of the final design. As the famous saying goes:

“Garbage in, garbage out.”

Or in the more recently used ironic form (in which the outcome of a black box process is taken as a holy, undisputed result):

“Garbage in, Gospel out.”

Indicating that the outcome of any (computerized) process is only as reliable as the data put into it in the first place. As the design task in many architectural engineering applications is complex -and even more so in the field of ventilation and CFD- computational methods are employed to help in the design process and increase the reliability of the outcome. Therefore, the correct set-up of the computational design process is extremely important, besides the correct design in the first place.

This setup for the computational design process is preceded by “Design Space Exploration” (DSE), in our case simply called the “design” phase. In the subsequent engineering phase, the ‘Design of Experiments’ or ‘DOE’, whose aim is to “determine the relationship between factors affecting a process and the output of that process” is performed. By using a systematic DOE process, it will be possible to identify and guide the design towards a direction of interest that is sufficiently narrowed down to be subjected to the optimization process. After all, even with current advances in computation, exploring many design options using CFD will take considerable amount of time and computing power.

To fine-tune the decisions taken in the design phase and in order to set up the design for optimization, the following aspects are analyzed:

1. Manual – CFD comparison

Validating the CFD model by checking its accuracy (convergence and energy balance). Total computing times for complex and surrogate (simplified) models. Comparing the manual design values from the Python scripts against the values from the CFD simulation and noting the final temperatures, thermal comfort parameters and airflow.

2. CFD settings exploration

Gauging the influence of the following aspects on the final accuracy and computing time of the results: convergence criteria, meshing settings, turbulence settings, solver types and radiation effects.

3. CFD design exploration

Exploring various designs, including changing inlet/outlet sizes, locations, air speeds, supply and ambient temperatures, geometry and solar chimneys and their effects on air distribution and thermal comfort.

4. Best practices, insights and difficulties

A sum-up of various insights gained during the process of experimental design with CFD simulations and how they can be used to narrow down the available design space.

5. Integration with GA's

Finally, the integration of the design process with genetic algorithms will be explored. Aspects such as available programs, objective functions, computation speed and initial gene selection will be considered.

4.4.2.3 Manual-CFD Comparison

In order to ensure that the CFD calculations are correct, a basic hall of 60x70x12m is designed and calculated based on the following parameters:

- Hall size: 60x70x12m (LxWxH)
- Floor area: 4200m²
- Level of Service: 1.8m²/person
- Occupancy: 2335 people
- Q_{internal} : 41.7W/m³ in the bottom 1.8m height of the terminal (based on 68W/m² people + 7W/m² generic loads)
- T_{ambient} : 18°C
- T_{supply} : 18°C
- $T_{\text{inside(target)}}$: 25°C
- $Q_{v,\text{req}}$: 37.1m³/s (133560 m³/h, 15.9L/s.person)
- $V_{\text{max, inlet}}$: 0.2m/s

- A_{inlets} : $185.5m^2$ (for $C_d=1$)
- # of inlets: 515 (for 60x60cm inlets, spaced in a 19x27 grid equaling 513 inlets)
- H_{stack} : 12m
- A_{eq} : $22.18m^2$ (if $C_d=1$)
- A_{outlet} : $22.34m^2$ (if $C_d=1$) (spaced in a 3x4 grid of 1.36x1.36m openings)

And the following settings:

- Energy equation: temperature
- Turbulence model: Chen-Kim KE
- Reference pressure: 101325Pa
- Initialization and buoyancy from ambient: ON
- Buoyancy model: density difference
- Reference density: $1.213219 kg/m^3$
- Buoyancy effect on turbulence: ON (0.3)
- Radiation models: ON (IMMERSOL)

Firstly, the model needs to be validated by checking the following parameters:

- Convergence: the total % error after 1500 runs was still not below the cutoff point of 0.01% for all variables. Especially kinetic energy (KE) was off, other values were either within cutoff range or very close.
- Maximum temperature: the highest temperature was noted at $25.91^\circ C$, which is above the expected value of $25^\circ C$. However, as will be shown later, this is due to the lower airflow rate. When corrected for the lower flow rate, the temperature is correct to within $0.3^\circ C$.
- Energy balance: the energy balance converged very well, with an overall residual of only 11W, equaling $5.13 \cdot 10^{-4}\%$ error.

Based on these results, it is possible to say that, although the model could use more refinement, in the main energy balance has settled and the outcomes can be deemed useful.

When considering the value differences between the manual calculations and the CFD simulation however, larger differences appear. The expected airflow rate was $37.1m^3/s$, while the model only produced $33.7m^3/s$, a difference of 11%. Similarly, the expected pressure difference due to buoyancy (stack pressure) was different: while the pressure difference between inlet and outlets is 2.13Pa in the CFD calculations, the expected pressure difference was 1.76Pa when based on average indoor temperature and 3.64Pa when based on maximum indoor temperature. The exact reason for this difference might depend on the manual calculation's temperature and stack height assumptions: the stack formula is normally only valid for an isothermal air column, which is not the case in the terminal as the cold

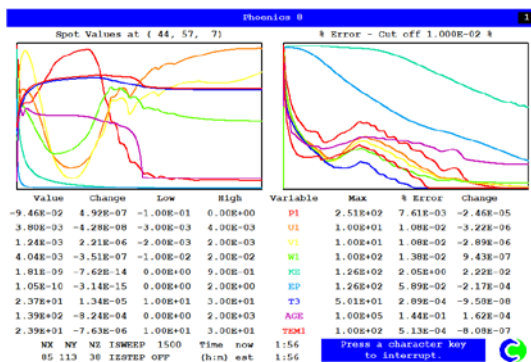


Figure 87 Convergence results for the simulation.

supply air creates a clear thermal stratification within the building. Additionally, according to the Bernoulli equation, as the outlet airspeed is significantly higher than the inlet airspeed, dynamic pressure changes also influence the expected outlet air pressure. Additionally, due to meshing constraints, determining precise outlet air pressures is more difficult.

This thermal stratification is also the most notable aspect for the temperature distribution inside the hall. The large quantity of inlets ensures that temperature is distributed very evenly, with thermal comfort criteria being reached at various heights. However, thermal stratification between inlets and head height (1.8m) also mean that vertical temperature differences are very large (in the range of over 7°C). This is a common problem with displacement ventilation, but is in part alleviated by the fact that local discomfort due to vertical temperature differences is felt less by people who are standing or have higher activity levels, as is the case in airports. Similarly, inlet speeds were half of the design speed: 0.11 m/s vs. 0.2m/s. This disparity is also difficult to explain, as the total airflow divided by inlet area (185.5m²) yields a result of 0.18m/s airspeed. The reason for the lower airspeeds might be in the resistance caused by air, pushing incoming air downward and to the sides or meshing, as inlet speed drops immediately before reaching the first measurement cell. The results of the analysis can further be seen below:

- T_{inlet} : 18.05-18.9°C (depending on inlet)
- T_{outlet} : ~25.6 °C (depending on inlet)
- T_{max} : 25.92 °C
- v_{inlet} : 0.092-0.11 m/s
- v_{outlet} : 1.25m/s
- P_{inlet} : -0.27Pa
- P_{outlet} : 1.96Pa
- P_{max} : 3.19Pa
- AGE_{max} : 2294s (1122s average)
- Ventilation efficiency: 0.74
- $q_v = 33.7m^3/s$ ($n=2.14ACH$)

Height	T_{air}	v_{air}	PMV	PPDR	PPD	AGE
0.10m	19.9°C	0.050m/s	-0.55	4.18%	11.8%	35.6s
0.50m	21.6°C	0.024m/s	-0.26	0.14%	6.6%	73.3s
1.10m	24.0°C	0.013m/s	0.14	0.02%	5.5%	163.6s
1.80m	24.7°C	0.018m/s	0.41	0.16%	8.5%	748.8s

Figure 88 Thermal comfort at various heights, including air temperature, airspeed, PMV, PPDR, PPD and age of air.

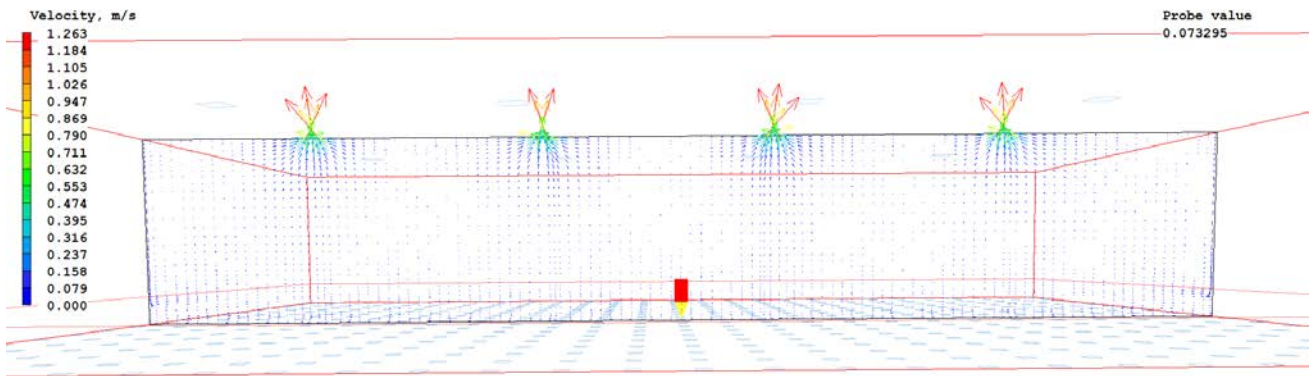
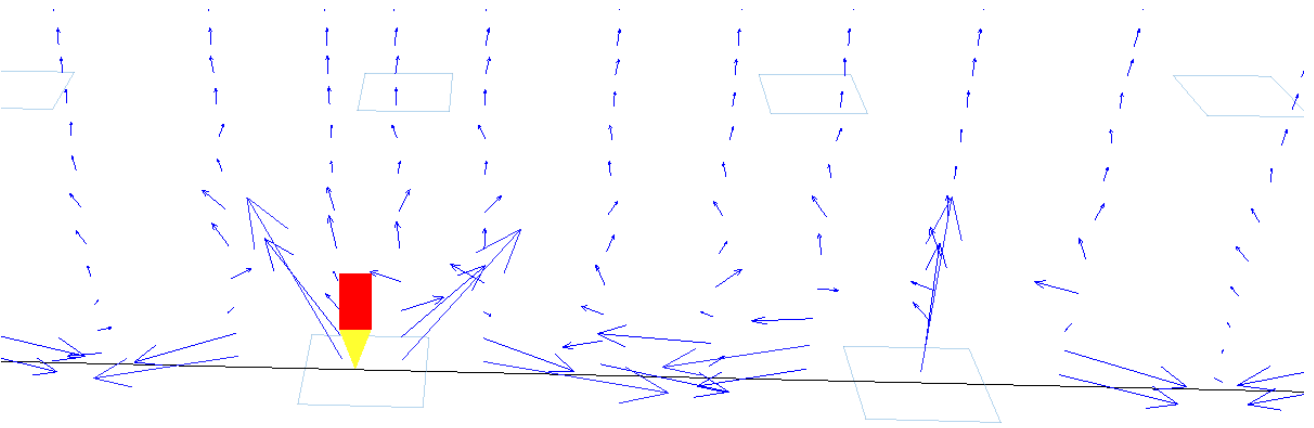
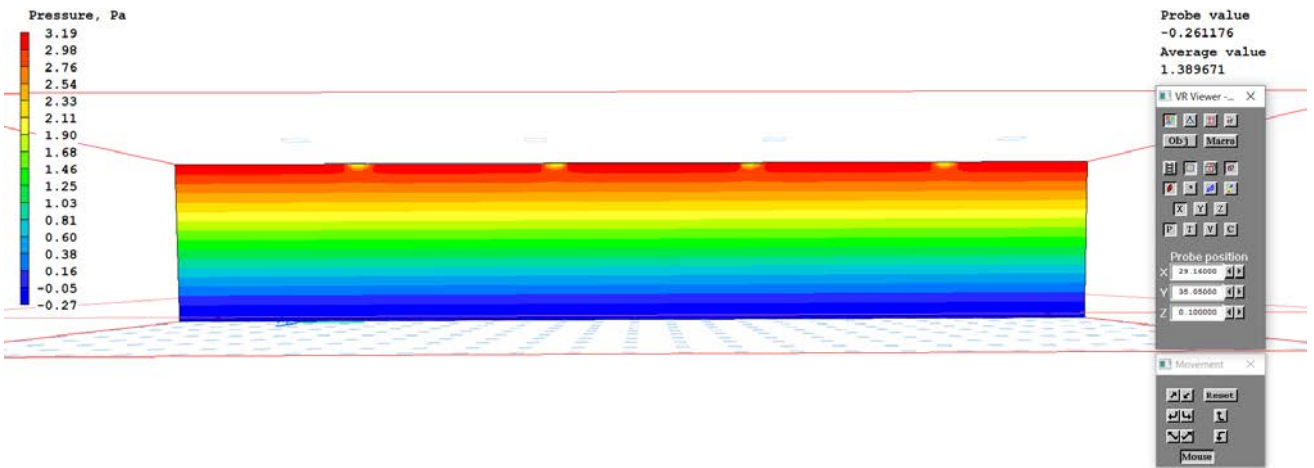
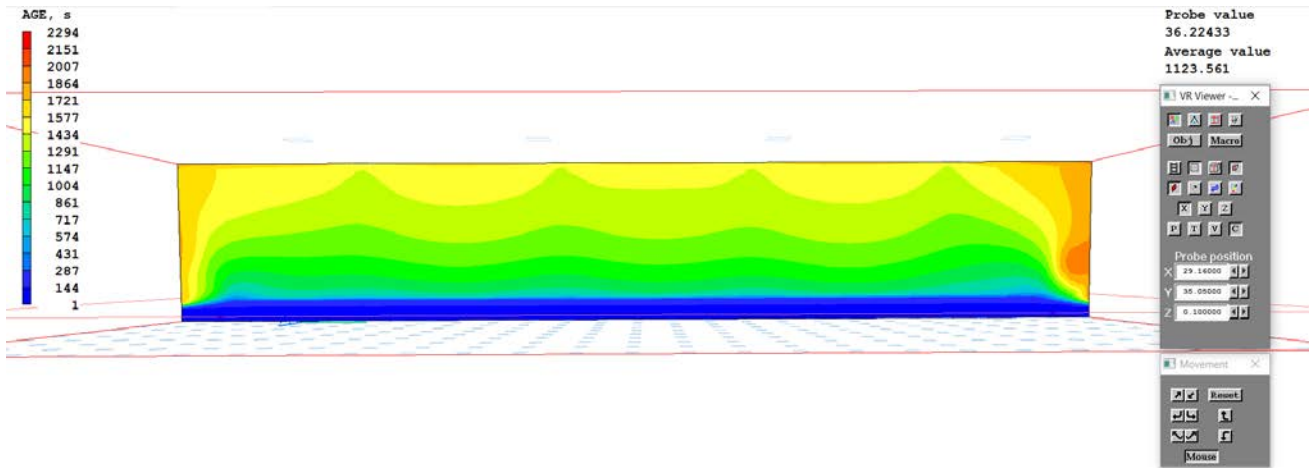


Figure 89 Results of the analyzed hall, showing pressure distribution, age of air, a zoom-in of the inlet and the velocity profile.

As can be seen from the results, the natural ventilation concept provides very high levels of thermal comfort and high ventilation effectiveness: with an effectiveness of 0.74, it is right in the middle between common mixing systems (0.5) and ideal displacement systems (1). Air distribution nearly everywhere is very good, with thermal stratification being well-visible in the results. Similarly, besides for the envelope and in the corners of the hall, air ages are low, meaning that air is replaced quickly.

Thermal comfort levels at a height of 1.1 m (neck height of sitting people) is excellent, reaching Category A, while at head level for standing people a thermal comfort level Category B is reached. The thermal comfort at 1.8m is mainly compromised due to high temperatures (high PMV), while at lower heights closer to the in-lets Category A and B levels are still possible. Local discomfort other than draught rate, however, is not taken into account. Even so, if air can be supplied at such temperatures and speeds, an excellent thermal comfort level can be attained for an ambient temperature of 18°C.

However, there are some notes to be made on the simulation itself. Firstly, losses or gains through the façade are not considered, while this can cause additional downdraught at the envelope, less heat buildup and additional discomfort due to radiant asymmetry. Secondly, the number of inlets is high, covering nearly 4.4% of the floor area, which would clearly influence placement of objects/equipment and separations. Additionally, current values are taken without considering the losses due to the orifice itself: normally, if a C_d value of 0.6-0.8 is assumed (now 1), this would result in a significantly higher required inlet area as well. Finally, the values do not correspond exactly to the initial assumptions made for the design, including inlet airspeeds which influence draught effects greatly.

The biggest caveat to the current analysis however is the time required to conduct the simulation: with a duration of over 7000s, the analysis is extremely slow yet has not converged enough to provide for high reliability in all aspects. If we consider a genetic algorithm to conduct the same analysis with an initial gene pool of 72 results and 7 mutations, this would result in a computation time of over 1008 hours or 42 days: an impossible amount within the scope of this –and probably any building- design.

4.4.2.4 CFD Settings Exploration

To speed up the CFD analysis, the development of a faster-running simulation is essential. Additionally, exploring different settings from the ones we took initially from experience in the simulation software to see the results on accuracy and speed can be useful to make the workflow more accurate or faster.

Specifically, within the scope of genetic algorithms, surrogate models can be developed that accelerate the analysis process, such as by using response surface approximation (RSA) or artificial neural networks (ANN). These models accelerate the design by evaluating the impact that input variables have on the outcome faster. Although such models are outside the scope of this thesis, the aim of these manual studies is to create a ‘manual surrogate model’, which in this case is basically a smaller version of the terminal that we intend to design. The aim of this model is to provide reasonably fast (with analysis times not exceeding 10 minutes) and accurate analyses in order to test different assumptions and concepts.

To test the speed and accuracy interrelation, both the initial full-size model as well as a smaller ‘surrogate’ model were put analyzed and their accuracy and convergence determined in a parametric multi-run using Phoenix CFD. The smaller hall has a size of 20x20x12m, equaling roughly a tenth of the real hall in terms of floor area. The same values were used as for the larger variant, as if the design were a section of the real terminal. The results are given in the tables below.

	Run 1	Run 2	Run 3	Run 4	Run 5
Sweeps	140	280	430	860	1500
Run time [s]	306	604	927	1851	3186
Residence time [s]	853	850	851	854	851
Difference vs 1500 sweeps	0.24%	-0.12%	0.00%	0.35%	n/a
ACH [1/h]	4.22	4.23	4.23	4.21	4.23
Difference vs 1500 sweeps	-0.24%	0.00%	0.00%	-0.47%	n/a
Volume flow rate [m3/h]	5.62	5.65	5.67	5.62	5.64
Difference vs 1500 sweeps	-0.35%	0.18%	0.53%	-0.35%	n/a
% error - P1	1.86E-01	2.25E-01	3.80E-01	3.64E-02	1.32E-02
% error - U1	2.02E-01	1.19E-01	2.04E-01	1.19E-01	7.52E-02
% error - V1	1.80E-01	1.13E-01	1.98E-01	1.18E-01	8.07E-02
% error - W1	3.24E-01	2.10E-01	3.52E-01	2.07E-01	1.46E-01
% error - KE	1.16E+02	1.05E+02	8.37E+01	8.95E+00	9.11E-01
% error - EP	7.95E+01	2.75E+01	6.97E+00	3.95E-01	2.20E-01
% error - T3	3.19E-02	2.47E-02	1.85E-02	6.28E-03	1.96E-03
% error - AGE	7.89E-01	9.15E-01	1.63E+00	6.06E-01	2.04E-01
% error - TEM1	2.76E-02	5.03E-02	7.97E-02	4.44E-03	9.09E-04
Average PMV at 1.5m height	-0.16	-0.155	-0.146	-0.212	-0.21
Difference vs 1500 sweeps	-23.81%	-26.19%	-30.48%	0.95%	n/a

Figure 90 Results of the surrogate model in amount of sweeps

	Run 1	Run 2	Run 3	Run 4	Run 5
Sweeps	140	280	430	860	1500
Run time [s]	660	1322	2083	8658	7003
Residence time [s]	1587	1499	1468	1487	1493
Difference vs 1500 sweeps	6.30%	0.40%	-1.67%	-0.40%	n/a
ACH [1/h]	2.27	2.4	2.45	2.42	2.41
Difference vs 1500 sweeps	-5.81%	-0.41%	1.66%	0.41%	n/a
Volume flow rate [m3/h]	31.7	33.6	34.3	33.9	33.8
Difference vs 1500 sweeps	-6.21%	-0.59%	1.48%	0.30%	n/a
% error - P1	6.27E-01	2.71E-01	7.64E-01	1.05E-01	2.30E-03
% error - U1	9.69E-02	4.19E-02	9.42E-02	2.53E-02	3.11E-04
% error - V1	8.86E-02	3.68E-02	7.94E-02	2.17E-02	2.77E-04
% error - W1	1.96E-01	5.64E-02	1.17E-01	2.21E-02	3.91E-04
% error - KE	1.16E+02	1.09E+02	9.92E+01	2.81E+01	7.35E+01
% error - EP	8.14E+01	2.87E+01	8.09E+00	5.85E-01	9.97E+01
% error - T3	1.42E-01	4.06E-02	3.76E-02	8.00E-03	0.00E+00
% error - AGE	1.37E+00	9.16E-01	2.23E+00	1.25E+00	1.84E+05
% error - TEM1	7.27E-02	6.83E-02	1.30E-01	1.29E-02	0.00E+00
Average PMV at 1.5m height	0.278	0.365	0.408	0.37	0.332
Difference vs 1500 sweeps	-16.27%	9.94%	22.89%	11.45%	n/a

Figure 91 Results of the main model in amount of sweeps

The results from the analysis show clearly that the difference in the amount of runs for the overall balance of the hall is minimal, especially in the case of the surrogate model. Differences between making 140 sweeps against 1500 is below 0.35% regarding the total thermal balance (residence time, air changes per hour and volumetric flow rate) for the surrogate model and below 6.3% for the main model. In the case of the PMV at 1.5m height however, there is a larger inconsistency measured. This could be explained by the fact that thermal comfort is measured

from a range of parameters, of which the cumulative error will account for a larger final difference.

Additionally, increasing the amount of runs does not necessarily lead to a trend of increasing accuracy. Especially at 430 sweeps, values differ greatly from the expected pattern. However, this inconsistency might also be continued as the amount of runs increases: after all, 1500 runs is still not a fully converged solution either.

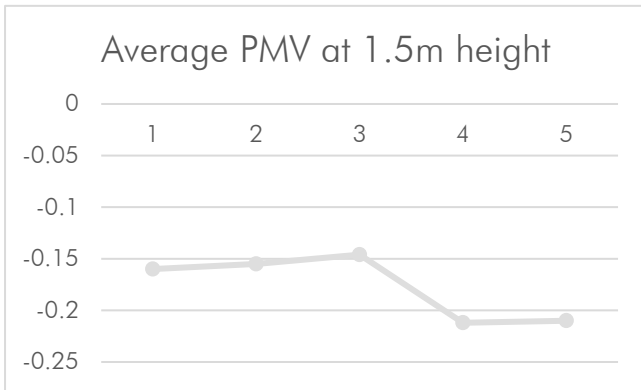


Figure 92 Average PMV results of the surrogate model for runs 1 through 5 (140 through 1500 sweeps). Notice the results at 430 sweeps (3rd run).

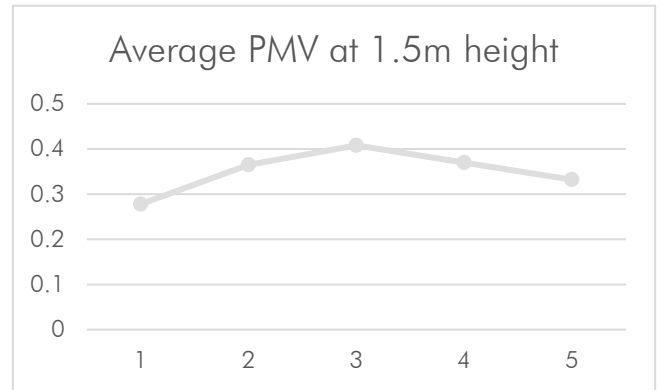


Figure 93 Average PMV results of the main model for runs 1 through 5 (140 through 1500 sweeps). Notice the results at 430 sweeps (3rd run).

However, the most noticeable trend is that a larger model has larger differences in accuracy between the amount of sweeps. While the difference is negligible in the case of the surrogate model, it reaches over 6.3% in the case of the main model. Although this is over 20x larger in terms of differences, it is still an error that is very small when considering that 95% accuracy (5% difference) is a normally held benchmark.

In a second exploration of the CFD solver, the meshing was investigated in order to see the effects of meshing on the final results. To this extent, a parametric multi-run was performed in Phoenix CFD with meshing in the initial amount of grid cells determined by Phoenix and multiple factors of it. Increasing the mesh amount does not yield a more accurate result for the aspects analyzed, for instance by grading more cells towards the bottom floor plane or increasing total cell count. This is also reasonable, because the Phoenix meshing initially is already of (adequate) fineness.

Similarly, various types of solvers were tested for the CFD simulations in Phoenics, including:

- Radiation: OFF (normally: Immersol)
- Buoyancy Solver: Constant, Boussinesq (normally: density difference)
- Turbulence: Laminar (normally: Chen-Kim KE)

To speed up the testing itself, a standard setting of 860 sweeps was conducted with each setting. The effects of testing these various solver settings are listed in the table below and will be elaborated thereafter. Laminar flows were not run with the settings presented in the thermal buoyancy solver and are therefore left blank.

	Boussinesq	Constant Rho	Laminar	Radiation OFF	Regular
Sweeps	860	860	-	860	860
Run time [s]	2134	1605	-	1679	1851
Residence time [s]	882	61	-	851	854
Difference vs 1500 sweeps	3.28%	-92.86%	-	-0.35%	n/a
ACH [1/h]	4.08	59	-	4.23	4.21
Difference vs 1500 sweeps	-3.09%	1301.43%	-	0.48%	n/a
Volume flow rate [m ³ /h]	5.44	78.64	-	5.64	5.62
Difference vs 1500 sweeps	-3.20%	1299.29%	-	0.36%	n/a
% error - P1	1.07E-01	1.32E-02	-	1.48E-02	3.64E-02
% error - U1	2.15E-01	7.52E-02	-	5.21E-02	1.19E-01
% error - V1	1.77E-01	8.07E-02	-	5.37E-02	1.18E-01
% error - W1	3.54E-01	1.46E-01	-	9.68E-02	2.07E-01
% error - KE	4.93E+01	9.11E-01	-	1.80E+01	8.95E+00
% error - EP	1.63E+00	2.20E-01	-	7.03E-01	3.95E-01
% error - T3	5.05E-01	1.96E-03	-		6.28E-03
% error - AGE	1.18E-02	2.04E-01	-	3.65E-01	6.06E-01
% error - TEM1	3.65E-02	9.09E-04	-	1.27E-03	4.44E-03
Average PMV at 1.5m height	-0.93	-1.66	-	-0.23	-0.212
Difference vs 1500 sweeps	338.68%	683.02%	-	8.49%	n/a
dP	1.84	193	-	1.96	1.95

Figure 94 Results of testing various CFD solver settings in Phoenics.

As can be seen from the testing of various CFD settings, there are very diverging results depending on what initial assumptions are made. The least difference is seen between turning radiation on or off: the difference between including radiation in the analysis or not varies the results of the surrogate model by only 0.5% in the case of the total energy balance. However, regarding thermal comfort, the differences are greater. There, a difference of over 8.5% is measured, which could be explained by the fact that mean radiant temperature is one of the aspects incorporated into a PMV calculation.

The difference in thermal comfort is even more pronounced for different solvers of thermal buoyancy, however. Using constant

density or the Boussinesq approximation to model thermal buoyancy yields results that are much more different than using other approximations: differences of over 1300% are measured. While the Boussinesq approximation yields similar results for the total thermal balance when compared to the density difference method, the results for thermal comfort are still off by over 600%. On the other hand, for the constant density method, results are very different across the range.

To understand why these differences occur, it is important to realize both how thermal buoyancy is calculated as well as how the driving force of our ventilation concept is structured. Firstly, thermal buoyancy is caused by the difference in density between air pockets of differing temperatures, causing them to be pulled more -or less- by gravity. In our case, the increase in temperature of the air inside of the terminal means that the lighter air is pushed out as heavier air replaces it. This is exactly how the standard 'density_difference' method calculates the gravitational force on an air particle. This force is then used in the momentum equations that dictate the final result of the CFD simulation.

The constant formula is computed as:

$$F = \rho \cdot g \left[\frac{N}{m^3} \right]$$

Where F= force per unit volume [N], ρ = density of air [kg/m³] and g= gravitational acceleration [m/s²].

While in the case of density difference ('reduced pressure method'), the gravitational pull per unit volume is based on the difference in density between the air particle and the average air density of the space, the so-called perturbation density:

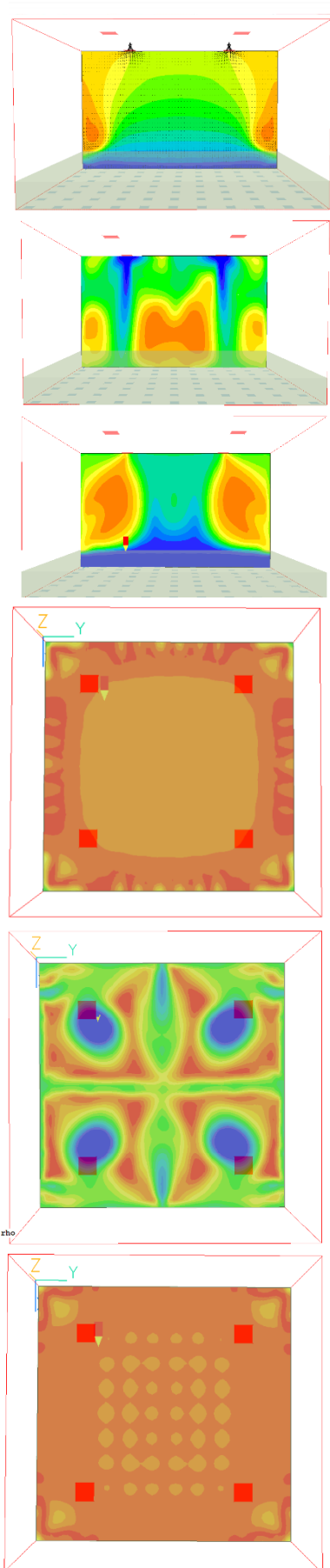
$$F = (\rho - \rho_{ref}) \cdot g \left[\frac{N}{m^3} \right]$$

Where F= force per unit volume [N], ρ = density of air [kg/m³], ρ_{ref} = average air density [kg/m³] and g= gravitational acceleration [m/s²].

In the case of the Boussinesq approximation, the force per unit volume needed for the momentum equations are solved using the assumption that density differences can be ignored everywhere except for the gravitational term. The density that is still considered for that is calculated based on:

$$\rho = \rho_0(1 - \beta \Delta T) \left[\frac{kg}{m^3} \right]$$

Where ρ = density used in the gravitational momentum equations [kg/m³], β = thermal expansion coefficient [1/K] and ΔT = temperature difference [K].



This approximation is especially used in cases of natural ventilation and thermal buoyancy. The flow is caused by density difference (a difference in temperature), yet the difference in density is ignored in the remaining continuity equations because it is very small except for the equations of gravitational pull (the buoyancy term in the momentum equation), which causes the movement. The Navier-Stokes equations are therefore simplified and the computational costs reduced (Nozaki, n.d.). However, the approximation is not suited to calculations in which there is combustion or large density differences. According to Ferziger, Peric, & Leonard (2001), the error of the approximation is in the order of 1% when differences are smaller than 15°C.

Coming back to the accuracy of thermal comfort, it is possible to understand that the option of constant density yields so differing results that it is not usable for the calculation of thermal buoyancy and natural convection. The usage of the Boussinesq approximation, however, is slightly more debatable. Differences in total thermal balance are very small (<3.3%), meaning that the total volume flow rates are nearly identical. However, thermal comfort values vary greatly, with the Boussinesq method yielding lower thermal comfort results (colder).

Upon investigation of the airflow, it is possible to see that the two models react different with regards to the air movement inside the terminal. Temperature distribution with the density difference model is nigh perfect, not changing at all once the height is above the 1.8m in which the heat is generated. On the other hand, the Boussinesq approximation has a greater temperature variance, with pockets of colder air following the general upward motion of airflow. Assuming a certain level of mixing and upward motion, the Boussinesq approximation seems to yield a more accurate airflow pattern compared to the density difference method.

Figure 95 Results of the CFD settings exploration in section (top three) and plan at 1.5m height (bottom three). The variants are from top to bottom: Boussinesq, constant rho and density difference (regular).

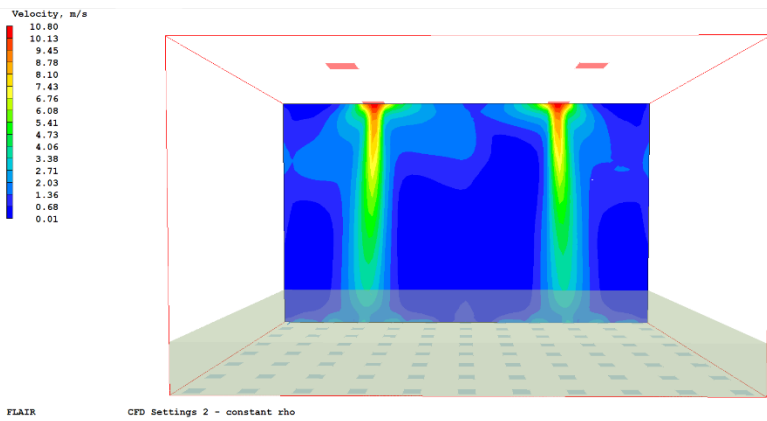


Figure 96 Obvious impossible airflow results generated by using constant rho in the CFD settings.

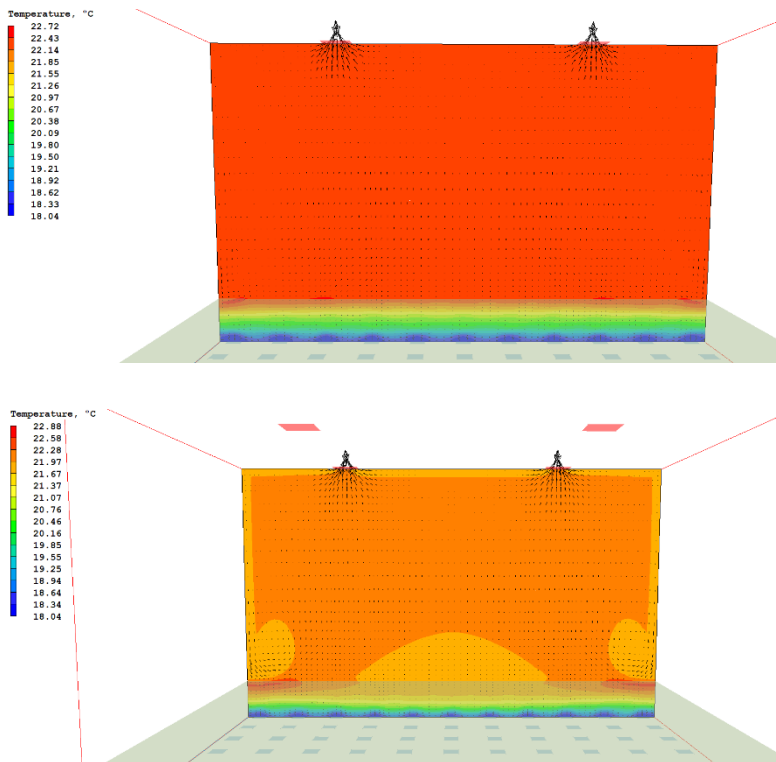


Figure 97 The difference in air temperature distribution between the density difference (regular, above) buoyancy solver and the Boussinesq solver (below).

From the aforementioned simulations, it is possible to discern that both the Boussinesq as well as the density difference methods have expectable and reasonable accuracy. Depending on the situation, both methods could be used to simulate and are able to realistically visualize expected results from manual calculation. Therefore, the decision to take either cannot be made right now and will depend on the situation in conjunction with the optimization process.

4.4.2.5 CFD Design Exploration

As part of the initial CFD design exploration, it is very important to look at the effect of conceptual design decisions that were taken. For instance, in the case of our earlier explanation of air distribution methods, the claims and assumptions were not

backed up by a CFD simulation. Although it is possible to make the optimization process find this out for us, the sheer amount of added variables and its drastic influence on the final design - such as the shape, location and type of openings and its relation to the building plan, façade and roof- means that eliminating less feasible options from the starts is more sensible.

To this extent, various options will be analyzed in terms of thermal comfort and air distribution. The variants that are analyzed include:

- Air distribution through façade or floor/roof
- Geometry of inlets/outlets
- Geometry of the roof and chimneys
- Air supply through ground ducts and plenums
- Usage of solar chimneys for summer ventilation
- Testing for 3 seasons: winter, summer and annual average

Air distribution through the façade or floor is analyzed to reach a conclusion on whether air should be supplied from below or from the side. The geometry of the inlets and outlets is analyzed to see if square openings or rectangular openings are preferable. Additionally, their size and amount could differ to play with the inlet/outlet airspeeds as well as the required amount of air distribution.

By also analyzing the initial idea of a 'fluid' geometry with smoothed chimneys it is possible to see if air distribution is enhanced by changing from a rectangular hall shape with high 'dead spots' to one that is more geared towards making air move.

Supply and removal of air is analyzed to ensure that air can be supplied in an even and balanced way if the underground option is chosen. A supply plenum from below could be used to distribute air more evenly, as more air will pass through the openings closed to the inlets outside. Towards the middle of the floor plan, supply air amounts would normally decrease.

Specifically, for the case of summer ventilation, it is possible to use solar chimneys to force air being drawn upward rather than its natural tendency to drop downward as the interior of the building is cooler than outside. To this extent, a short Python script is used to calculate the necessary solar chimney height to guarantee air will flow upward in the case of summer ventilation.

Finally, the natural ventilation concept will be tested for winter, summer and annual average conditions to ensure that in all three cases a sufficient level of thermal comfort is achieved. Additionally, the effect of heating or cooling incoming air is investigated.

	Air distribution Floor 1	Air distribution Floor 2	Air distribution Floor 2B	Air distribution Floor 3	Air distribution Floor 4	Air distribution Floor 5	Air distribution Façade 1	Air distribution Façade 2	Hall Geometry 1	Hall Geometry 2	Supply Plenum 1	Supply Plenum 2	Supply Plenum 3	Solar Chimney 1	Wind load	Season Testing - Winter	Season Testing - Summer
Model Used	AD_F_1	AD_F_2	AD_F_2B	AD_F_3	AD_F_4	AD_F_5	AD_F_6	AD_F_7	AD_F_8	AD_F_9	AD_F_10	AD_F_11	AD_F_12	AD_F_13	AD_F_14	AD_F_15	AD_F_16
Description									Roof tapers towards openings at shallow angles	Trumpet shaped roof towards openings	1m deep supply plenum under floor, open all sides	1m deep supply plenum under floor, open all corners	1m deep supply plenum under floor, open one side	Solar chimneys of 4m high with 300W/m2 radiation	1m deep supply plenum under floor, open all corners		
Sweeps	140	140	140	140	140	140	140	140	140	140	140	140	140	140	140		
Run time [s]	659	362	373	181	179	180			876	937	294	295	224	847			
Residence time [s]	1587	1644	1750	1616	1703	1673			812	862	1090	1245	2085	1988			
ACH [1/h]	2.27	2.19	2.06	2.23	2.11	2.15			4.43	4.18	3.3	2.89	1.73	1.81			
Volume flow rate [m3/s]	31.7	30.6	28.8	31.2	29.6	30.1			55.9	55.5	5.77	5.05	3.02	25.3			
# of inlets	512	36	18	6	4	3			4	4	512	1	1	512			
A inlets [m2]	184	432	216	420	440	210			440	210	184	184	20	20	20	184	
Inlet geometry	0.6x0.6m square	2.16x2.16m square	2.16x2.16m square	1.0x70.0m gutter	1.7m wide gutter along perimeter	1m wide gutter			1.7m high opening along perimeter (2.1m high)	0.85m high opening along perimeter (2.1m high)	0.6x0.6m square	0.6x0.6m square	1.0x20m gutter in middle	1.0x20m gutter in middle	1.0x20m gutter in middle	0.6x0.6m square	
# of outlets	12	12	12	12	12	12			12	12	12	4	4	4	4	12	
A outlets [m2]	22.2	56	56	56	56	56			56	56	56	5.4	5.4	5.4	56		
Outlet geometry	1.36x1.36m square	2.16x2.16m square	2.16x2.16m square	2.16x2.16m square	2.16x2.16m square	2.16x2.16m square			2.16x2.16m square	2.16x2.16m square	2.16x2.16m square	1.16x1.16m square	1.16x1.16m square	1.16x1.16m square	2.16x2.16m square		
v inlat, max [m/s]	0.2	0.2	0.4	0.2	0.2	0.4			0.2	0.2	0.2	0.2	0.2	0.2	0.2		
dP [Pa]	3.26	4.16	4.12	3.4	4.16	3.6			2.47	2.98	2.24						
Average PMV at 1.5m height	0.278	0.291	0.3	0.291	0.109	0.228			-0.105	-0.098	-0.284	-0.18	0.374	1.07			
Average PMV at 1.1m height	0.271	0.271	0.267	0.274	0.064	0.175			-0.12	-0.116	-0.298	-0.197	0.352	1.06			
Average PMV at 0.1m height	-0.032	0.003	-0.031	0.033	-0.137	-0.14			-0.66	-0.68	-0.646	-0.603	-0.128	0.624			

Figure 98 Results from the CFD design experiments

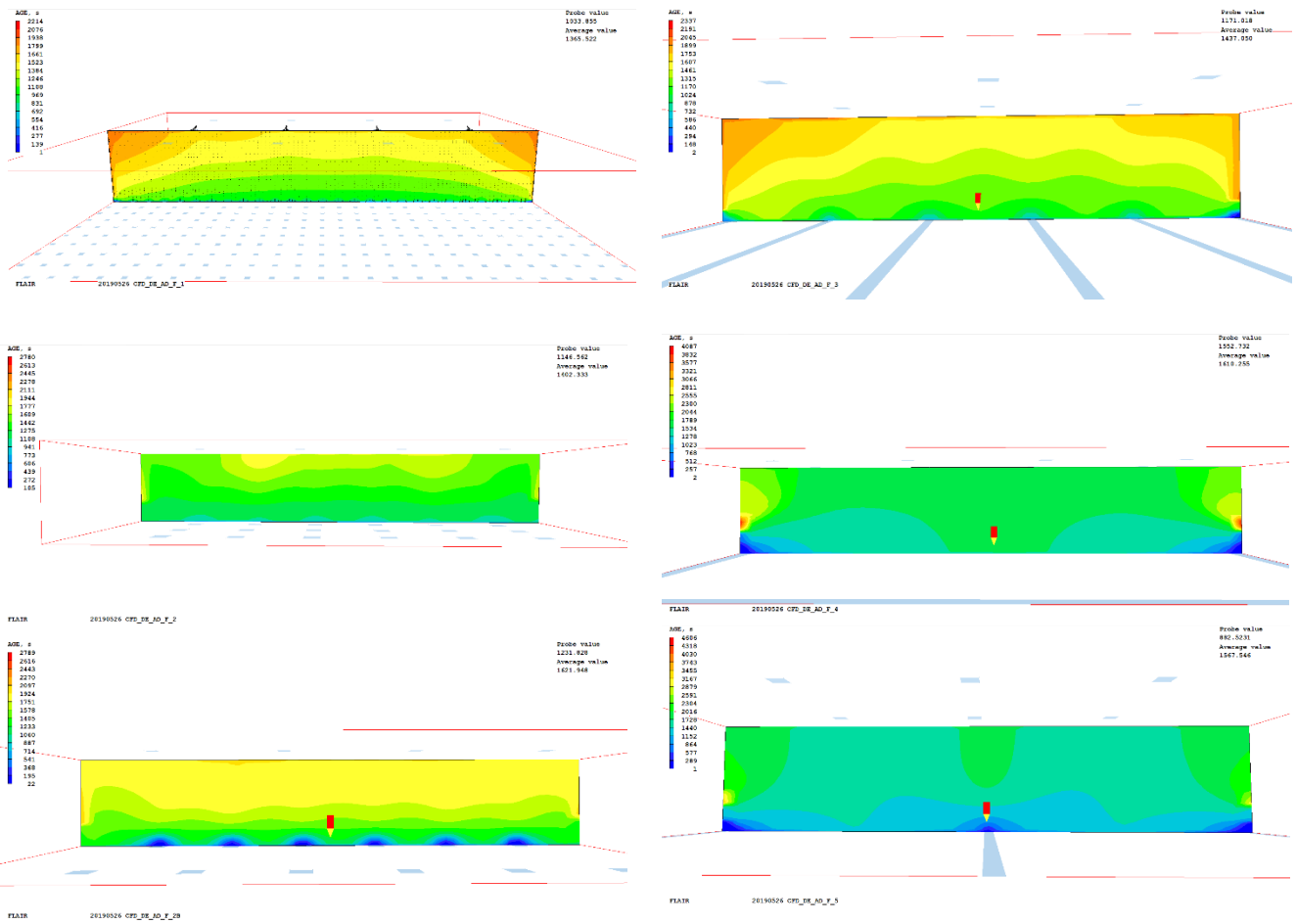


Figure 99 Results from analyses 1 through 5, showing the age of air

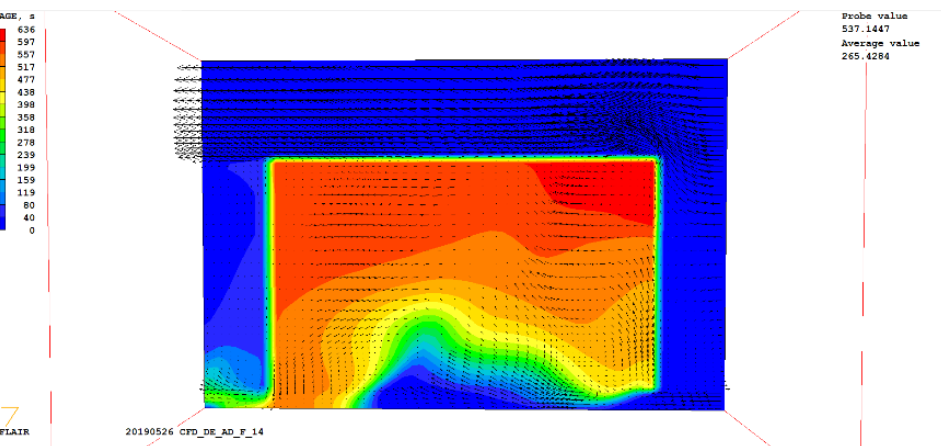
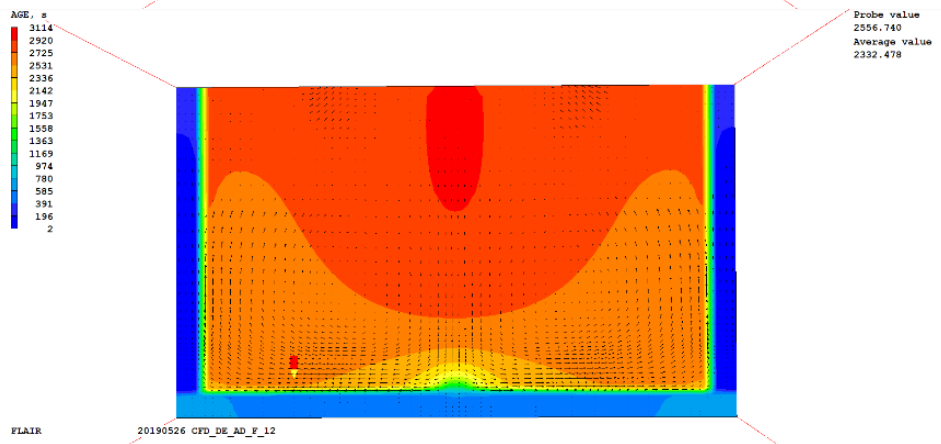
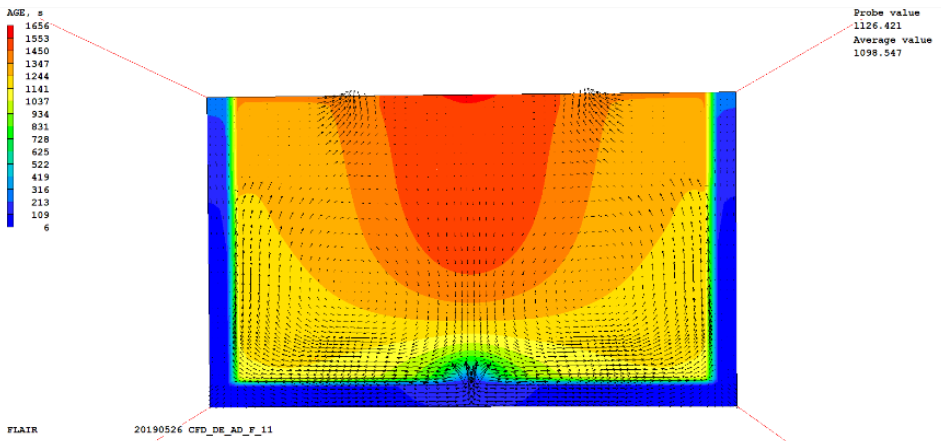
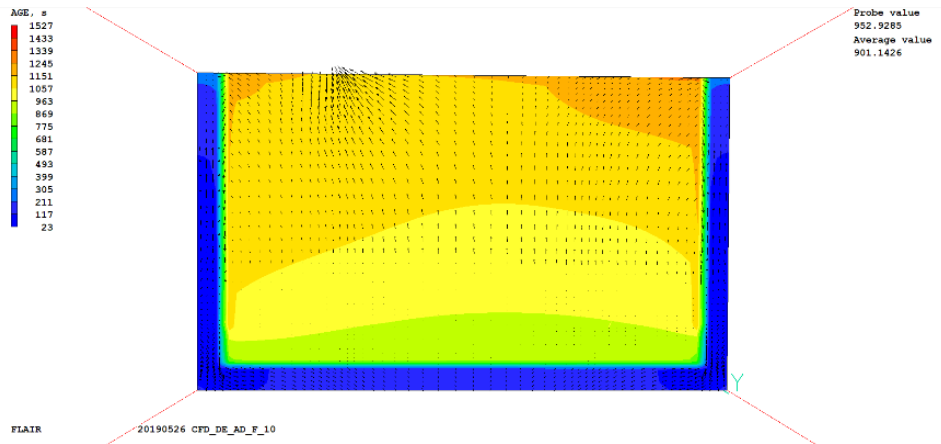


Figure 100 Results for the implementation of a supply plenum under the floor

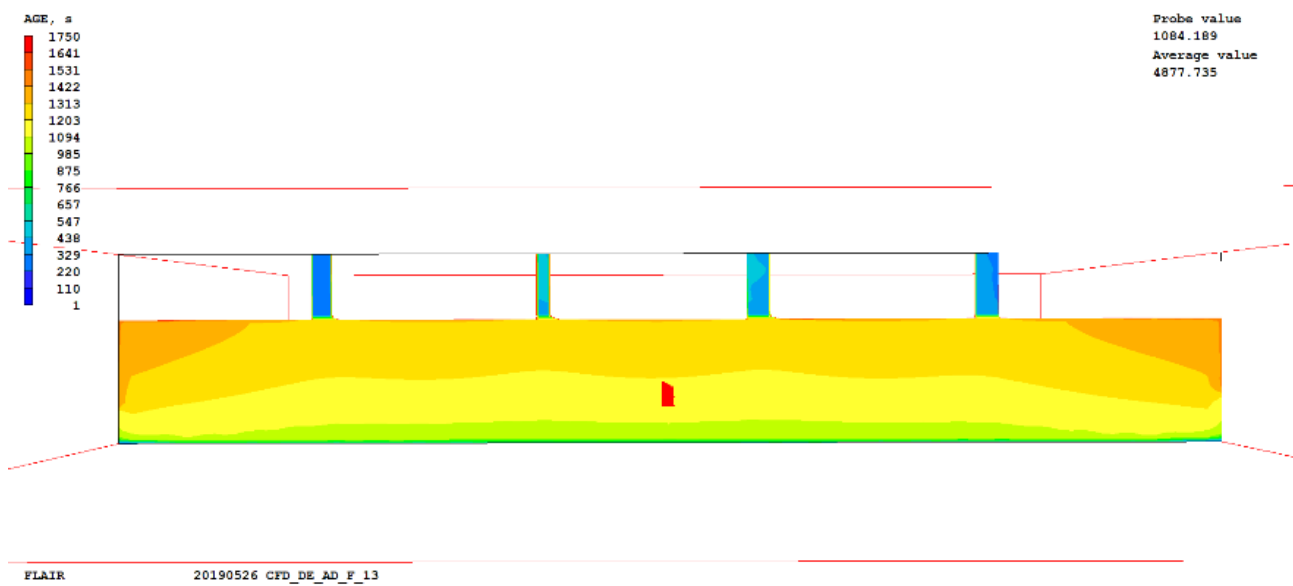
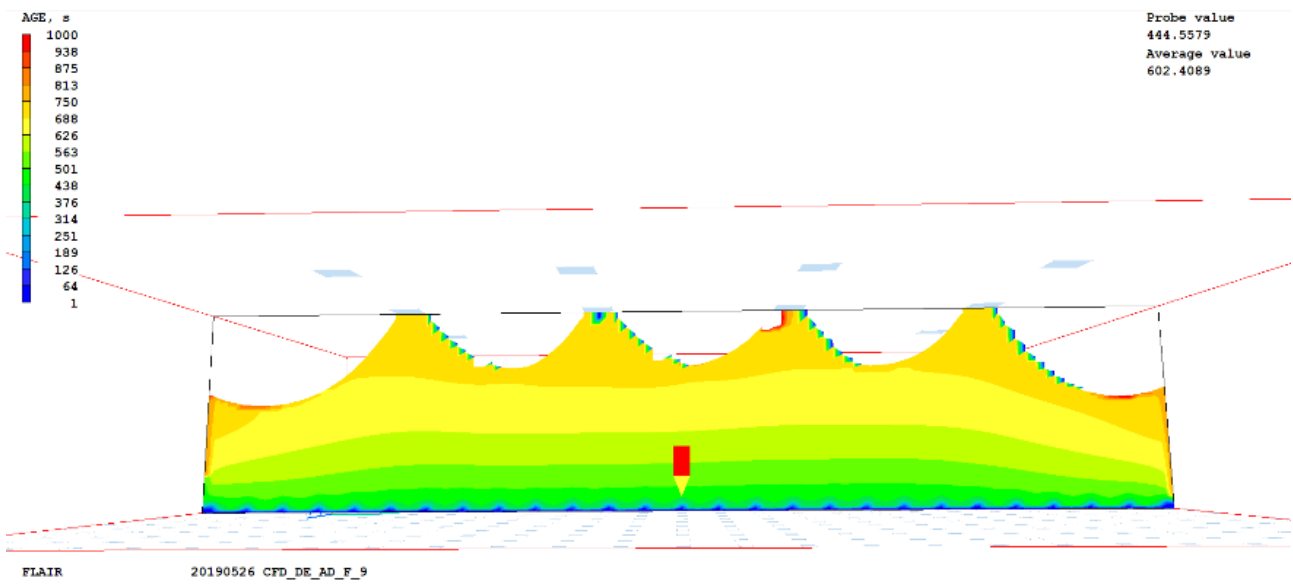
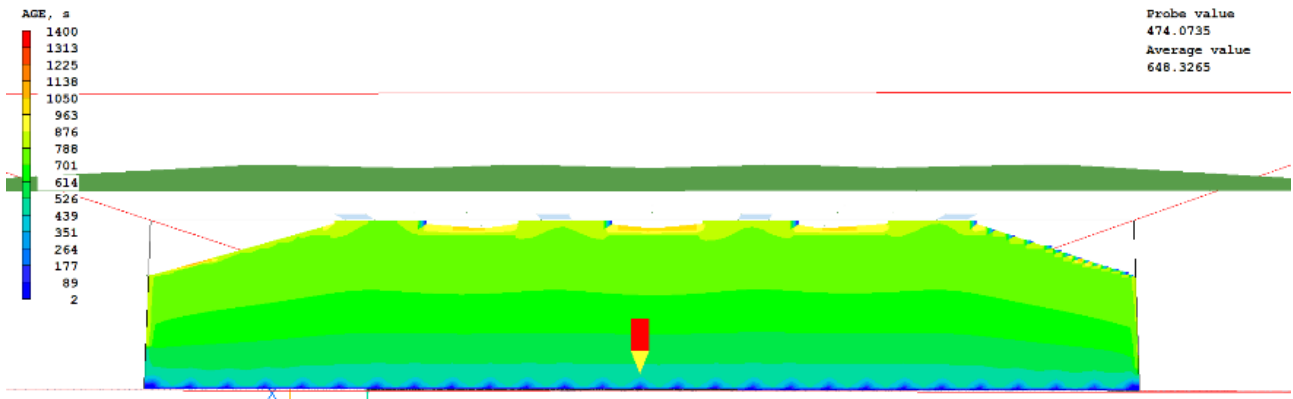


Figure 101 Age of air results for the edited geometries (top two) and chimney stacks (bottom)

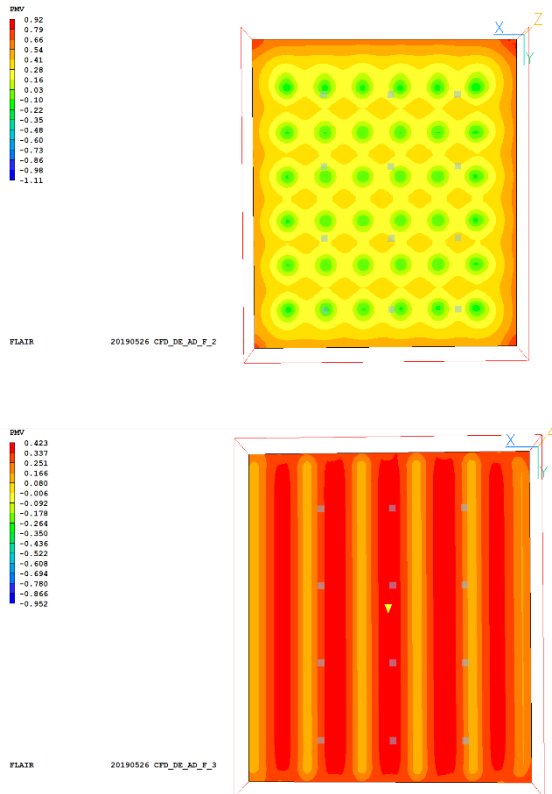


Figure 102 Example of small inlets versus gutter inlets in thermal comfort distribution

In short, when looking at average thermal comfort values, it is possible to see that low inlet airspeeds with high amounts of inlets perform the best as expected. However, options with 0.4m/s airspeeds still perform within nearly identical range yet with half the inlets; however, differences over the range of the whole floor area increase.

Similarly, the variance in distribution between average PMV vs. the extents are more noticeable in the case of gutters as inlets. As the amount of gutters is drastically lower than square inlets (3-4 gutters against over 200-500 inlets) 'dead spots' start to emerge in between the gutters themselves. This effect is also pronounced when supply is only from the façade sides, in which case hotspots appear in the middle of the plan. However, even there, an average of 1ACH is attained, with air distributing visibly in the structure even if supplied from over 30m away.

This distribution pattern changes visibly upon alteration of the room geometry towards higher laminar and displacement-like ventilation, rather than mixing. Even a slight slanting of the roof prevents dead spots from occurring at greater heights, meaning an increase of over 50% in volume flow rate and halving of the average residence time. The higher airflows do have an effect on thermal comfort, however, as the thermal comfort levels drop sharply at 0.10m height, yet increase in the subsequent 1.1m and 1.5m heights; this could be explained by the fact that the final stratification is reached at a higher level when there is more airflow, meaning that temperatures over the whole domain are lower for the people.

As part of the experimental designs, experiments were also conducted on how air could be supplied under the structure. Various alternatives, with large and small openings and either from single or both sides were tested. A 'supply plenum' under the structure with a height of 1 m (or other size if necessary) is able to provide sufficient area for ventilation and can be easily integrated into the design. Air is distributed equally, with only small differences between one side or the other of supply gutters. This indicates that such a solution is able to provide for natural ventilation without much pressure drop even in the case of deep supply into the terminal.

Additionally, the effect of wind on such a supply solution was investigated as well. Depending on the difference in pressure coefficients, it is possible to guarantee that air will flow from bottom to top when using chimneys and motorized valves. If an uncontrolled system were to be built, it is possible that air is supplied from the outtakes and flows are reversed, especially if no chimneys are used; they nearly always guarantee a negative pressure coefficient at the outtakes.

Finally, the usage of solar chimneys was investigated as well for summer ventilation cases. With an effective irradiation of $300\text{W}/\text{m}^2$, the 4m high stacks did not provide for a sufficient ventilation rate inside of the terminal. This might be partly due to the shape (boxes stacked on the terminal) or due to a lack of capacity. In such a case the chimney might actually be the limiting factor, requiring the design to be made taller in order to increase its effectiveness.

As can be seen from the results, a naturally ventilated terminal is still possible with very high levels of thermal comfort. Assuming that usually class B structures are designed, the PMV/PPD values are often reaching that target, sometimes even reaching class A fully naturally. However, on the other hand, the initial goal was to reach class A from the calculations, something which is not achieved. This is in part due to the difficulty in regulating and guaranteeing such levels of performance, especially without mechanical controls and heating/cooling, but also because of the fact that the initial Python models need to be adjusted to take into account for airspeeds and turbulence (currently they are merely temperature-based).

4.4.2.6 Air Distribution Proposal

As can be seen from the comparative studies, it is very favorable to supply air from below through a supply plenum and extract it through the roof. The amount of inlets can be reduced greatly by using higher inlet airspeeds (such as $0.4\text{m}/\text{s}$), while thermal comfort is not impacted greatly. The larger variance in comfort throughout the floor plan could even be seen as an advantage, as it allows users more choice between hotter and colder regions in the floor plan.

The geometry of the hall apparently plays a bigger-than-expected role in the final airflow of the design. Airflow rates increase greatly when a slanted or trumpeted shape is implemented, causing air to also behave more laminarly and according to ideal displacement principles. The exact method of determining the right geometry is however trivially chosen in the two studies. A more 'technical' approach will be implemented in more detail in the Optimization chapter instead. The culling of geometry removed dead spots in the terminal, increasing airflow and ventilation efficiency, but also reducing thermal comfort due to increased airspeeds. This could be corrected by adjusting the design temperatures slightly higher as to reach the desired level of thermal comfort.

The implementation of solar chimneys to create more updraft is finally also proven to be feasible within the chimney stacks. If they can be combined and integrated into the architectural expression of the structure, they will provide for additional pressure

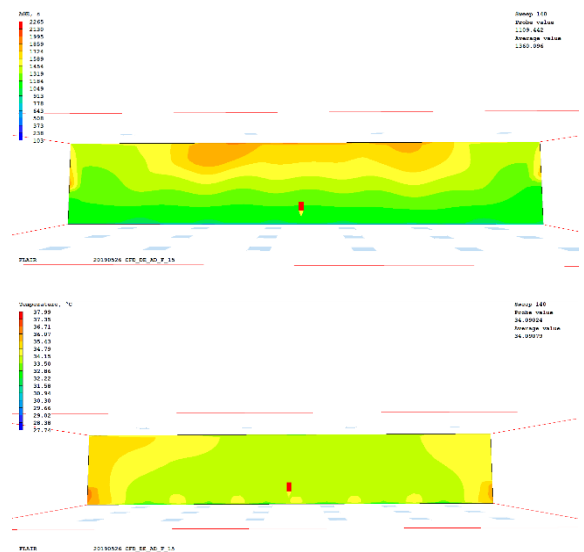


Figure 103 If no heating or cooling were to be used for the supply air, in winter (-10C) and summer (27C) indoor temperatures would be far out of acceptable thresholds

difference between the ground floor and roof. This additional pressure could be used to overcome pressure losses due to filters, inlet and outlet vents and possible heat recovery elements. The pressure difference caused by the usage of a ground duct to precool or preheat the air could then be overcome by a supply fan or by integrating it into the thermal buoyancy of the structure.

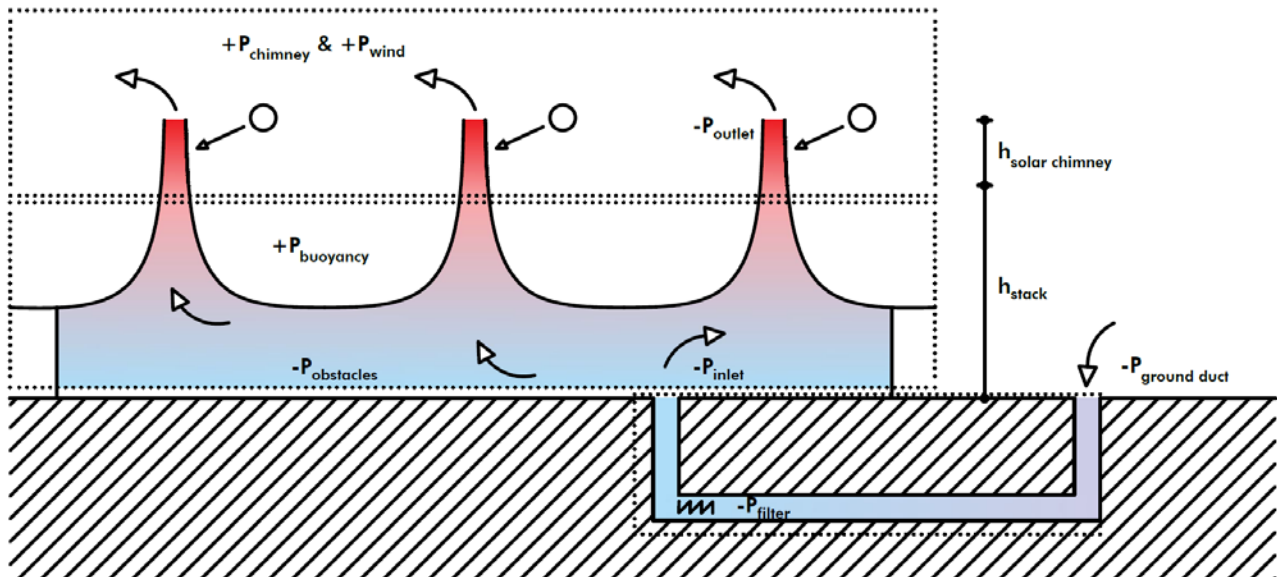


Figure 104 The proposal: pressure from buoyancy is dimensioned for providing enough ventilation for the space itself. Additional pressure drops are taken by the pressure generated by the chimney and wind. A fan is added to the ground duct if necessary.

4.4.2.7 Air Distribution Scripts

According to the outlined principles of the air distribution proposal, inlets are placed on the floor while outlets are placed in the roof. For the sake of simplicity and removing another design parameter, inlets and outlets are assumed as horizontal planar surfaces, even though they could still be another type of vent, such as a vertical air diffuser. This would yield a slightly different airflow pattern than a horizontal air diffuser, but not of a significant level to impact the design in any meaningful way.

Firstly, the number of inlets and outlets and the corresponding volumetric airflow per element is calculated in a GH_CPython script. This is also where the design parameters of inlet speeds and inlet and outlet areas are connected to. The script outputs the required number of inlets and outlets, their size and corresponding airspeeds and volumetric airflow and looks as follows:

Air Distribution Generator

```
import Rhino as rh
import rhinoscriptsyntax as rs
import math
import Grasshopper as gh

inlet_areas_list=[]
inlet_amounts_list=[]
qv_inlets_list=[]
for i in range(len(q_v_min_per_space)):
    a=q_v_min_per_space[i]
    b=v_air
    c= a/b
    inlet_areas_list.append(math.ceil(c))
    d=inlet_areas_list[i]
    e=float(A_inlet)
    f=d/e
    inlet_amounts_list.append(math.ceil(f))
    n_inlet=inlet_amounts_list
    j=inlet_amounts_list[i]
    v_inlet=v_air
    qv_inlets=a/j
    qv_inlets_list.append(qv_inlets)
qv_inlet = qv_inlets_list

outlet_areas_list=[]
outlet_amounts_list=[]
outlet_areas_corrected_list= []
outlet_speeds_list=[]

for i in range(len(q_v_min_per_space)):
    h=Aeff_per_space[i]
    g=(1/abs((1/h**2)-(1/d**2))))**0.5
    outlet_areas_list.append(g)
    k=outlet_areas_list[i]
    l=k/A_outlet
    outlet_amounts_list.append(round(l))
    n_outlet=outlet_amounts_list
    m=n_outlet[i]
    o=m*A_outlet
    outlet_areas_corrected_list.append(o)
    A_outlet_total=outlet_areas_corrected_list
    p=a/o
    outlet_speeds_list.append(p)
    v_outlet=outlet_speeds_list
```

After the necessary number of inlets and outlets are determined, they are distributed over the floor and roof areas. The inlets have to provide an even airflow over the whole floor plan, allowing for both sufficient air replenishment as well as cooling/heating. Because the air distribution plays such an important aspect for the thermal comfort -as airflow is used both for heating/cooling as well as ventilation- the placement of inlets and outlets also requires additional care.

In the case of large hall structures with very high internal loads such as at airport, heat transfer through the envelope is limited compared to heat gains from internal sources. Although this is the case, the regions close to the envelope still experience a different heat load than regions deeper inside the structure. To

accommodate for this, the placement of inlets should be done in accordance with the heat load on the floor. This way, the cooling capacity of each inlet is placed where cooling is also needed. This also allows for various spaces to have higher or lower heat loads within the same modeling environment.

Additionally, the fact that the air inlets take up space in the floor plan of the building means that they should only be placed in certain allowed zones. That is why the exclusion zones were used as an input from the start of the design. To consider both the exclusion zones as well as the heat load per grid point on the floor plan, the K-means Clustering algorithm is used.

K-means clustering is defined as an 'unsupervised machine learning algorithm' and is used to cluster unlabeled datasets based on a set number of clusters k - hence the name. The algorithm runs this process iteratively until the clusters stop changing, or when a limit is reached. Optionally, a weight can be allocated to each point in order to bias the algorithm towards clustering those points more intensively.

In the case of the inlets and outlets, the inlets are placed with a weighted K-means script to bias towards points with a higher heat load. Two options, one with exponential weighting and one with linear weighting, are investigated to this extent. A linear weighting is chosen with the highest weight of 1 being attributed to the point with the highest heat load, after which all points weighted against the maximum number by dividing its value with the maximum value. To initialize the K-means algorithm, the `k-means++` initialization setting is used without random states, while the `n_jobs` settings is -1, allowing for all cores of the processor to be utilized. 2800 probe points are processed in under 3.6 seconds on a 6-core 12-thread Intel i7-9750H running at 2.6GHz.

In order to make the K-means script run, the algorithm needs to be imported from `scikit.learn` with `numpy` imported as well. This means that the `GH_CPython` component needs to be utilized, which is unable to read geometric data from Grasshopper directly. Therefore, all points in the script are converted using a `GH_Python` script into a list of coordinates. As the K-means script did not run in a for-loop for multiple spaces, the whole algorithm is converted to a Grasshopper cluster containing the selection of the space, conversion from geometric data to numeric values using `GH_Python`, the K-means algorithm with re-conversion from numeric values to points and additional components for visualization. This also means that for each space within the design, a separate Grasshopper cluster is necessary.

The input for the two python scripts are as follows (see next page):

K-means Preparation

```
import Rhino.Geometry as rg
import Rhino
import rhinoscriptsyntax as rs

is_inside_list=[]
heat_points_out_list=[]
z_coordinates_list=[]

for point in heat_load_points:
    is_inside=(spaces.Contains(point,rg.Plane.WorldXY,0.01)==rg.PointContainment.Inside)
    is_inside_list.append(is_inside)
    if is_inside==True:
        heat_points_out_list.append(point)

for i in range(len(heat_load_points)):
    is_inside= (spaces.Contains(heat_load_points[i])==rg.PointContainment.Inside)
    is_inside_list.append(is_inside)
    if is_inside==True:
        z_coordinates_list.append(heat_load_values[i])

heat_points_out=heat_points_out_list
z_coordinates=z_coordinates_list

import sklearn
import sklearn.cluster as sk
from sklearn.cluster import KMeans
import numpy as np
import math as math
```

K-means Inlets (Weighted)

```
numbers=np.array(_z_coordinates)

highest_value=max(_z_coordinates)
print(highest_value)
weights=np.divide(numbers, highest_value)

a=list(weights)
weights=np.array(weights)
print(weights)
datapoints=np.array(_points)
kmeans=KMeans(n_clusters=int(_n_inlets),init="k-means++",random_state=0,n_jobs=-1).fit(datapoints, y=None, sample_weight=weights)
labels= list(kmeans.labels_)
centres=kmeans.cluster_centers_
x_centres=list(centres[:,0])
y_centres=list(centres[:,1])
z_centres=list(centres[:,2])
```

After the inlet and outlet points are determined, the next step is the preparation of the CFD simulation.

4.4.3 CFD Simulation

4.4.3.1 Simulation Preparation

In order to determine the performance of the intended design, a CFD analysis needs to be conducted. The CFD analysis is conducted using OpenFOAM v5.x, sometimes also written as v1706+. OpenFOAM is an open-source CFD that runs in a Linux environment (OpenFOAM Ltd, n.d.) using BlueCFD-Core. The package contains a large library of readily available CFD tools ranging from meshing to different types of CFD solvers. However, as OpenFOAM runs in a virtual Linux machine, Rhino Grasshopper cannot connect to it directly. Therefore, the Butterfly plugin v.0.0.05 is used to form the bridge between Rhino Grasshopper and OpenFOAM. Butterfly mimics the basic workflow required to set up any OpenFOAM case:

1. Case Generation
2. Boundary Conditions
3. Mesh generation
4. CFD settings (thermophysical models, turbulence, i/o control, numerical schemes, solver types)

As OpenFOAM does not contain any post-processing of results, it is paired with ParaView to view analysis results. In addition, the Butterfly plugin allows for a limited post-processing of results. However, it is nowhere near as memory-efficient as ParaView, which has the capacity to efficiently show complex meshes and results faster than Grasshopper.

In the developed design script, the geometry is converted to OpenFOAM geometries using Butterfly. The following Boundary conditions are applied to the various surfaces:

1. ZeroGradient
 - a. Floor (adiabatic)
 - b. Roof (adiabatic)
 - c. Walls (adiabatic)
2. FixedValue
 - a. Inlets (volume flow rate, inlet temperature)
 - b. Outlets (external pressure)

Additionally, refinement regions are defined at the inlets and outlets. The refinement regions will increase mesh density around the inlets and outlets by splitting the cells into smaller parts. For both inlets and outlets a refinement level of three was implemented.

All geometries are meshed using a twofold meshing, first by running blockMesh and then running snappyHexMesh. The blockMesh component splits the domain into a predefined amount of segments in x, y and z directions. Additionally, gradients can be supplied in any direction, refining the meshing in particular regions upon demand. snappyHexMesh will then generate three-dimensional hexahedra and split-hexahedra that are formed by

dividing a coarser, underlying mesh. It allows for a more refined mesh, which is especially useful around the inlet locations, where higher mesh accuracy is desirable. The following meshing parameters were used:

- BlockMesh: #divisions=length/2, i.e. meshes of 2m each, remaining settings at default
- snappyHexMesh: 1 extra cell between levels, remaining settings at default

Finally, the CFD settings that were implemented included the following:

- Parallel decomposition: method scotch, 12 CPU's
- Control dictionaries: starttime=0, endtime=15 (15 runs)
- Turbulence model: LES, model kEqn, delta=cubeRootVol, turbulence=ON
- CFD solver: buoyantBoussinesqSimpleFoam (steady-state SIMPLE buoyant solver based on Boussinesq approximation)
- Probe points: points in a 0.5m x 0.5m grid at 1.50m height from the floor pane

The turbulence model chosen was a moderately complex LES-kEqn model that is computationally more expensive than the Reynolds-Averaged Simulation (RAS) used more commonly. This was because the RAS simulation would cause convergence errors for the large hall geometries that were analyzed. Similarly, laminar flow was avoided because it caused incorrect flow results.

The amount of runs and meshing parameters was based on experience gained from tests executed in OpenFOAM. The result of these trials are given in the following figures. The model used was a simplified version of Lelystad Airport, with the landside, airside and main halls simplified as large building volumes.

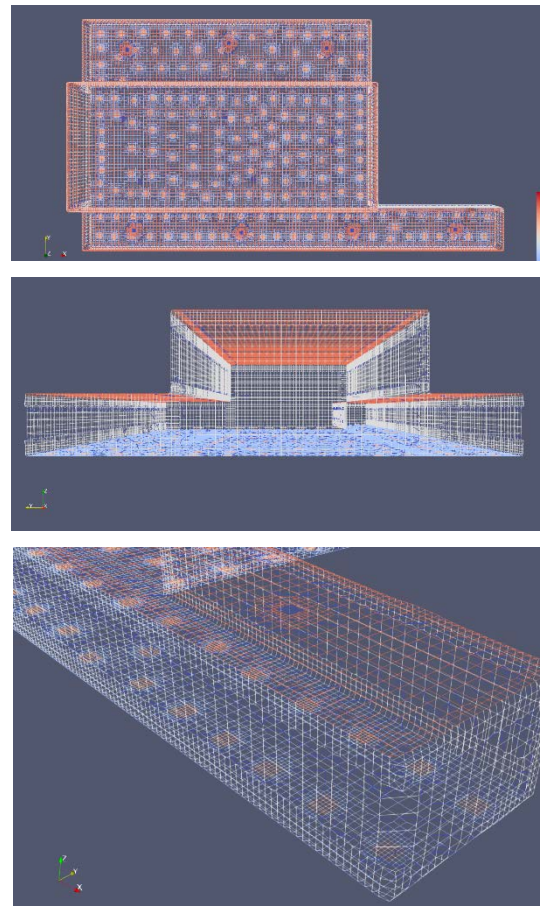


Figure 105 The Lelystad Airport model for testing OpenFOAM settings, opened in ParaView. Note how the mesh refines close to the floor and roof and in particular around the inlets and outlets.

	LS S 1	LS S 2 P5_test_12	LS S 3	LS S 4	LS S 5	LS S 6	LS S 7	LS S 8	LS S 9	LS S 10	LS S 11	LS S 12
Model Used	Lelystad Simplified 1											
Description	Simplified model of Lelystad with 3 boxes of xxx	Simplified model of Lelystad with 3 boxes of xxx	Simplified model of Lelystad with 3 boxes of xxx	Simplified model of Lelystad with 3 boxes of xxx	Simplified model of Lelystad with 3 boxes of xxx	Simplified model of Lelystad with 3 boxes of xxx	Simplified model of Lelystad with 3 boxes of xxx	Simplified model of Lelystad with 3 boxes of xxx	Simplified model of Lelystad with 3 boxes of xxx	Simplified model of Lelystad with 3 boxes of xxx	Simplified model of Lelystad with 3 boxes of xxx	Simplified model of Lelystad with 3 boxes of xxx
BlockMesh Factor	1	0.5	0.5	0.5	0.5	0.5	0.5	0.75	0.5	0.5	0.5	0.5
# of cells (BlockMesh)	2.5e^6	38000	38000	38000	38000	38000	38000	127000	38000	38000	38000	38000
Grid refinement (direction) (% length) (% cells)	Z-grading 20-80 50-50	Z-grading 30-70 55-45	Z-grading 20-80 50-50									
Refinement level inlets & outlets	(1,1)	(1,1)	(1,1)	(1,1)	(1,1)	(1,1)	(1,1)	(1,1)	(2,2)	(4,4)	(3,3)	(3,3)
ExpandMesh	OFF	ON										
SnappyHexMesh Cells between levels	2	2	4	8	2	2	2	2	2	2	2	1
SnappyHexMesh Extra Layers	OFF	OFF	OFF	OFF	OFF	OFF	ON	ON	ON	ON	ON	ON
SnappyHexMesh Surface feature level	2	2	2	2	4	2	2	2	2	2	2	2
time (BlockMesh) [s]	5.1	1.9	1.3	1.9	2	2.2	1.9	4.3	1.9	1.9	1.9	2
time (BlockMesh loading) [s]	72	6.5	4.3	6.5	6.6	6.6	6.5	21.3	6.5	6.5	6.5	6.6
time (SnappyHexMesh) [s]	318	84	96	138	156	60	66	144	90	318	168	24
time (SnappyHexMesh loading) [s]	324	28	30	33	90	31	28	66	28	288	90	7.3
PPDavg	-	-	-	-	-	-	-	-	-	-	9.69	8.29
Tavg	-	-	-	-	-	-	-	-	-	-	25.94	25.52

Figure 106 Effect of various meshing options on total runtimes for the analysis. The last two options were chosen and further analyzed for the actual analysis results, which proved to have little differences.

	LS S 12						
Model Used	Lelystad Simplified 1						
Description	Simplified model of Lelystad with 3 boxes						
# of cpu's	12	12	12	12	12	12	12
# of sweeps	25	50	100	200	300	500	1000
PPDavg	32.5	31.9	28.9	26.7	23.9	18.3	11.3
dT(min, max)	1.03	1.42	1.35	1.6	1.3	1	1.1

Figure 107 Effect of number of runs on the result of the CFD analysis.

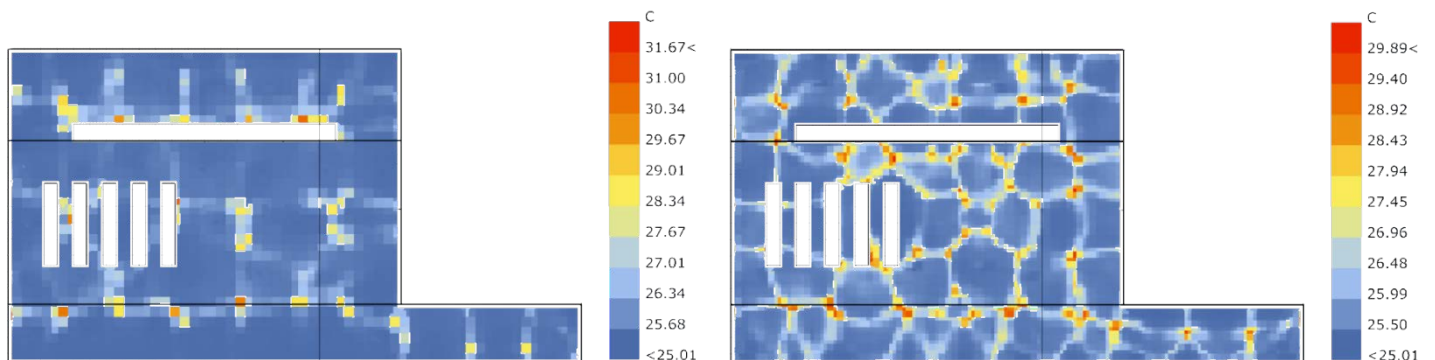


Figure 108 Running the Lelystad model with a coarse 2m mesh without grading in the lower heights (left) against having a graded and refined mesh in the lower 20% of the height; the accuracy differences are clearly visible. Runtime differences were 4 minutes in the graded mesh version against 2.6 minutes in the non-graded version.

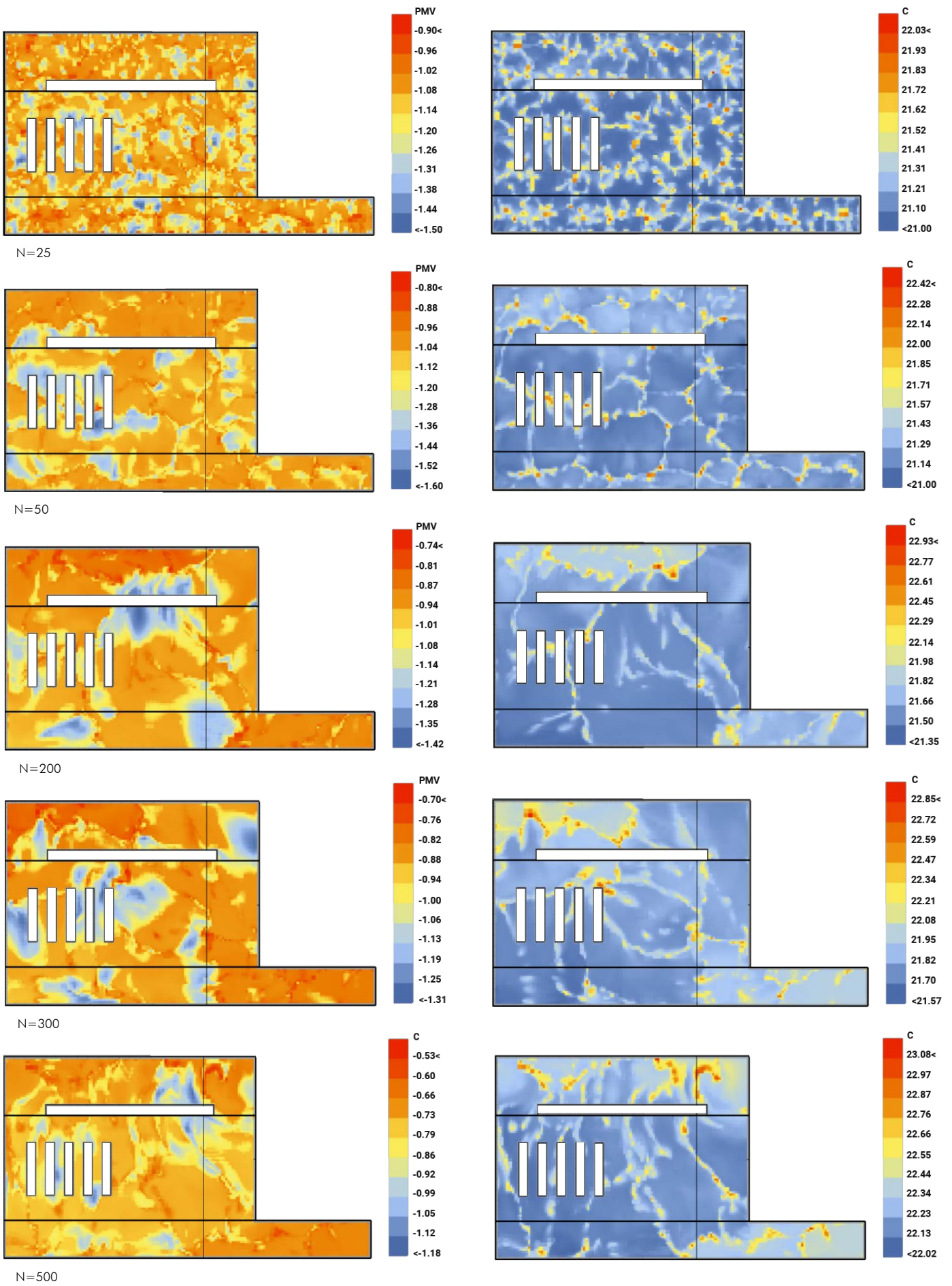
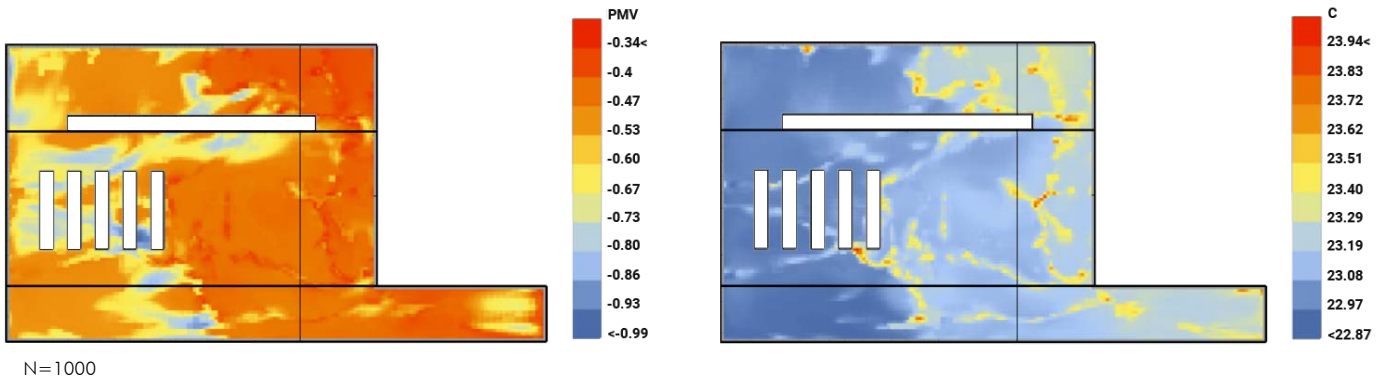


Figure 109 Comparison on the effect of runtimes on final comfort results. N = number of iterations run in the CFD analysis.



As can be seen from the CFD simulations, the number of runs and the meshing influence OpenFOAM results more than is the case at Phoenix CFD.

Finally, in order to link the volumetric heat load values that were generated earlier to the CFD simulation, a set of custom dictionary and options files need to be generated. This is because the Butterfly plugin does not support volumetric heat loads out of the box; instead, only an equivalent floor temperature can be used.

Therefore, a Python script was written in GH_CPython to implement two files that need to be added to the OpenFOAM case directories: *topoSetDict* and *fvOptions*. *topoSetDict* is a dictionary that is read by running the *topoSet* command, which is run additionally by entering a command into the standard Butterfly simulation component. The *topoSetDict* contains information on which cells to select and group together; in this case, the heat load boxes' coordinates and names are entered as a list, with which the Python script generates the file with the required amount data. The script then generates the *fvOptions* file, which contains the finite volume options to dictate which set of cells get what amount of volumetric heat load.

Although the generated set of files and additional command in the Butterfly component's code makes it possible for the heat loads to be added and entered into the analysis, the code does not always work properly. As of the writing of this thesis, these bugs are not fully resolved, which is why an additional method is also proposed in the form of equivalent floor temperature. The script that is used to generate both files is given on the next page:


```

topoFile.write(topoSetDictScript_A)
topoFile.close()

fvoptionsfile = case_folder_windows + '\\\' +
case_name + '\\\' + 'system\\\' + 'fvOptions'
fvFile=open(fvoptionsfile, "w")
fvFile.write(fvOptionsScript_A)
fvFile.close()

topoFile=open(toposetfile, "a")
fvFile=open(fvoptionsfile, "a")

for i in range(len(box_loads)):
    topoSetDictScript_B = """
    {
        name "" + 'heatSourceset' + str(i)
+""";
        type cellSet;
        action new;
        source boxToCell;
        sourceInfo
        {
            box ("" + bottom_coordinates[i] +
""") ("" + top_coordinates[i] + "");
        }
    }"""
    topoSetDictScript_C = """
    {
        name "" + 'heatZone' + str(i) +""";
        type cellZoneSet;
        action new;
        source setToCellZone;
        sourceInfo
        {
            name "" + 'heatSourceset' + str(i)
+""";
        }
    }"""
    topoFile.write(topoSetDictScript_B)
    #topoFile.write(topoSetDictScript_C)
    fvOptionsScript_B = """
"" + 'heatSource' + str(i) + """
    {
type scalarSemiImplicitSource;
active true;
selectionMode cellSet;
cellSet "" + 'heatSourceset' + str(i) +""";

scalarSemiImplicitSourceCoeffs
    {
        volumeMode specific;
        injectionRateSuSp
        {
            h ("" + str(volumetric_heat_load[i]) + "" 0);
        }
    }
    }
    """
    fvFile.write(fvOptionsScript_B)
topoFile.write("""
);""")
topoFile.close()
fvFile.close()
topoFile=open(toposetfile, "r")

```

```

with open(toposetfile, "r") as data:
    plaintext = data.read()
plaintext = plaintext.replace(',',' ')
topoFile=open(toposetfile, "w")
topoFile.write(plaintext)
topoFile.close()

buoyantfile= case_folder_windows + '\\\\' +
case_name + '\\\\' + 'log\\\\' + 'buoyantBous-
sinesqSimpleFoam.err'
buoyantFile=open(buoyantfile, "w")
buoyantFile.write(' ')
buoyantFile.close()

reconfile= case_folder_windows + '\\\\' +
case_name + '\\\\' + 'log\\\\' + 'reconstruct-
Par.err'
reconFile=open(reconfile, "w")
reconFile.write(' ')
reconFile.close()

rmfile= case_folder_windows + '\\\\' + case_name +
'\\\\' + 'log\\\\' + 'rm.err'
rmFile=open(rmfile, "w")
rmFile.write(' ')
rmFile.close()
done=True

```

4.4.3.2 Simulation Results Analysis

After the CFD simulations are completed, the results from the T and U fields (temperature and velocity, 'v' in the thesis python scripts) are loaded into a Rhino Grasshopper environment using Butterfly components. All analysis surfaces are offset 500mm off from other building surfaces. The loading of such probe points however is limited to selected section slices only, with many section slices and datapoints slowing down the model considerably. This is because of the way Grasshopper handles memory and constitutes the same issue as with loading the mesh into Grasshopper when compared to viewing it in ParaView.

The results of airspeed and temperature are put into the Ladybug PMV calculator used earlier in the script. Clothing and metabolic rates are taken from the initial values from the start of the script, while relative humidity is assumed to be 50%. Radiation is not considered for the comfort calculation as radiation is not included in the CFD analysis. However, earlier simulations run in Phoenics already confirmed that the effect of radiation on the final thermal comfort was limited.

5

OPTIMIZATION

5 OPTIMIZATION

5.1 Introduction

After a working proof of concept is given in the engineering design, the challenge is to find a correct combination of parameters that will yield the desired level of performance for a set of constraints. Even though all results from the engineering stage are usable and meet a minimum level of quality, not all solutions are created equal. In a first stage of optimization, the aim is to find the best-performing combination of parameters to select for further geometric refinement. In the second stage of the optimization phase, a geometry is sought to be found for which the airflow inside the structure is improved and redundant parts are culled with the aim of increasing ventilation performance and thermal comfort.

5.2 Optimization I: Air Distribution

5.2.1 Description

Within the design method, achieving a set level of thermal comfort is a constraint to which any generated design has to conform. A certain level of robustness is already ensured for in the engineering stage by selecting a relatively broad range of possible options that all still fall within the constraints set. Within the developed method, the number of possible options is only limited by user input; the number of parameters and variables can be as high as desired. During the testing of the method, the maximum number of possible combinations was 3150. If each CFD study took 10 minutes, that would still yield a calculation time of 525 hours if all iterations were to be calculated.

Within this open realm of possible combinations, the objective is to attain a minimum level of thermal comfort while reducing the total number of inlets and outlets. As the sum of inlets and outlets stands in direct proportion to construction costs, difficulty of implementation and added losses and complexity in remaining climatization systems, minimizing supply and removal points is critical. Also, it would make no sense to complicate the building construction itself with inlets and outlets when the main goal of the thesis is to reduce the amount of building services in the construction industry.

However, in order to prevent the optimization algorithm from 'beelining' to the solution with the least inlets -endangering the even distribution of thermal comfort- an aggregate single objective function is developed in which the average PPD over the whole analysis field is multiplied with the amount of inlets and outlets. This way an objective function can be stated that is simple, still oriented towards minimization and yet take into account the effect of thermal comfort better.

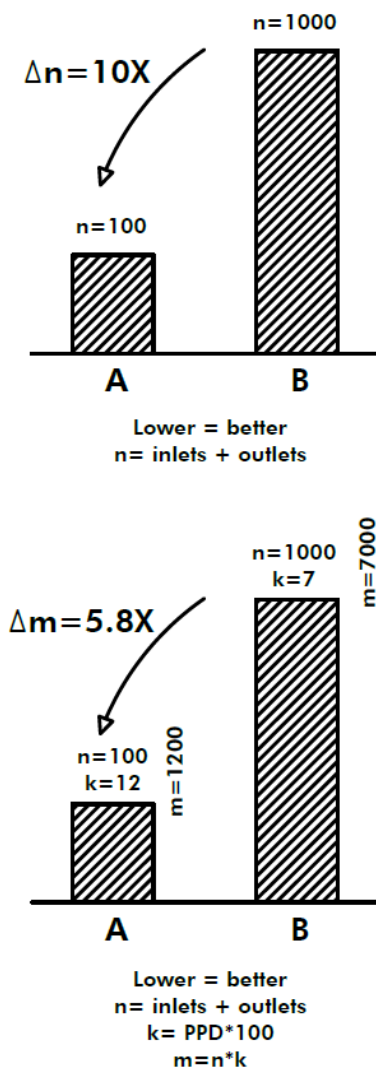


Figure 110 Aggregate objective function to increase the weight of thermal comfort.

By such, the description of the objective function becomes:

$$\min_{a,b,c,d} (|inlets| + |outlets|) PPD_{avg}$$

$$\text{subject to: } = \begin{cases} a \in [a_{min}, a_{max}] \\ b \in [b_{min}, b_{max}] \\ c \in [c_{min}, c_{max}] \\ T_{inlet} = d \\ q_{v,min} = e \end{cases}$$

Where a = inlet airspeeds [m/s], b = inlet areas [m²], c = outlet areas [m²], d = supply air temperature [°C] and e = minimum ventilation rate [m²/s].

As there is no direct mathematical link between the objective and the constraints, it is not possible to use linear or deterministic methods in a fast and reliable way. Therefore, a heuristic algorithm, that ‘searches’ the domain of possible options, is preferable for the design challenge posed in the thesis. However, it is up to designer to choose another optimization method if so desired.

For the scope of this thesis, an evolutionary solver in the form of Galapagos is proposed. Galapagos is readily integrated into Rhino Grasshopper is part of the standard set of components. However, it is also relatively simple in its settings and possibilities, meaning that it is a relatively crude tool. For instance, due to the expensive nature of CFD simulations, methods such as Artificial Neural Networks can be implemented to speed up the total optimization process. However, as such integration would constitute a fully specialized topic in and of itself, they are left outside of the scope of this thesis.

5.2.2 Result Aggregation I

In order to analyze the results of the OpenFOAM simulation, the results from the T and U fields (temperature and speed) are imported into Rhino Grasshopper. The results are first aggregated: temperatures are converted from °K to °C, while the air velocity magnitudes of the x, y and z coordinates are multiplied to gain one airspeed indicator.

The results are then input into the Ladybug PMV calculator and logged using a data recorder and panel component per iteration of the genetic algorithm. This is done as a safeguard, because the Galapagos component might have issues in registering all data after the simulation is run. The Galapagos component stores data of all variables and fitness, which is displayed graphically on the user interface. All data from the simulation is exported to a text file at the end of the analysis and the most successful iteration is reinstated into Grasshopper for further optimization.

5.3 Optimization II: Geometric

5.3.1 Description

The output of the first optimization is a volumetric model that has been selected as fitting the initial objective function best. The geometry itself contains the outermost bounding box of each space volume and corresponding inlets and outlet with their sizes and dimensions. In order to go from this box shape to one that is better able to allow for air movement, a second optimization is performed.

The second optimization is intended to 'cut away' geometry from the large bounding box that was generated by the script. This geometric optimization removes stale and recirculating spots of air and prevents recirculation and curling of the airflow. This has the benefit of allowing for a higher ventilation efficiency, reducing radiant temperature by removing pockets of hot air (and large planar surfaces that can cause heat radiation) and by showing the ventilation concept in the design of the structure itself.

To do this, three methods are firstly investigated:

1. Adjoint Shape Optimization
2. Culling of probe points with a particular airspeed
3. Manual approximation

The first method investigated is 'adjoint shape optimization', a computational optimization method developed first in the 70's to give a method that can scan large design spaces effectively independent of the number of design variables. The adjoint method was firstly intended for structural mechanics and has been adapted to fluid mechanics since the start of the new millennium (Othmer, 2014). It has found particular attention in the aerodynamic and car industry, where many examples of the optimization of aerodynamically important shapes or engine parts are performed.

The method computes the derivative of the objective function and detects to which variables the objective is most sensitive. Regions least sensitive to the variables are shown visually and can be removed from the space by adding an incremental porosity to the regions that need to be removed, meaning that they block the airflow through these cells.

However, the application of adjoint shape optimization has remained in the aerospace and automotive industry. Examples of the method are only tested on small elements such as cars or engine manifolds. Due to the computational complexity of such a method, adjoint optimization is left outside of the scope of the thesis, although its potential for building design is also acknowledged.

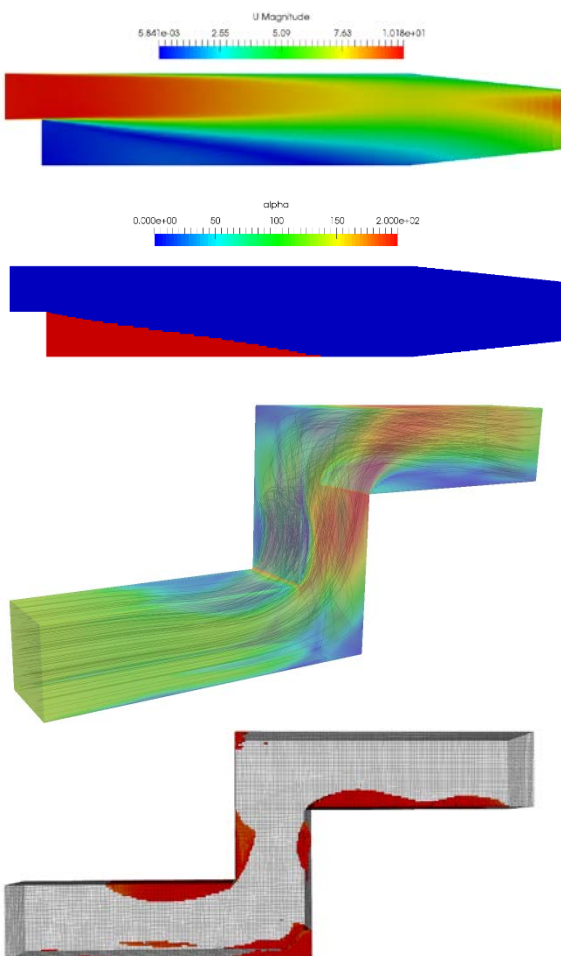


Figure 111 Images showing adjoint shape optimization for two duct sections. Red regions are areas that cause pressure losses and can be culled (CFDSupport.org).

The second investigated method is based on the CFD results that are generated from the analysis. Cell centers contain both coordinate data as well as the velocity magnitude. By selecting a right set of velocities to cull, an indication of the desired geometry could be achieved.

Therefore, culling of geometry using airspeed data is tested in various configurations:

1. Removing cells with a negative Z component
2. Removing of cells with a small magnitude ($v < a$)
3. Removing of cells with magnitude close to zero ($a < v < b$)

The example considered is a simplified model of Lelystad Airport, where the whole bounding volume is filled with probe points spaced at 1m interval throughout the terminal. These probe points are entered into the CFD simulation to log their values and later imported back from the OpenFOAM simulation together with their respective airspeed and temperature data. The cells are visualized using small voxels of 1x1 m with the cell center corresponding to the probe point.

The following results are obtained from the various geometric trials:

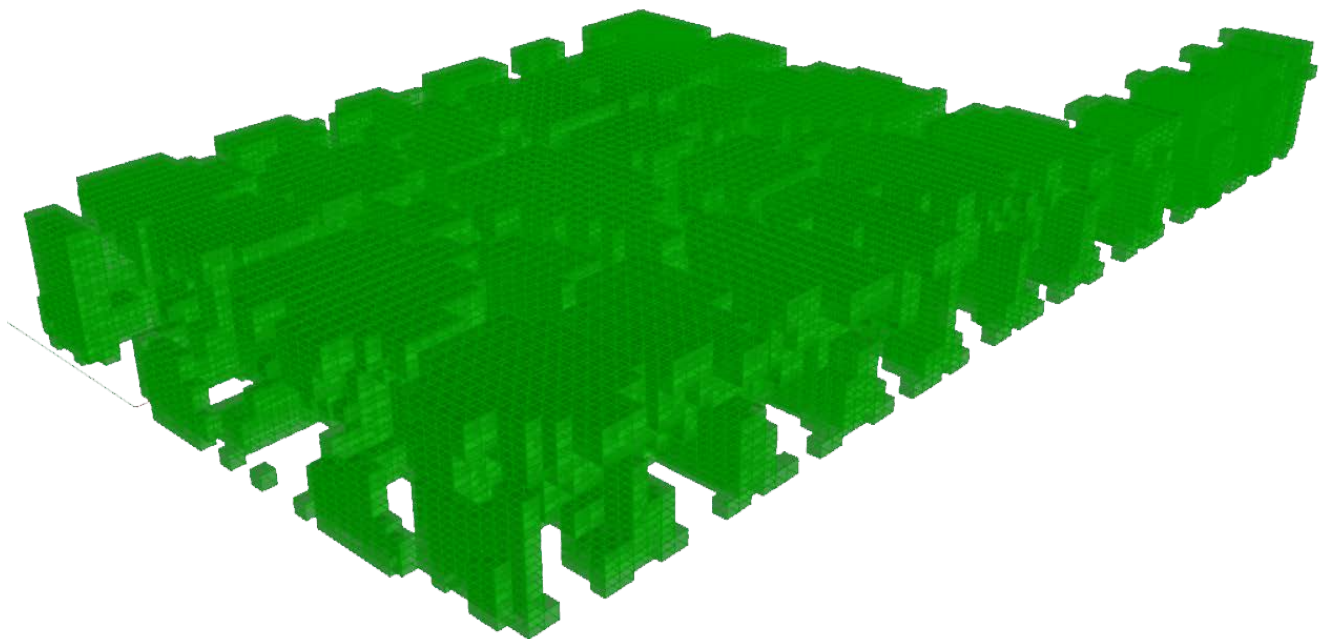


Figure 112 Resulting voxels when all voxels with z component < 0 are culled.

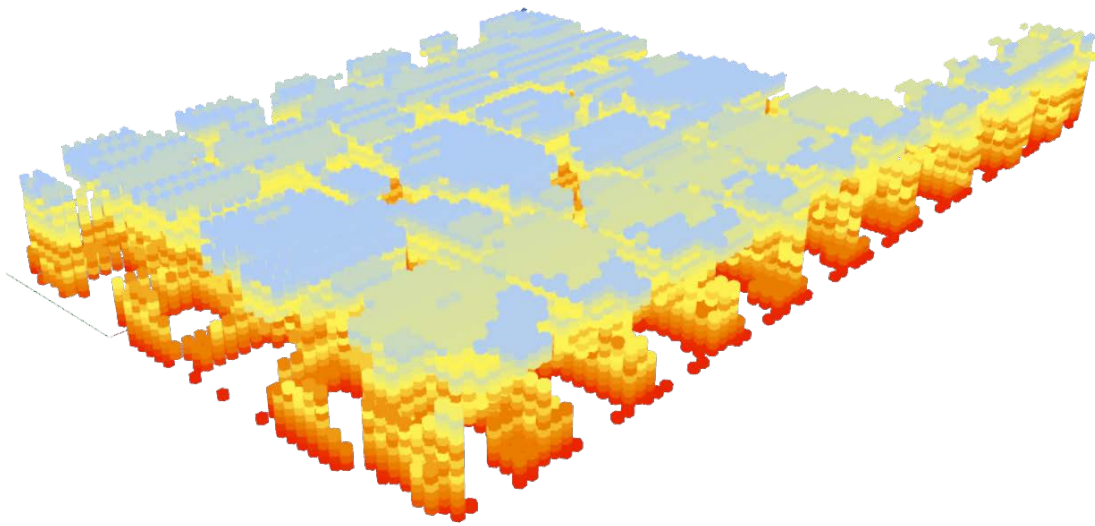


Figure 113 Resulting voxels when all voxels with z component < 0 are culled, with color.

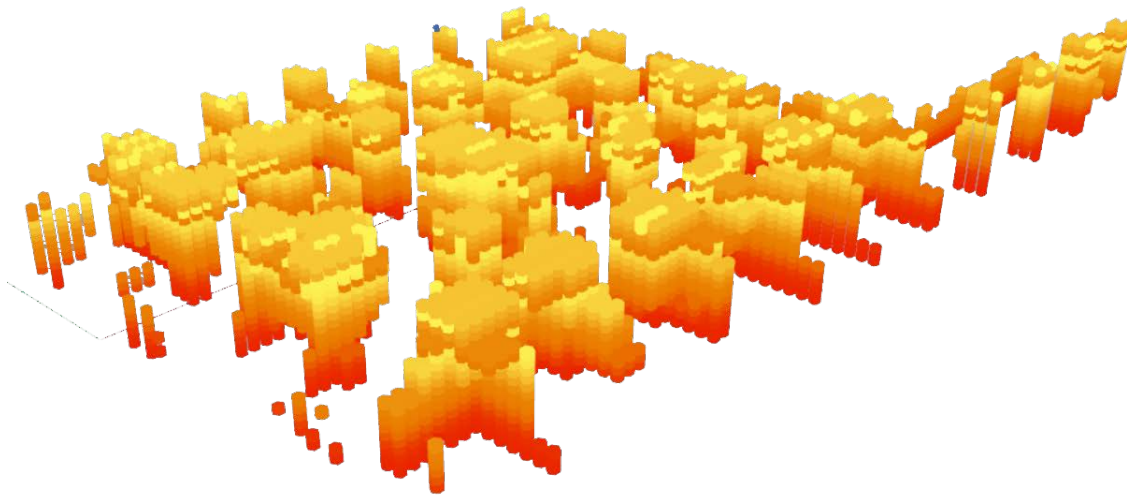


Figure 114 Remaining voxels when all points with z component < 0.4 are culled.

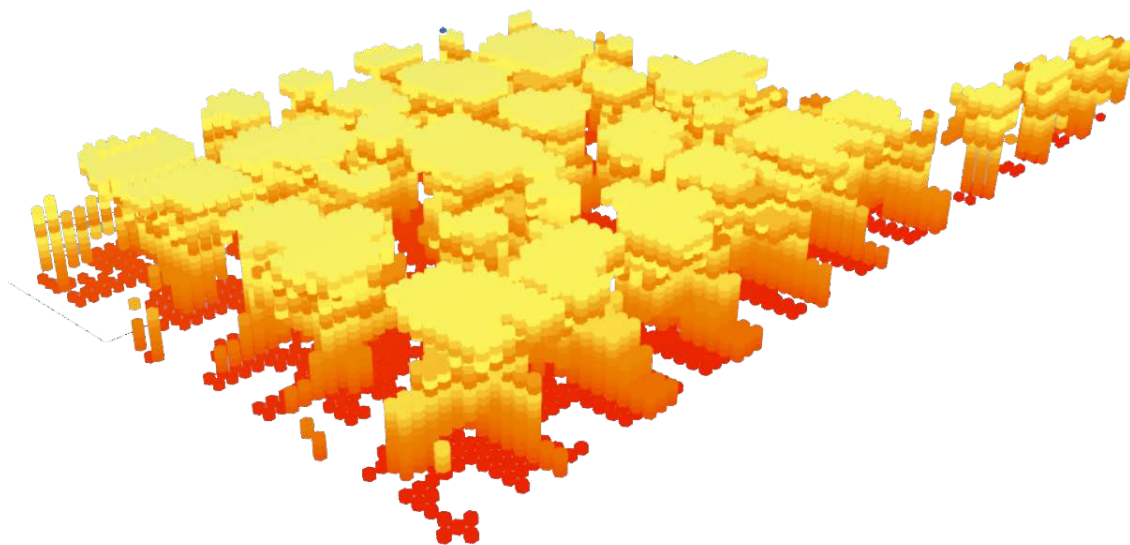


Figure 115 Removing voxels with velocity magnitude < 0.35 .

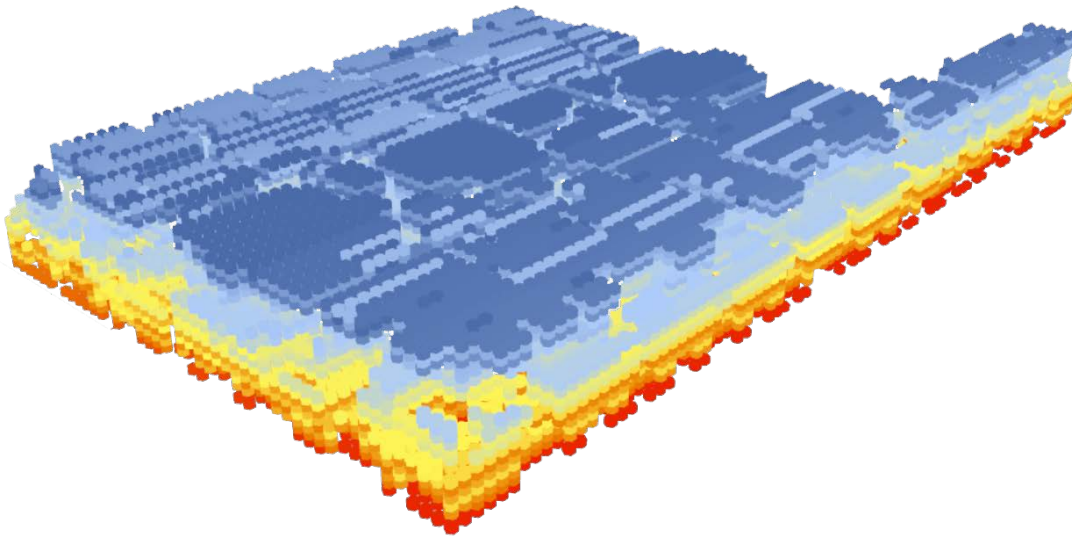


Figure 116 Remaining voxels when all points with magnitude < 0.25 are culled.

As can be understood from the previous method, the culling of geometry does not always yield a coherent result that can be used for developing a geometry for the terminal. Trials with disabling turbulence in the CFD model had additionally no effect either.

Therefore, a manual approximation is also developed using Bezier curves that connect the inlets to the outlets in the design. The result can be viewed as a set of curves, or as a set of pipe sections that represent a volume better. The visualization can be directly used, with various curve tangents being modified by the designer to allow for design freedom. Additionally, the curves can be turned into solids by offsetting them with a circular section. The points that fall inside of these solids can then be selected through a Boolean operation, which yields a final resulting geometry. In all cases, a minimum height can be specified per space that prevents the culling of points below that height.

The intention of the aforementioned methods is to provide insight for various designs to the designer, but not dictate the final shape of the building. However, more deterministic methods that would dictate the final shape can still be theorized. For instance, as one of the objectives is to prevent recirculation and curling of air, the *curl* of each (which is a derivative property of each vector in the field) could be analyzed. Similarly, the *kinematic energy dissipation* could be analyzed per gridpoint and areas that cause high dissipation could then be culled. However, due to the complexity of such methods it is left outside of the scope of the thesis.

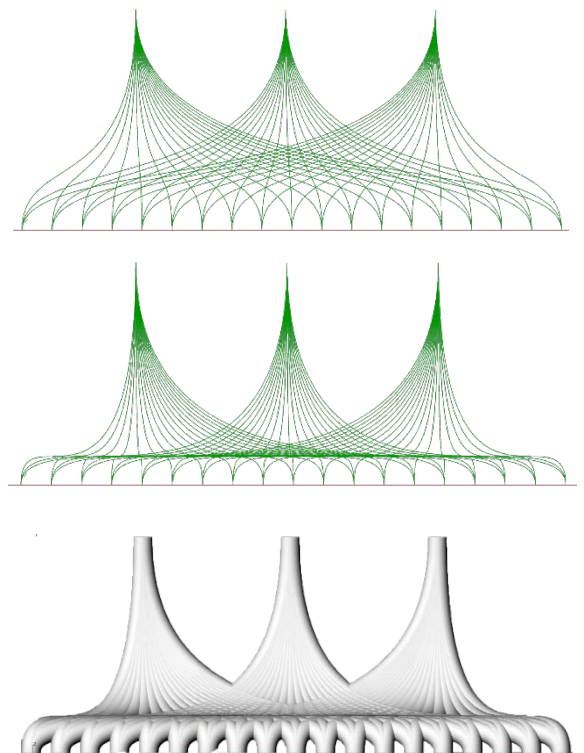


Figure 117 Examples of generating geometry based on Bezier curves.

5.3.2 Result Aggregation II

The results of the various types of proposed geometric culling are indicative of a final geometry and propose a design indication, rather than the geometry of the design. This way, the designer is left with the final control over the shape of the building with clear indications on how the geometry could look like. The geometry therefore needs to be reconstructed manually for the final stage of the design, which is the verification and analysis of the final design results.

6

APPLICATION

6 APPLICATION

6.1 Introduction

In order to test the functioning of the model and gain insight into the effect of various design parameters on the final performance and geometry of the design, the example structure that was used throughout the model's development -Lelystad Airport- is full run through the script. Additionally, various design proposals are shown and discussed and the effect of more specific elements such as solar chimneys and ground ducts are investigated.

6.2 Description of Lelystad Airport

Lelystad Airport (IATA code: LEY, ICAO code: EHLE) is a general aviation airport in the Lelystad province of The Netherlands and started service in 1973. The airport was bought by the Schiphol consortium in 1993 and has since been frequently used as its satellite. Since 2019 a new terminal and runway extension has been completed in order to facilitate the airport's new role in reducing (especially holiday) traffic from Schiphol Airport.

The new terminal is located at the north corner of the airport terrain and is designed as a linear terminal model that is easily expandable depending on growth of the airport. In its initial form, the airport has an apron for four aircraft to be parked simultaneously. The linear model allows for an expansion of up to twelve airplanes, equaling a capacity of 7 mln passengers annually. However, this growth is not foreseen until after 2023, even soon after that; due to protest from the local governments and population, the opening of the airport terminal has been delayed as of August 2019.

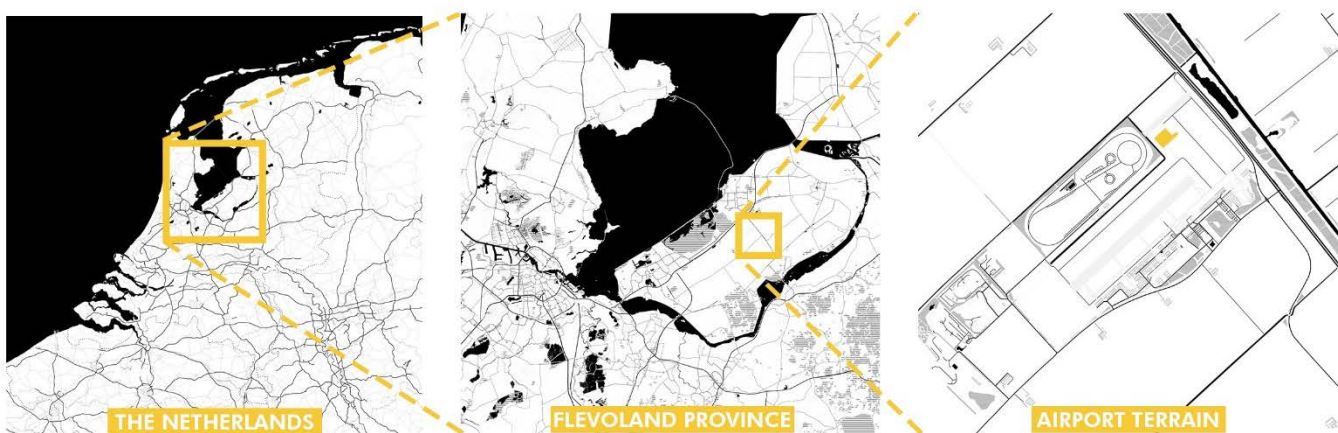
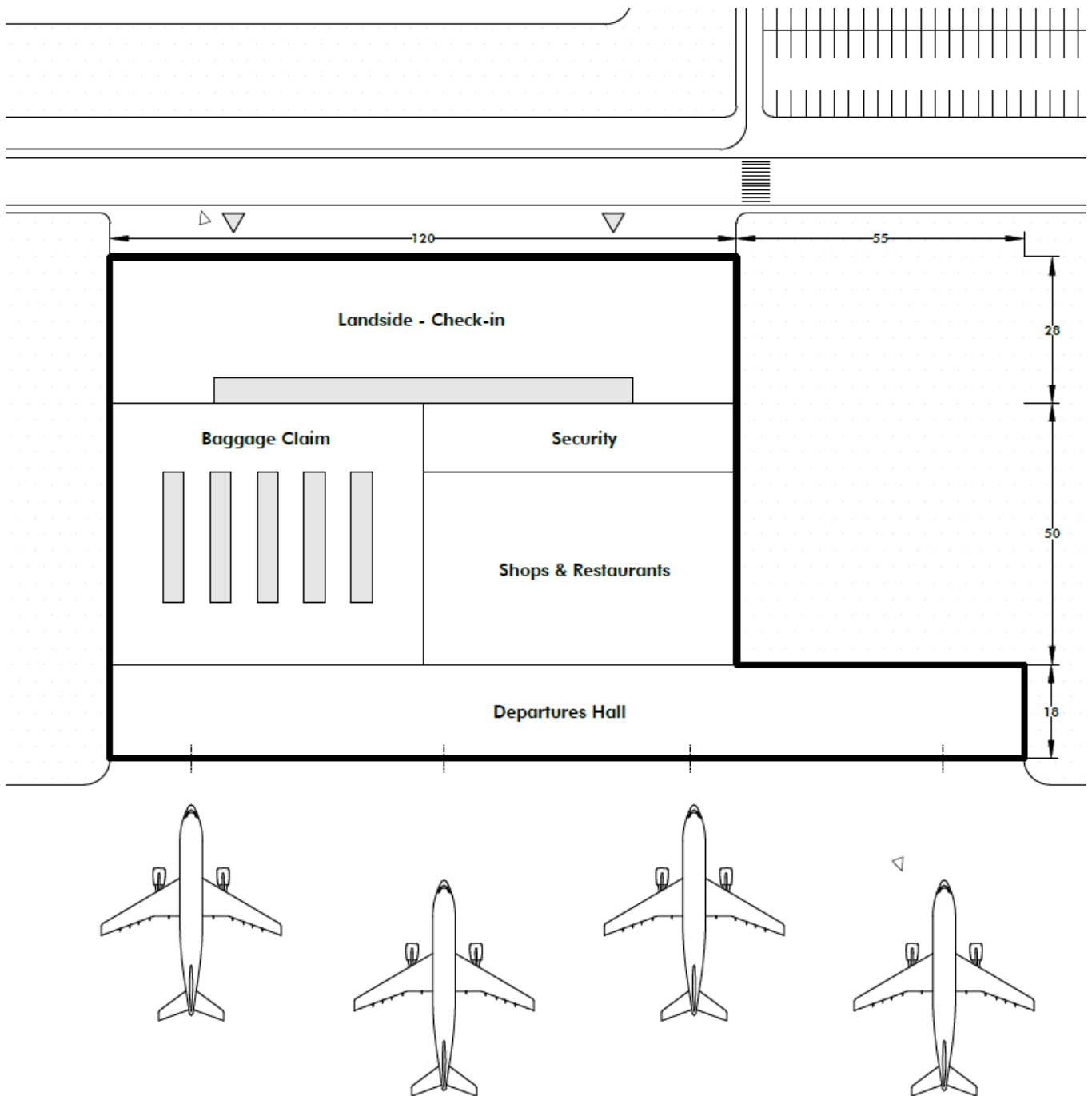


Figure 118 The location of Lelystad Airport.

The airport terminal consists of three main areas: the landside entrance hall with check-in, the main terminal area with security, restaurants and shops and the airside boarding pier. Due to safety reasons, the exact layout of the airport is confidential and was not shared, which is why the layout of Lelystad Airport has been slightly changed and simplified for the sake of testing the model and its performance.

The airport terminal is split into three main areas as mentioned earlier. Exclusion zones are defined on the floor plan to indicate various service and off-limit zones or zones that need to be ventilated mechanically for different reasons.



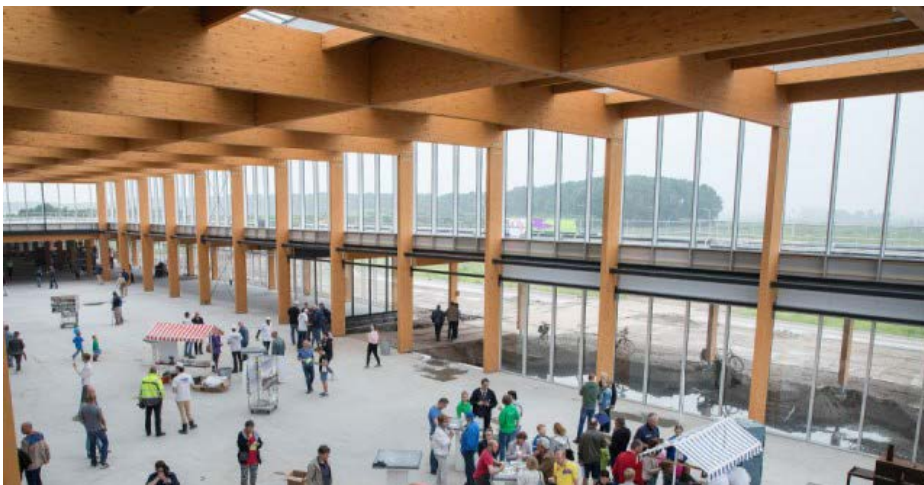


Figure 119 Images of the actual airport. From top to bottom: aerial picture (HollandLuchtfoto), landside hall (luchtvaartnieuws.nl) and entrance (fd.nl).

6.3 Input Parameters

The parameters put into the model are summed up in the figure to the right. The space is simply divided into three main spaces and exclusion zones are calculated accordingly. This results in the following output of the script in terms of thermal loads:

Solar Loads (avg) [W/m2]	20.8	12.7	35.5
Transmission Loads (avg) [W/m2]	0.96	0.58	1.6
Total Heat Load [W/m2]	96.5	88	111.9
Total Heat Load [kW]	285.7	484.1	352.4
dT stratification	1		
Ttarget	27.2	24.7	27.2
qv,min [m3/s]	25.7	59.6	31.7

Figure 121 Heat loads in the design as calculated by the script.

Space Name	Landside Check-in	Main Hall	Airside Departures
Level of Service	1.8	1.4	1.8
PPD	15	5	15
Comfort Class	III	I	III
Design Season	Summer		
Outside Temperature	27		
Air Supply Temperature	18		
Clothing Level	0.5		
Metabolic Rate	1.2		
Façade Area [m2]	1760	3480	3192
Façade WWR [-]	70	40	70
Façade Ug [W/m2K]	1	1	1
Façade Rc [m2K/W]	6.5	6.5	6.5
Façade gcombined [-]	0.1		
Equipment Loads [W/m2]	7	7	7

Figure 120 Inputs for running the test script.

This results in the following heat loads on the floor surfaces:

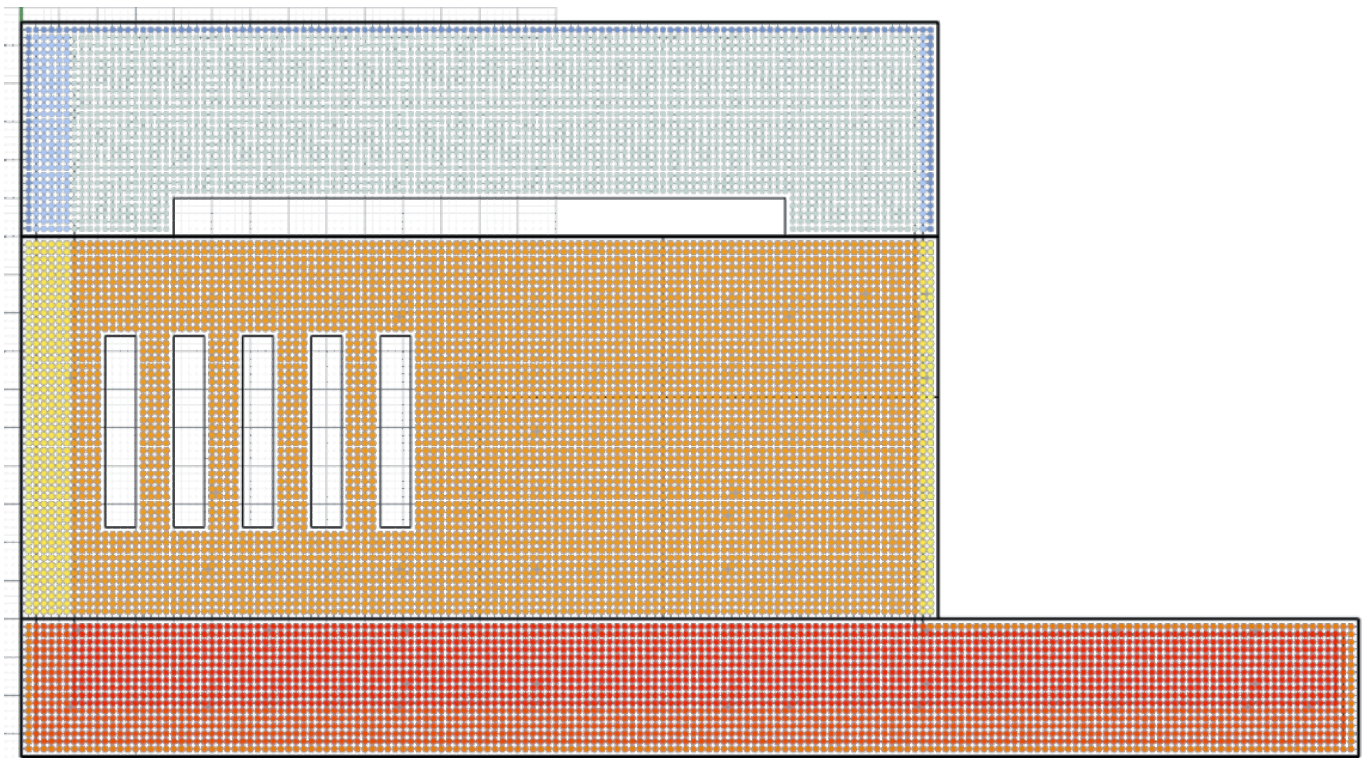


Figure 122 Heat loads projected on the floor surface.

In order to make the optimization with the genetic algorithm, the following design parameters were entered into the script:

1. Inlet airspeeds: 0.2, 0.4, 0.6, 0.8 and 1.0m/s
2. Inlet area: 0.36, 0.81, 1.44, 2.25 and 3.24m²
3. Outlet area: 3.24, 5.76, 12.96, 23.04 and 51.84 m²
4. Stack height: 12, 16, 20, 24, 24, 28m, with check-in and departure heights linked and main hall height independent

The CFD simulation was run with 12 CPU's running in parallel, the buoyantBoussinesqSimpleFoam script, LES turbulence with the kEqn model and 25 runs per optimization run. Galapagos Evolutionary Solver was run with a population of 10 per generation, with a total of 40 generations. 5% of the genes were maintained, while inbreeding was set at 75%. The meshing was set at a coarse mesh of 2m cells size with refinement in the bottom 20% height of the model, where the analyses were carried out.

6.4 Genetic Algorithm Results

The evolutionary solver was set to run and complete a total of 350 iterations. The total simulation took 27 hours in this configuration, equaling 4.6 minutes per iteration. The 350 iterations cover roughly 10% of the total design space in the case of the selected input parameters. The results of the genetic algorithm indicated that the 'best' solution reached a fitness of 348.25, which had a total of 42 inlets and outlets and an average PPD of 8.3%. The results of this analysis are also given below:

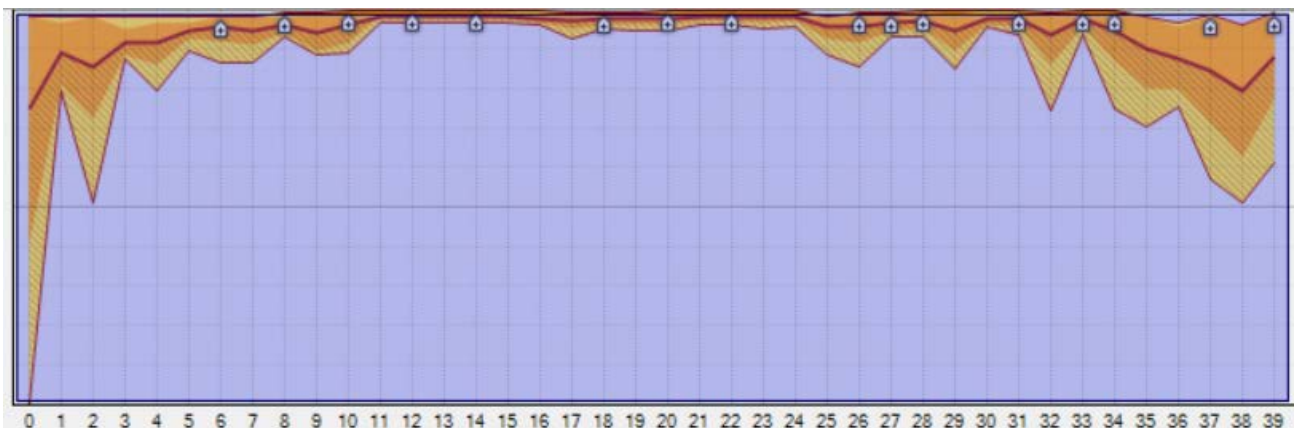
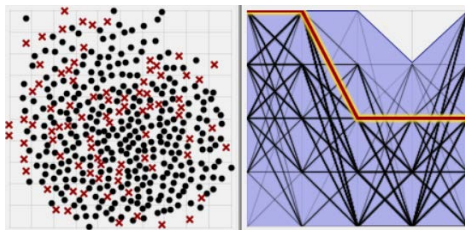


Figure 123 The total set of solutions showing the design space. The optimum result was found in the 16th generation.

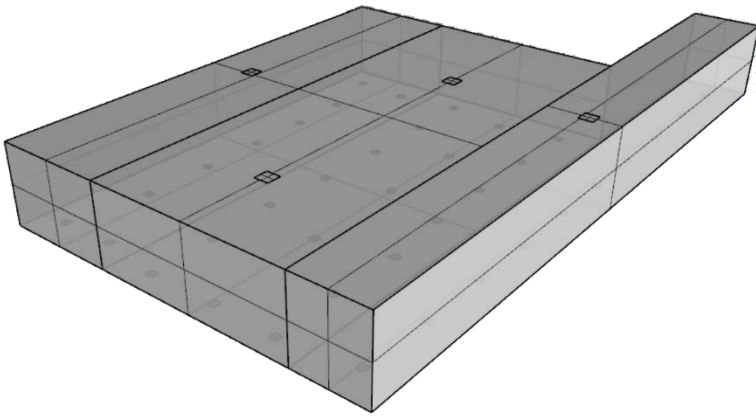


Figure 1244 Final air distribution geometry. Only four outlets are necessary with this combination of parameters.

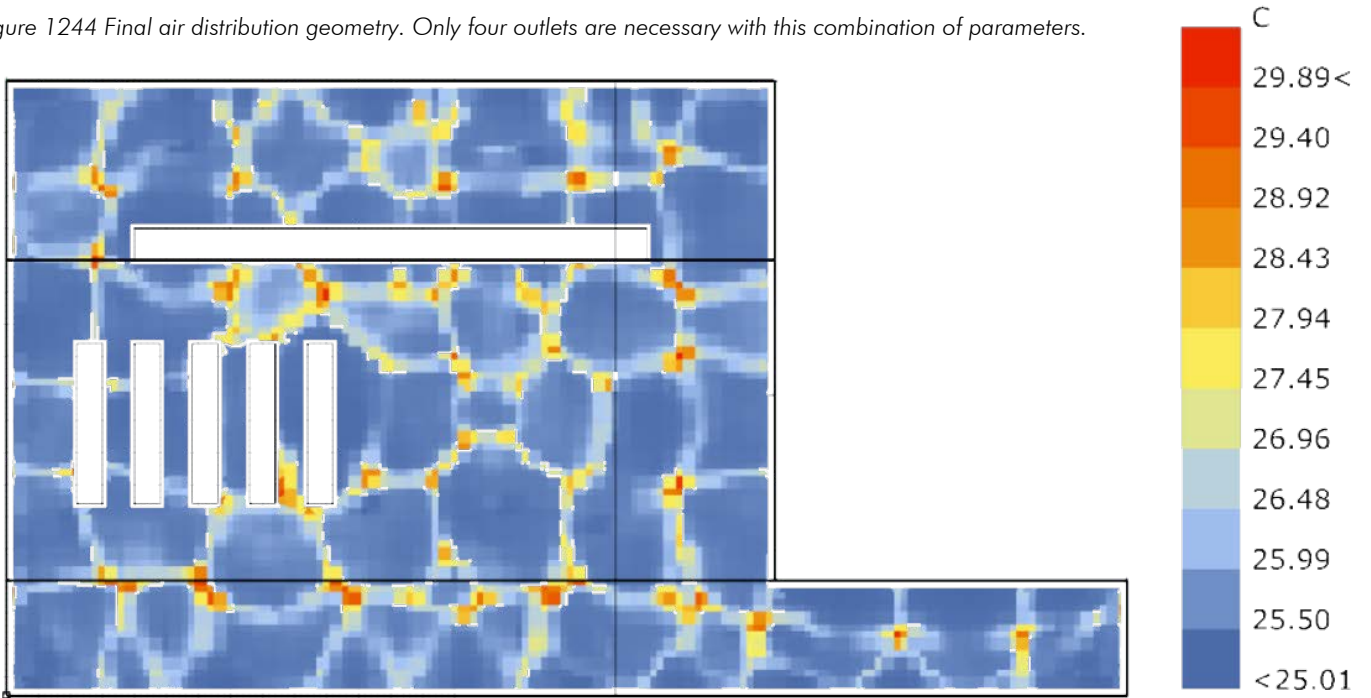


Figure 1255 Distribution of temperature over the floor field. Note the hot spots in the floor field due to the fact that the inlets do not reach there.

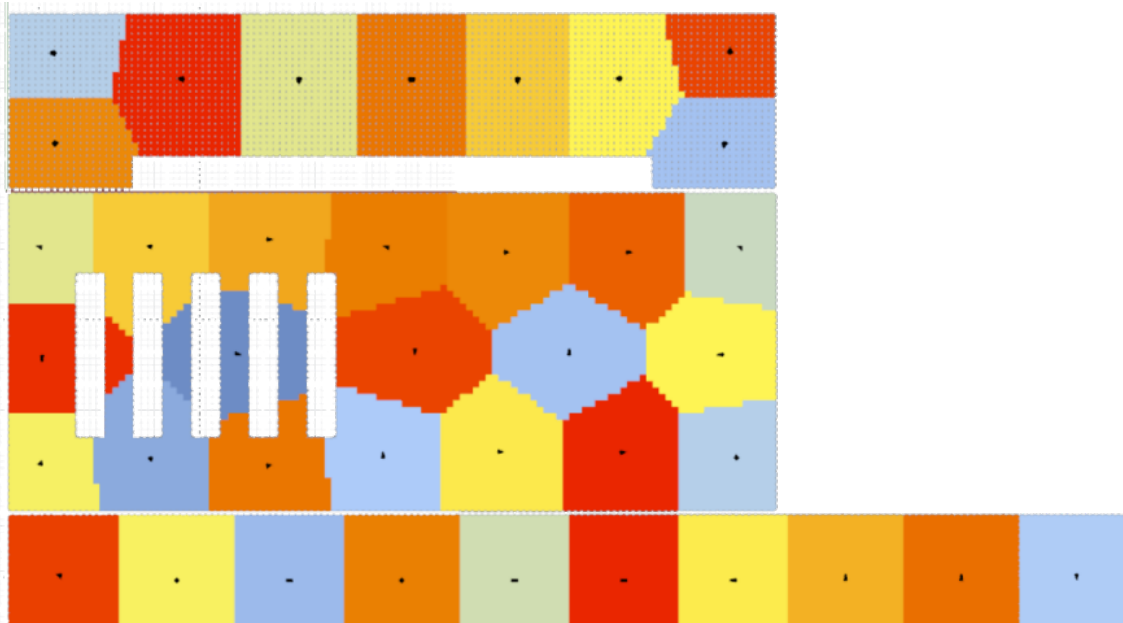


Figure 126 Distribution of the inlets per space.

The best-performing result had 38 inlets that were distributed through the spaces. Outlets were minimal: only one in the check-in and departures hall and two in the main hall. Inlet speed was 1.0m/s and its area 3.24m², equaling an opening of 1.80x1.80m for instance. The outlet has an area of 51.84m², equaling a square opening of 7.2x7.2m for instance. Although challenging, opening with such large free area's are devisable. Additionally, the small amount of inlets and outlets simplifies the placement and incorporation into the architecture.

When looking at the best performing results, a clear pattern does emerge from the analysis. Not to any surprise, the top five results all share the largest inlet and outlet areas possible. Interestingly however, the stack heights are not the highest ones available, with all spaces having an equal 20m stack height.

6.5 Geometric Optimization Results

After the best iteration is selected, its geometry is put into the various geometric possibilities. The option of culling cells with a velocity magnitude smaller than 0.25m/s yields the best result in this process, with a hint of what regions to cull. In all cases, the corners of the boxes can be culled, as they provide the biggest dead zones. This is for instance visible in the top view of the culled geometry when colored:

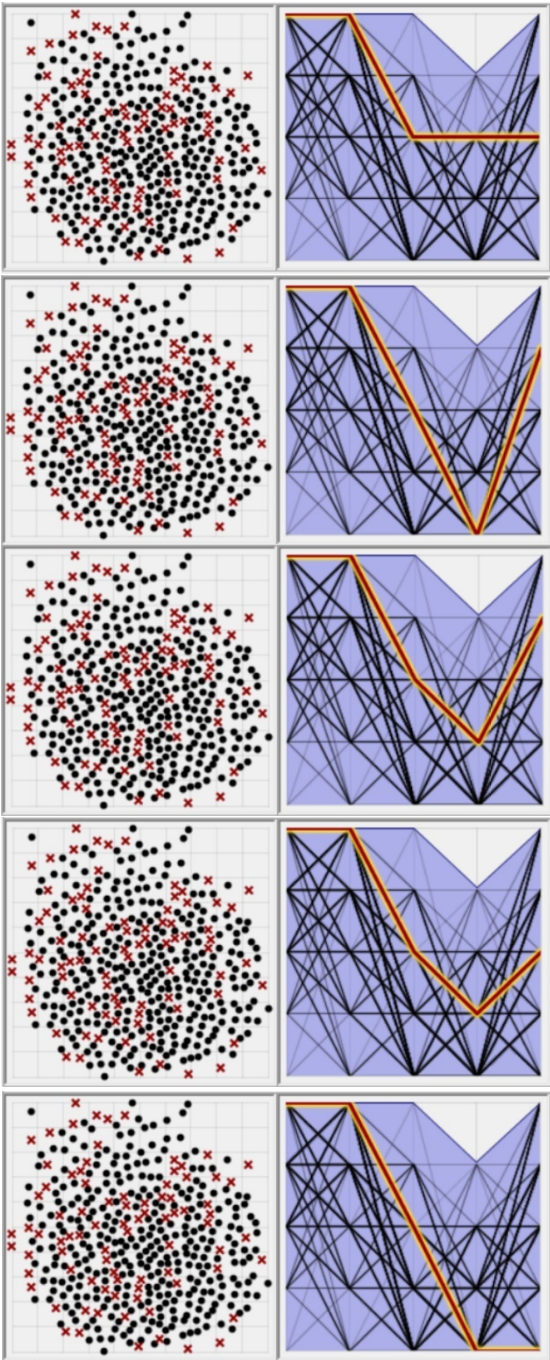


Figure 127 The top 5 results show a clear trend: high values for parameters 1, 2 (inlet speed and size), medium values for the remaining ones (stack height).

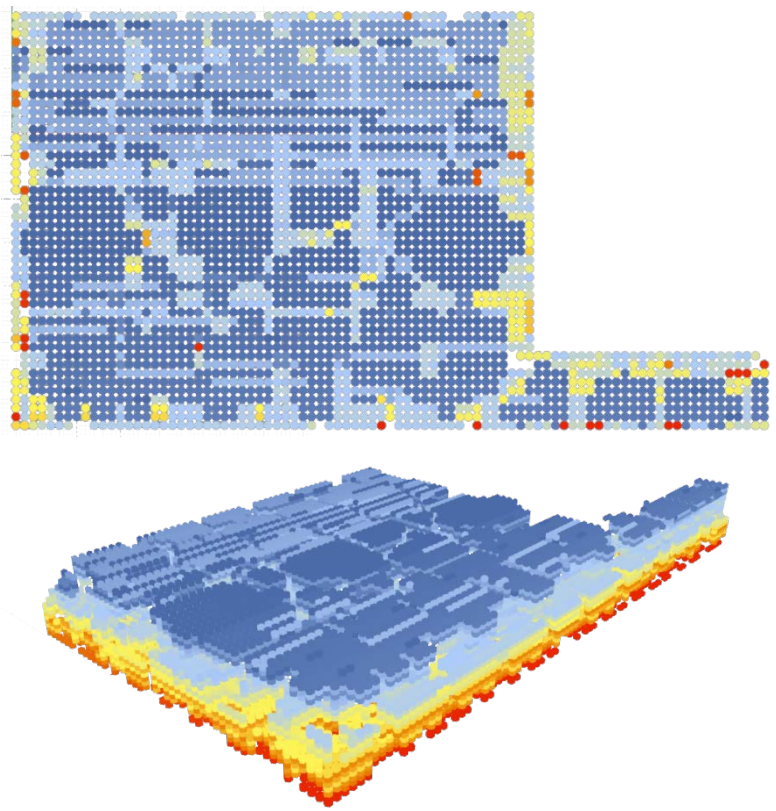


Figure 128 Geometry culling with voxels with magnitude < 0.25 culled. Note how the corners of the hall are the main parts to be culled.

However, if the bezier curves are used for the creation of the geometry, a far more diverse result appears. A sample of various ratios between the outlet points and the inlet points are provided in the following figures.

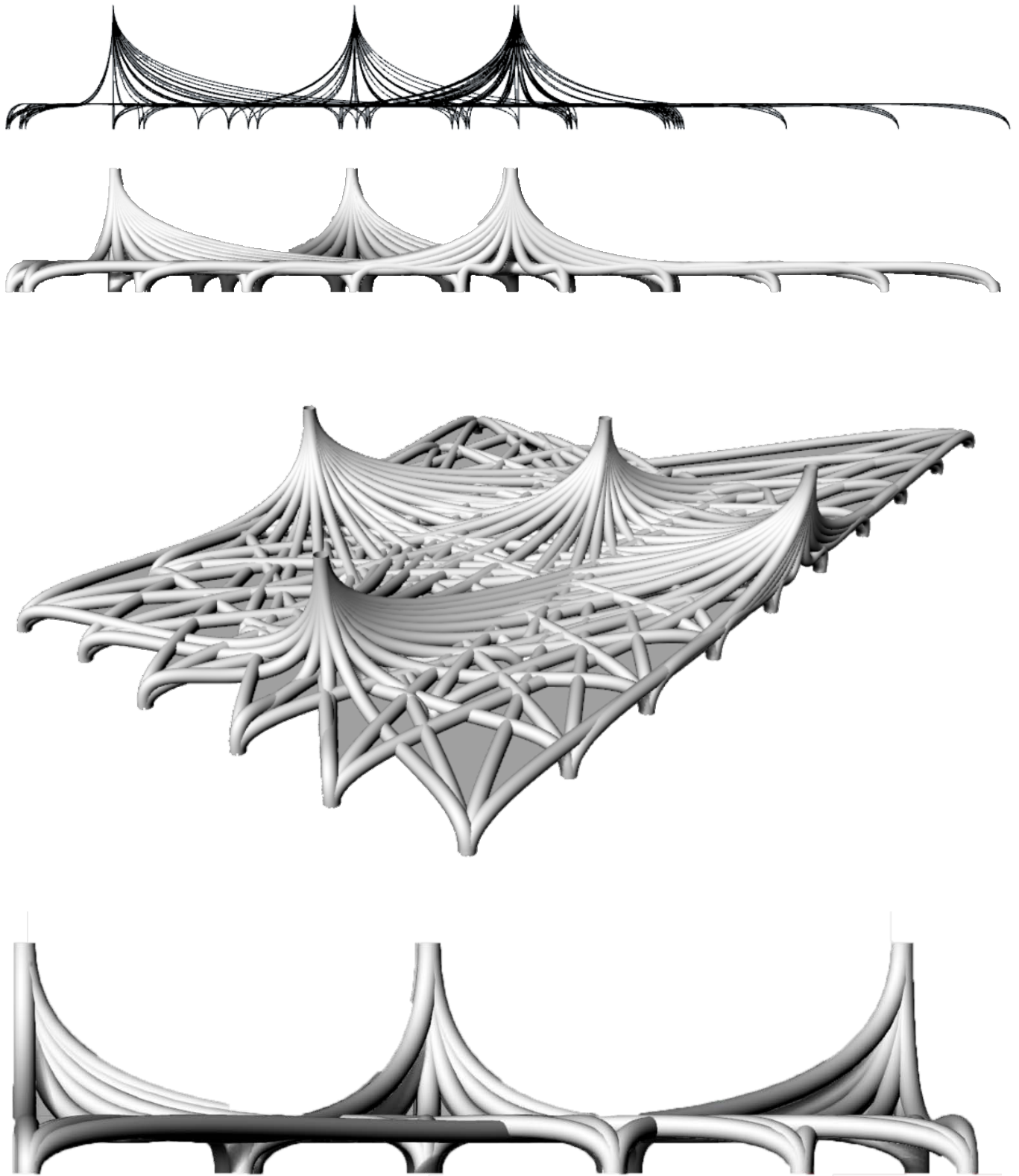


Figure 129 Impressions from connecting bezier curves between inlets and outlets with a very steep tangent for the outlet side.

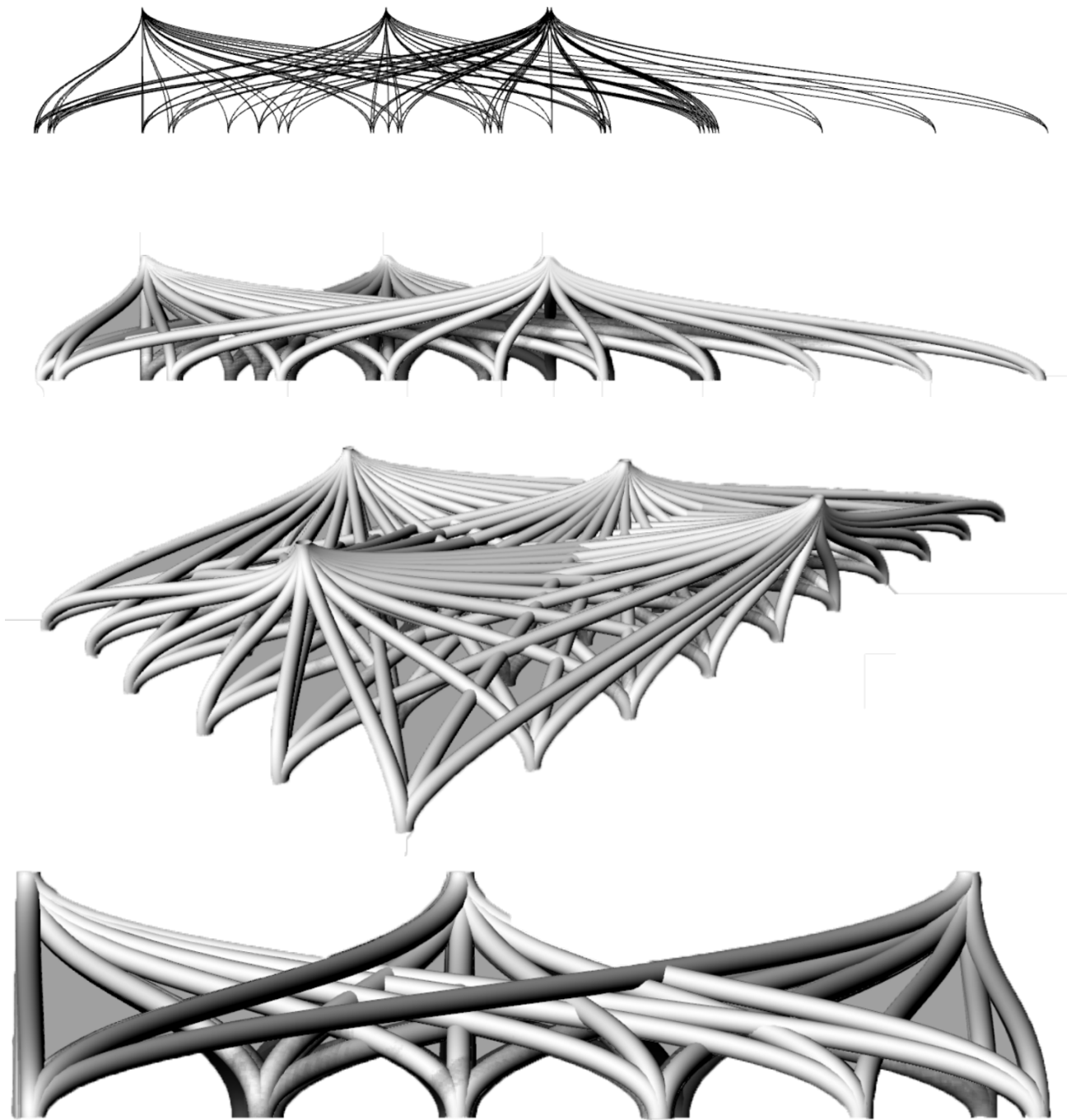


Figure 130 Impressions from connecting bezier curves between inlets and outlets with a very shallow tangent for the outlet side.



CONCLUSION

7 CONCLUSION

7.1 General Conclusion

This thesis focused on the development of a computational model for early-stage design optimization of naturally ventilated terminals. To this extent a computational method was developed after initial background studies and manual and CFD-assisted studies. The final product is a working model that allows for users to quickly set up and run CFD simulations in a parametric workflow and optimize the air distribution parameters and gain insight into how the geometry of the structure should be.

The development of naturally ventilated structures requires integration into the architecture from an early design stage. However, designing with natural ventilation is most accurate when combined with CFD simulations, which are difficult to implement in early-stage design. However, as HVAC systems can constitute between 20 to 66% of an airport's energy consumption and up to 15% of operational expenditures, it is evident that significant savings can be gained in this field. Additionally, airports themselves are a very energy-intensive building typology while the aviation sector in general has a very negative image in terms of its carbon footprint. Therefore, especially for the aviation sector where large terminals are the main building typology, the proposed method allows for the integration of natural ventilation into the design quickly.

The proposed model for natural ventilation relies mainly on thermal buoyancy as the driving force of air movement. Air is supplied through openings in the floor in the form of floor supply elements or vertical diffusers. Air is pre-cooled in a ground duct that can be placed under the structure or constructed under the apron of the airport and supplied to an underfloor supply plenum. Conditioning of air can be done at supply inlets or centrally at the entrance of the underfloor plenum. Removal of air occurs through tall stacks that have wind-assisted extraction of the air in the terminal. Pressure drops due to the ground duct and conditioning and filtering elements can be taken by fans in the ground duct or in the chimneys or by means of wind assistance by using the chimneys to generate negative pressure.

The script utilizes Rhino Grasshopper for the total interface and geometry generation. Integrated into the Rhino Grasshopper script are Python coding components that are used for a variety of geometric and mathematical purposes. The Ladybug/Honeybee plugin is needed for thermal comfort calculations, while the Butterfly plugin is necessary to run OpenFOAM CFD simulations from a virtual Linux machine. Additional coding was performed to edit and add functionality to the parametric workflow that is normally not possible with the listed software as well.

The optimization of air distribution parameters is performed using Galapagos evolutionary solver and has the objective to minimize an aggregate of inlets/outlets multiplied with the average PPD value of the floor field. Inlets are placed on the weighted heat load of each gridpoint in the floor field, with the script being able to take into account exclusion zones and regions of higher thermal loading. The geometric optimization performed afterwards mainly allows for users to gain insight into regions of low or negative airspeeds and how the final geometry of the structure could look like.

7.2 Research Questions

The main question of the thesis was to investigate what various air distribution and geometry input parameters affect the thermal comfort in naturally ventilated terminals. To his extent, the model itself provides the answer by using the answer of this question as design variables.

The biggest influence on the thermal comfort is the temperature and airspeed in the space. Effects of radiation or local discomfort indicators play a far smaller role, especially in large terminals where people are more standing and walking, rather than sitting. Parameters that influence the temperature in the space are mainly the internal heat generation and the cooling power of the ventilation air. It is noteworthy that, even though internal generation is very dominant in the total heat balance of a terminal, locally speaking solar and façade transmission can cause heat values that are 3-4 times as large as the internal heat generated by occupants and equipment.

Air inlet speeds are very important to the final thermal comfort as well, especially when supplied in regions close to where the occupants are, such as the floor. This is especially the case for the proposed design method, where air is supplied from the floor.

Even so, best-performing results from the evolutionary solver indicated that high inlet airspeeds of 1 m/s provided the optimal result, with small number of inlets and outlets and large inlet and outlet areas. Stack height did not impact the result as greatly, with an average stack height being implemented of 20m. This did result in pockets of very hot spots however, meaning that the manual verification of the results is absolutely critical for the final performance of the design. On the other hand, the simulated heat load in the CFD study is simultaneous, while normally the occupancy in the terminal will never.

The geometric optimization of the design clearly indicated that the interior corners of rectangular halls often form dead spots and can be removed easily. However, there is no computation-

ally inexpensive and fast method of generating a single geometry from CFD studies found in the thesis. This leaves the designer with a certain level of design freedom which is supported by a curve model in the design script. An indication of the possible geometry is given by connecting all inlets and outlets through a set of Bezier curves with variable start and end tangents, allowing for a level of design freedom.

Manual and early studies performed indicated that the optimization of the roof geometry increases ventilation efficiency and total airflow between up to 50%, but therefore also decreases the resulting thermal comfort. The increase in airspeed can be compensated by lowering the number of inlets and outlets or increasing supply air temperature (when cooling). However, there is nearly no difference observed between the 'trumpeted' shape as shown in the later geometric optimization against a more tapered and slightly slanted roof geometry. Early studies also indicated that the effect of wind on air distribution was minimal, as the supply is performed through a pressure-equalizing plenum under the floor that is little affected by wind.

7.3 Limitations

As a model for early-stage design optimization, the proposed model has clear limitations. Firstly, the model does not simulate with a high level of accuracy, as the goal is to iterate through many design options and decide which parameters influence the design to what effect. The total amount of runs is small and the meshing is relatively coarse, meaning that the model cannot be relied on for a final verification. However, due to the flexibility of the simulation settings, a final verification could be run within the same environment.

Similarly, the model does not take into account the complex interaction between supply plenum, ground ducts, solar chimneys, wind and infiltration. All those elements can constitute a great disturbance to the final airflow and comfort in the terminal. Similarly, the time-based effect of occupancy, solar loading or other time-dependent occurrences are not modeled. Similarly, dampening due to thermal mass or dynamic heat transfer is left outside the model.

From a computational point of view, the proposed method also has its limitations due to the integration of many software packages that each have their own bugs and limitations. A 'cleaner' interface between Rhino Grasshopper and OpenFOAM and the integration of OpenFOAM into windows would therefore be desirable.

7.4 Recommendations

As part of the process, a list of recommendations can be given to both future users as well as future development possibilities of this topic. Firstly, the design and development of naturally ventilated structures requires the integration of all stakeholders in the design and a clear understanding of its principles by the architects and users. Even though the process tries to simplify the process as much as possible, an understanding of the underlying physical models as well as an understanding of coding and optimization is necessary to work with the model.

A clear way of streamlining the whole process itself would be to add additional code to the standard Butterfly to expand its capability in running more complex OpenFOAM commands and options; after all, the most difficult part of entering geometry into OpenFOAM stays the same and is handled very efficiently by the plugin. Similarly, overall performance improvements in the memory handling of the Grasshopper plugin to Rhino is necessary to be able to visualize the large amounts of data that the CFD simulations generate. To this extent, the fact that the plugins did not work with Rhino 6 and Grasshopper v1.0, which have improved some of the performance issues, is another indicator that the large amount of plugins that need to interact is an additional cause of complexity.

8

REFERENCES

- Alba, S. O., & Manana, M. (2016). Energy research in airports: A review. *Energies*, 9(5), 1–19. <https://doi.org/10.3390/en9050349>
- Arcadis. (2018). *Vormfactoren & Kosten Kerngetallen*. Retrieved from <https://www.arcadis.com/media/E/C/1/%7BEC11C305-B768-4D5D-952D-39F22681A441%7D15-1058> Brochure VF-KK 1024-768digital_DEF_144dpi.pdf
- ATAG. (2004). *Air Transport Action Group Report: The Economic and Social Benefits of Air Transport*. Retrieved from http://www.icao.int/Meetings/wrdss2011/Documents/JointWorkshop2005/ATAG_SocialBenefitsAirTransport.pdf
- Attia, S. (2018). Modern History of Sustainable Architecture. *Regenerative and Positive Impact Architecture: Learning from Case Studies*, (Porteous 2013), 7–12. https://doi.org/10.1007/978-3-319-66718-8_2
- Autodesk. (2018). Embodied CO2. Retrieved January 18, 2019, from <https://sustainabilityworkshop.autodesk.com/>
- Bhardwaj, M., & Agrawal, G. D. (2018). Optimization of solar chimney for ventilation in buildings using Taguchi method. *Proceedings of 2017 IEEE International Conference on Technological Advancements in Power and Energy: Exploring Energy Solutions for an Intelligent Power Grid, TAP Energy 2017*, 1–6. <https://doi.org/10.1109/TAPENERGY.2017.8397217>
- Bluyssen, P. M. (2009). *The Indoor Environment Handbook: How to make buildings healthy and comfortable*. Earthscan Publishers, Abingdon.
- Bluyssen, P. M. (2014). *The Healthy Indoor Environment: How to Assess Occupants' Wellbeing in Buildings*. <https://doi.org/10.4324/9781315887296>
- Bluyssen, P. M. (2018a). *Indoor air quality & sources of pollution*.
- Bluyssen, P. M. (2018b). *Indoor Environmental Quality*.
- Brager, G. S., & de Dear, R. (2001). *Climate, Comfort, & Natural Ventilation: A new adaptive comfort standard for ASHRAE Standard 55*. <https://doi.org/10.1021/jm00120a002>
- Büyükbay, M. N., Özdemir, G., & Üstündağ, E. (2016). Sustainable aviation: Energy and environmental issues. In T. H. Karakoç, M. B. Özerdem, & M. Z. Sogut (Eds.), *Sustainable Aviation: Energy and Environmental Issues*. <https://doi.org/10.1007/978-3-319-34181-1>
- C2ES. (2018). Global Emissions. Retrieved January 18, 2019, from <https://www.c2es.org/content/international-emissions/>
- Cagney, D. (2018). New study reveals the real economic impacts of airports. Retrieved January 18, 2019, from

<http://www.airport-business.com/2015/04/new-study-reveals-real-economic-impacts-airports/>

- CAPA. (2018a). The world's top 20 international airports in 2025 will mostly reflect hub connectivity expansion. Retrieved January 18, 2019, from <https://centreforaviation.com/analysis/airline-leader/the-worlds-top-20-international-airports-in-2025-will-mostly-reflect-hub-connectivity-expansion-295056>
- CAPA. (2018b). USD1 trillion for airport construction globally - but it's not enough. CAPA Database. Retrieved January 18, 2019, from <https://centreforaviation.com/analysis/reports/usd1-trillion-for-airport-construction-globally---but-its-not-enough-capa-database-356495>
- CASCADE. (2012). CASCADE: ICT for Energy Efficient Airports. Retrieved January 18, 2019, from <http://www.cascade-eu.org/cms/>
- CBE. (2018). CBE Thermal Comfort Tool. Retrieved January 18, 2019, from <http://comfort.cbe.berkeley.edu/EN>
- Chen, X., Xue, P., Liu, L., Gao, L., & Liu, J. (2018). Outdoor thermal comfort and adaptation in severe cold area: A longitudinal survey in Harbin, China. *Building and Environment*, 143(73), 548–560. <https://doi.org/10.1016/j.buildenv.2018.07.041>
- Choufani, E. El. (2016). Energy Reduction in Airports. *Energy Reduction in Airports*, 5(December), 1–50. Retrieved from [http://www.cibse.org/getmedia/70ea2227-e8e8-4df5-bf60-24ce50084a18/Energy-Reduction-in-Airports-2016-\(1\).pdf.aspx](http://www.cibse.org/getmedia/70ea2227-e8e8-4df5-bf60-24ce50084a18/Energy-Reduction-in-Airports-2016-(1).pdf.aspx)
- Chu, C. R., & Chiang, B. F. (2013). Wind-driven cross ventilation with internal obstacles. *Energy and Buildings*, 67, 201–209. <https://doi.org/10.1016/j.enbuild.2013.07.086>
- Disch, R. (2018). Rolf Disch Solar Architektur. Retrieved from <http://www.rolfdisch.de/en/architects-office/>
- EnergyStar. (2013). *Technical Reference: US Energy Use Intensity by Property Type*. (July), 1–6. Retrieved from <https://portfoliomanager.energystar.gov/pdf/reference/CanadianNationalMedianTable.pdf>
- Engel, P. van den, & Roaf, S. (2017). *HYBRID VENTILATION – A DESIGN GUIDE*.
- European Commission. (2016). *Energy Performance of Buildings*. <https://doi.org/10.1007/978-3-319-20831-2>
- European Commission. (2018). Energy Efficiency in Buildings. Retrieved January 18, 2019, from <https://ec.europa.eu/energy/en/topics/energy-efficiency/buildings>
- FAA Airport Engineering Division. (2014). *FAA Airport Advisory Circular*.

- Ferziger, J. H., Peric, M., & Leonard, A. (2001). Computational Methods for Fluid Dynamics. In *Physics Today* (Vol. 50). <https://doi.org/10.1063/1.881751>
- Fuller, S. (2016). Life Cycle Cost Analysis (LCCA). Retrieved January 18, 2019, from <https://www.wbdg.org/resources/life-cycle-cost-analysis-lcca>
- GEA. (2012). Energy End-Use: Buildings. In E. Jochem (Ed.), *Global Energy Assessment: Towards a Sustainable Future* (pp. 649–760). Cambridge University Press, Cambridge UK.
- Gou, Z., Gamage, W., Lau, S., & Lau, S. (2018). An Investigation of Thermal Comfort and Adaptive Behaviors in Naturally Ventilated Residential Buildings in Tropical Climates: A Pilot Study. *Buildings*, 8(1), 5. <https://doi.org/10.3390/buildings8010005>
- Guo, W., Liu, X., & Yuan, X. (2015). Study on Natural Ventilation Design Optimization Based on CFD Simulation for Green Buildings. *Procedia Engineering*, 121, 573–581. <https://doi.org/10.1016/j.proeng.2015.08.1036>
- Hanaoka, S., & Saraswati, B. (2011). Low cost airport terminal locations and configurations. *Journal of Air Transport Management*, 17(5), 314–319. <https://doi.org/10.1016/j.jairtraman.2011.03.009>
- Heathrow Airport Limited. (2018). Heathrow Airport - About Us. Retrieved January 18, 2019, from <https://www.heathrow.com/more/about-us>
- Hitchin, R. (2013). *Embodied Carbon and Building Services*. 1–16.
- IATA. (n.d.). *IATA Airport Development Reference Manual.pdf*.
- IATA. (2018a). Address Infrastructure Crisis to Secure Aviation's Future. Retrieved January 18, 2019, from <https://www.iata.org/pressroom/pr/Pages/2018-02-05-01.aspx>
- IATA. (2018b). Level of Service Concept. Retrieved January 18, 2019, from <https://www.iata.org/services/consulting/airport-pax-security/Pages/level-of-service.aspx>
- Initiafly. (2018). How does construction impact the environment? Retrieved January 18, 2019, from <https://www.initiafly.com/blog/how-does-construction-impact-the-environment/>
- International Airport Review. (2017). A budget terminal for budget airlines. Retrieved January 18, 2019, from <https://www.internationalairportreview.com/article/1676/a-budget-terminal-for-budget-airlines/>
- Khan Academy. (2018). Khan Academy: Fluid Dynamics. Retrieved January 18, 2019, from <https://www.khanacademy.org/science/physics/fluids/flui>

- Klein, K., & Sc, M. (2015). *Building Automation Data Supported Energy Management*.
- Kotopoulos, A., & Nikolopoulou, M. (2016). Thermal comfort conditions in airport terminals: Indoor or transition spaces? *Building and Environment*, 99, 184–199. <https://doi.org/10.1016/j.buildenv.2016.01.021>
- Li, K., Xue, W., Xu, C., & Su, H. (2013). Optimization of ventilation system operation in office environment using POD model reduction and genetic algorithm. *Energy and Buildings*, 67, 34–43. <https://doi.org/10.1016/j.enbuild.2013.07.075>
- Liu, Z., Wang, X. L., & Zhang, A. L. (2013). Construction Ventilation Scheme Optimization of Underground Main Powerhouse Based on CFD. *Applied Mechanics and Materials*, 368–370(1), 619–623. <https://doi.org/10.4028/www.scientific.net/AMM.368-370.619>
- Ma, J. S., Liu, X. T., Zhuang, D. M., & Wang, S. G. (2011). CFD-Based Design of the Natural Ventilation System of the Traffic Center of T3 in Beijing International Airport. *Advanced Materials Research*, 291–294(1), 3292–3295. <https://doi.org/10.2139/ssrn.1836674>
- Malik, K. (2017). Assessment of energy consumption pattern and energy conservation potential at Indian airports. *Journal of Construction in Developing Countries*, 22(November), 97–119. <https://doi.org/10.21315/jcdc2017.22.suppl.6>
- Méndez, C., San José, J. F., Villafruela, J. M., & Castro, F. (2008). Optimization of a hospital room by means of CFD for more efficient ventilation. *Energy and Buildings*, 40(5), 849–854. <https://doi.org/10.1016/j.enbuild.2007.06.003>
- Nakayama, Y. (1998). *Fluid Mechanics*.
- NASA. (2018). Climate change: How do we know? Retrieved January 18, 2019, from <https://climate.nasa.gov/evidence/>
- National Geographic. (2018). See how termites inspired a building that can cool itself. Retrieved from <https://video.nationalgeographic.com/video/magazine/decoder/00000163-4f96-de63-afe7-7fdf708d0000>
- NEN. (2005). *ISO 7730: Ergonomics of the thermal environment - Analytical determination and interpretation of thermal comfort using calculation of the PMV and PPD indices and local thermal comfort criteria*. (015).
- Neufert, E., & Neufert, P. (2003). *Architects' Data* (p. 683). p. 683.
- Nitsopoulos, I., Stephan, M., Böhm, M., Karlsruhe, F., & Sofia, F. (2009). *An Efficient Approach for CFD Topology*

Optimization of interior flows FE-DESIGN Locations in Europe.

- Nozaki, F. (n.d.). Solvers for heat transfer problems in OpenFOAM – buoyantBoussinesqPimpleFoam. Retrieved from <https://caefn.com/openfoam/solvers-buoyantboussinesqpimplefoam>
- Ohio Airports. (2014). *Ohio Airports Focus Study*. 1–16.
- OpenFOAM Ltd. (n.d.). OpenFOAM - About. Retrieved from <https://www.openfoam.com/>
- Othmer, C. (2014). Adjoint methods for car aerodynamics. *Journal of Mathematics in Industry*, 4(1), 1–23. <https://doi.org/10.1186/2190-5983-4-6>
- Parry, J., Bornoff, R. B., Stehouwer, P., Driessen, L. T., & Stinstra, E. (2004). Simulation-based design optimization methodologies applied to CFD. *IEEE Transactions on Components and Packaging Technologies*, 27(2), 391–397. <https://doi.org/10.1109/TCAPT.2004.828554>
- Parsons, K. (2014). *Human Thermal Environments*. <https://doi.org/10.1201/b16750>
- Passivhaus Institute. (2018). Passivhaus. Retrieved from <https://passivehouse.com/>
- Pearce, M. (2018a). Eastgate Centre. Retrieved January 18, 2019, from <http://www.mickpearce.com/Eastgate.html>
- Pearce, M. (2018b). Mick Pearce Architect. Retrieved January 18, 2019, from <http://www.mickpearce.com/>
- Pérez-Lombard, L., Ortiz, J., & Pout, C. (2008). A review on buildings energy consumption information. *Energy and Buildings*, 40(3), 394–398. <https://doi.org/10.1016/j.enbuild.2007.03.007>
- Poh, E. (2007). *Airport Planning and Terminal Design*. (April).
- Prendergast, E. (2016). *Trends in Energetische Maatregelen*.
- Rithcie, H., & Roser, M. (2018). Urbanization. Retrieved January 18, 2019, from <https://ourworldindata.org/urbanization>
- RVO. (2018). Wettelijke eisen - BENG. Retrieved January 18, 2019, from <https://www.rvo.nl/onderwerpen/duurzaam-ondernemen/gebouwen/wetten-en-regels-gebouwen/nieuwbouw/energieprestatie-beng/wettelijke-eisen-beng>
- Sacht, H., Bragança, L., Almeida, M., & Caram, R. (2016). Study of Natural Ventilation in wind Tunnels and Influence of the Position of Ventilation Modules and Types of Grids on a Modular Façade System. *Energy Procedia*, 96(October), 953–964. <https://doi.org/10.1016/j.egypro.2016.09.173>
- Schiphol Airport. (2018a). A CO2 neutral airport. Retrieved January 18, 2018, from <https://www.schiphol.nl/en/schiphol-group/page/a-co2-neutral-airport/>

- Schiphol Airport. (2018b). Schiphol Airport Annual Report 2017. Retrieved January 18, 2019, from <https://www.annualreportschiphol.com/>
- Schlanger, Z. (2018). Why do all our climate data start in 1880? Retrieved January 18, 2019, from <https://qz.com/1055629/why-does-all-our-climate-data-start-in-1880/>
- Short, C. Alan. (2011). Sustainable Buildings in 2030 ' Environmental Design Strategies for a Changing Climate .' *Plateau*, (May).
- Short, C. Alan. (2018). The recovery of natural environments in architecture: Delivering the recovery. *Journal of Building Engineering*, 15(November 2017), 328–333. <https://doi.org/10.1016/j.jobe.2017.11.014>
- Short, C A, & Cook, M. J. (2015). *Technical note Design guidance for naturally ventilated theatres*. 3(2005), 259–270.
- Spence, R., & Mulligan, H. (1995). Sustainable development and the construction industry. *Habitat International*, 19(3), 279–292. [https://doi.org/10.1016/0197-3975\(94\)00071-9](https://doi.org/10.1016/0197-3975(94)00071-9)
- Su, Y. X., Lei, F. N., & Xue, Y. F. (2013). Modeling of Natural Ventilation in Solar Chimney and Optimization of the Channel Profile by CFD Method. *Applied Mechanics and Materials*, 368–370, 549–553. <https://doi.org/10.4028/www.scientific.net/AMM.368-370.549>
- The Strait Times. (2017). Changi's T4 is model airport of the future for budget airlines, says AirAsia chief Tony Fernandes. Retrieved from <https://www.straitstimes.com/singapore/changis-terminal-4-model-airport-of-the-future-for-budget-airlines-airasia-chief-tony>
- United Nations. (2014). *Brundtland Report*.
- Vitruvius, M. P. A.-M. H. M. (1914). *The ten books on architecture*.
- Voorde, E. Van de. (n.d.). *The future of low-cost airlines and airports*.
- Vranes, S., Tomasevic, N., Batic, M., Keane, M. M., Costa, A., Blanes, L. M., ... Ohr, F. (2012). *Energy and Technical Characterization, Operational Scenarios of European Airports as Open Spaces D1.1: CASCADE ICT for Energy Efficient Airports*.
- Weisstein, E. W. (2019). Algebraic Topology. Retrieved from Mathworld - A Wolfram Web Resource website: <http://mathworld.wolfram.com/AlgebraicTopology.html>
- Wendover Productions. (2018). How Airports Make Money. Retrieved from <https://www.youtube.com/watch?v=wdU1WTBJMIO&t=2>

- Zhou, L., & Haghghat, F. (2009a). Optimization of ventilation system design and operation in office environment, Part I: Methodology. *Building and Environment*, 44(4), 651–656. <https://doi.org/10.1016/j.buildenv.2008.05.009>
- Zhou, L., & Haghghat, F. (2009b). Optimization of ventilation systems in office environment, Part II: Results and discussions. *Building and Environment*, 44(4), 657–665. <https://doi.org/10.1016/j.buildenv.2008.05.010>
- Zimmermann, K. A. (2018). Pleistocene Epoch: Facts About the Last Ice Age. Retrieved January 18, 2019, from <https://www.livescience.com/40311-pleistocene-epoch.html>